The Thesis Committee for Mohammad Hamad AlTwaijri
Certifies that this is the approved version of the following thesis:

A Comprehensive Numerical Model for Simulating Two-Phase Flow in Shale Gas Reservoirs with Complex Hydraulic and Natural Fractures

APPROVED BY
SUPERVISING COMMITTEE:

Supervisor:

Kamy Sepehrnoori

Wei Yu

A Comprehensive Numerical Model for Simulating Two-Phase Flow in Shale Gas Reservoirs with Complex Hydraulic and Natural Fractures

by

Mohammad Hamad AlTwaijri

Thesis

Presented to the Faculty of the Graduate School of

The University of Texas at Austin

in Partial Fulfillment

of the Requirements

for the Degree of

Master of Science in Engineering

The University of Texas at Austin

August 2017

Dedication

For my loving mother, my wonderful wife, and my sweet little boy.

Your love, kindness, and encouragement have been my backbone.

Acknowledgements

Above all, I give thanks to Allah for his countless blessings.

This work would not have been possible without contributions from several individuals and organizations. Their help, input, and support had been substantially valuable throughout my graduate studies at the University of Texas at Austin.

Firstly, I would like to express my sincerest gratitude for my research advisor Dr. Kamy Sepehrnoori for his guidance and help during my research and studies at the University of Texas at Austin. In addition, my deepest appreciation goes to Dr. Wei Yu for his endless support and motivation throughout the research's period. Furthermore, a great deal of appreciation goes to my follow research mate Yifei Xu for his help and comments on several aspects of the research.

Secondly, I would like to acknowledge my academic sponsors at Saudi Aramco for giving me the opportunity to pursue a master's degree and supporting me financially throughout the process. Additionally, the library at the University of Texas at Austin is appreciated for providing access to resources and journal papers reviewed during my research. Moreover, my thanks go to the Computer Modeling Group (CMG) for software utilization.

Finally, my outmost gratitude and love are to my wife for being there every step of the way. My family, friends, and colleagues are also hugely appreciated for their love, support, and kindness.

Abstract

A Comprehensive Numerical Model for Simulating Two-Phase Flow in Shale Gas Reservoirs with Complex Hydraulic and Natural Fractures

Mohammad Hamad AlTwaijri, M.S.E.
The University of Texas at Austin, 2017

Supervisor: Kamy Sepehrnoori

Increase in energy demand has played a significant role in the persistent exploitation and exploration of unconventional oil and gas resources. Shale gas reservoirs are one of the major unconventional resources. Advancements in horizontal drilling and hydraulic fracturing techniques have been the key to achieve economic rates of production from these shale gas reservoirs. In addition to their ultra-low permeability, shale gas reservoirs are characterized by their complex gas transport mechanisms and complex natural and induced (hydraulic) fracture geometries. Production from shale gas reservoirs is predominantly composed of two-phase flow of gas and water. However, proper modeling of the two-phase behavior as well as incorporating the complex fracture geometries have been a challenge within the industry. Due to the limitation of the local grid refinement (LGR) approach, hydraulic fractures are assumed to be planar (orthogonal), which is an unrealistic assumption. Although more flexible approaches are available, such as the use of unstructured grids, they require significantly high computational powers.

In this research, an efficient embedded discrete fracture model (EDFM) is introduced to explicitly model complex fracture geometries. The EDFM approach is capable of explicitly modeling complex fracture geometries without increasing the computational demand. Utilizing EDFM alongside a commercial simulator, a 3D reservoir model is constructed to investigate the effect of complex fracture geometries on the two-phase flow of a shale gas well. In this investigation, varying degrees of hydraulic fracture complexity with 1-set and 2-set natural fractures were tested. The simulation results confirm the importance of properly modeling fracture complexity, highlighting that it plays an integral part in the estimation of gas and water recoveries. In addition, the simulation results hint to the pronounced effect of fracture interference as fracture complexity increases. Finally, variable fracture conductivities and initial water saturation values were analyzed to further assess their effect on the two-phase production behavior of the shale gas well.

This study examines the effect of non-orthogonal complex fracture geometry on the two-phase flow of shale gas wells. The work can provide a significant insight toward understanding the extent to which fracture complexity can affect the performance of shale gas wells.

Table of Contents

List of Tables

List of Figures

Chapter 1: Introduction

1.1. Background and Motivation

There is an estimated 7,570 Tcf of technically recoverable shale gas within the countries assessed by (EIA, 2013) and highlighted on **Figure 1.1**. This compares to 6,600 Tcf of global total proven gas reserves (BP, 2017). Shale gas therefore has the potential to be a greatly significant source of natural gas and help increase the overall production of natural gas across the globe. As a matter of fact, using the United States as an example, shale gas is projected to dominate domestic production of natural gas, as depicted on **Figure 1.2**. Specifically, alongside gas from tight oil resources, shale gas is forecasted to account for nearly two-thirds of the US natural gas production by 2040 (EIA, 2017).

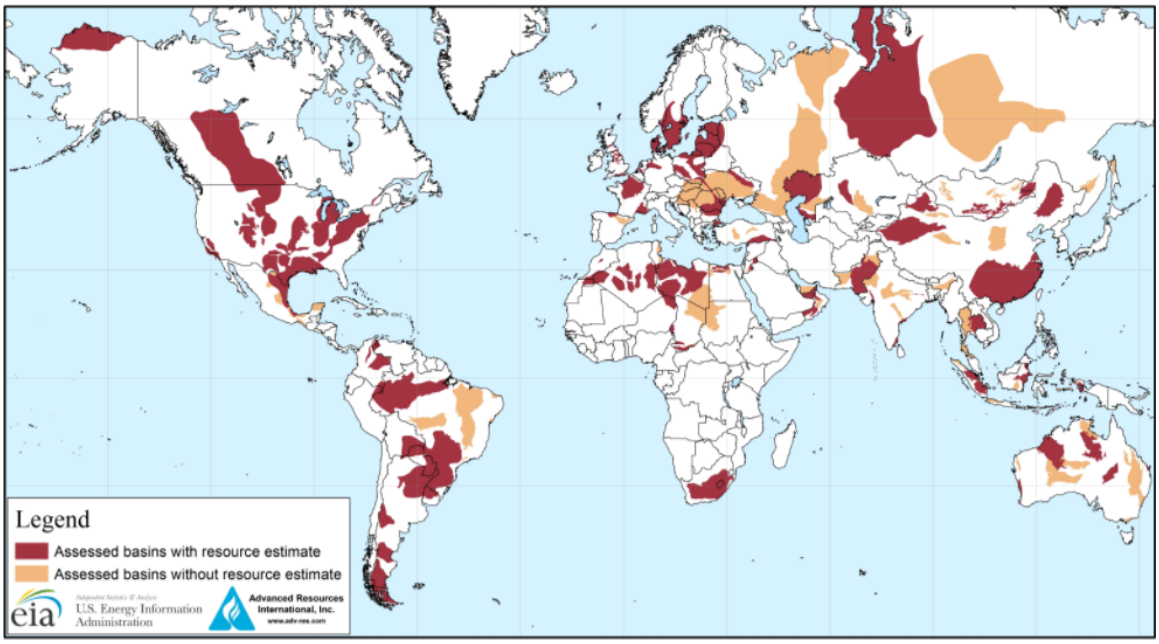

Figure 1.1: Map of worldwide assessed shale basins (EIA, 2013).

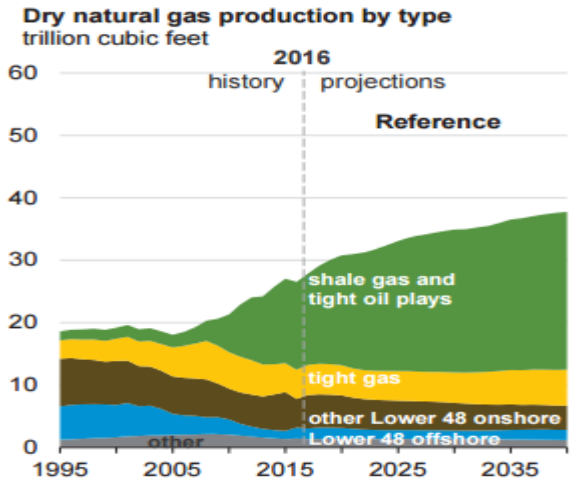

Figure 1.2: Historical and projected sources of natural gas in the United States (EIA, 2017).

Unlike conventional gas reservoirs, shale gas reservoirs are characterized by greater heterogeneity, several gas storage mechanisms, and intricate gas transport phenomena (Jenkins and Boyer, 2008). Shale gas reservoirs are comprised of both organic and inorganic matters. In addition, they are characterized by small pores that are connected by tiny throats. Hence, these reservoirs are considered to have ultra-low permeability. All this giant variation in pore scale makes the flow of gas and water inside the reservoir and into the hydraulic fractures very complex.

Hydraulic fracturing has been the cornerstone in the development of shale gas reservoirs. Hydraulic fracturing involves pumping thousands of barrels of water into the reservoir at a high pressure to break down the rock and create conduits for gas to flow freely to the surface. Due to the prevalence of stress anisotropy and the presence of natural fractures in shale gas reservoirs, hydraulically created conduits (fractures) are seldom orthogonal (planar). The geometrical complexity of these induced fractures has been established by several recorded microseismic events of hydraulically-fractured shale gas wells, as depicted in **Figures 1.3** and **1.4**.

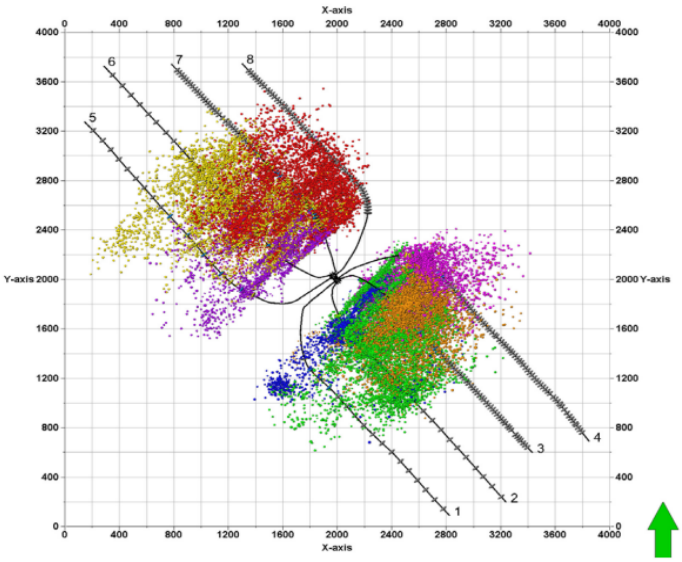

Figure 1.3: Microseismic events recorded in the Horn River Basin in Canada highlighting fracture complexity (Virues et al., 2015).

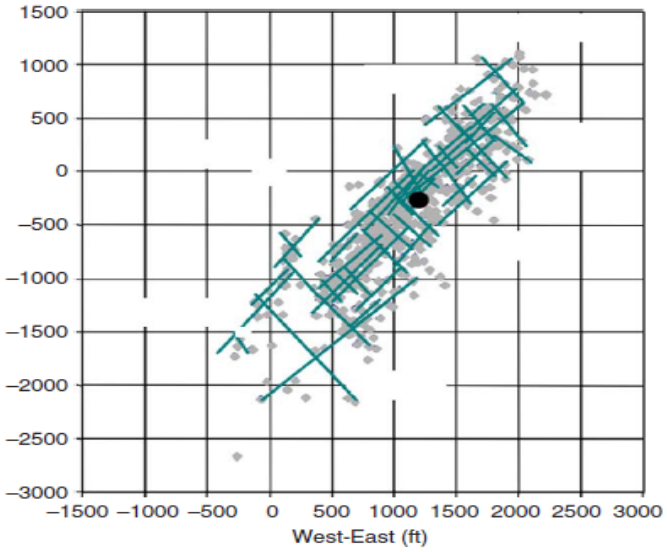

Figure 1.4: Microseismic events recorded in the Barnett Shale highlighting complex fracture geometries (Fisher et al., 2004).

A major challenge in the appraisal phase of shale gas plays has been the inadequacy of classic conventional reservoir engineering modeling tools to capture the changing characteristics of hydraulically-fractured shale formations (Vassilellis et al., 2010). Proper modeling of these complex shale gas reservoirs is imperative for accurately predicting long-term production and recovery. A major obstacle typically arises when trying to accurately model complex hydraulic fractures. The hydraulic fracturing process of shale gas reservoirs often creates complex fracture networks, particularly when the fracture propagates in a formation with pre-existing natural fractures. Nevertheless, this complex fracture geometry is rarely captured in simulation models of shale gas reservoirs. As a matter of fact, due to the limitation of local grid refinement (LGR) approach, fractures are usually assumed to be planar (orthogonal). Other flexible approaches were attempted to incorporate fracture complexity, such as unstructured grids. However, these approaches require high computational powers. Yet, the embedded discrete fracture modeling (EDFM) approach, which will be utilized in this research, is capable of reducing these computational demands while efficiently handling complex fracture geometries. In addition to being able to explicitly model complex hydraulic fracture geometries, the EDFM approach is capable of simultaneously incorporating large number of natural fractures to the reservoir model to examine their effect on the production performance.

This research thesis investigates how complexity in fracture geometry can affect the two-phase (Gas and water) flow of shale gas wells. The investigation approach is solely focused on numerical simulation of different synthetic cases. In this study, a horizontal well with 25 hydraulic fractures is constructed to model gas and water flowback performances from a shale gas reservoir.

1.2. RESEARCH OBJECTIVES

The overall objective of this research is to provide knowledgeable insight toward understanding the extent to which fracture complexity can affect the performance of shale gas wells. An investigation of multiple levels of fracture complexities in shale reservoirs is carried out to reach a consensus on the significance of incorporating such complexities in simulation modeling of shale gas reservoirs in particular and perhaps shale reservoirs in general. Such fracture complexities include geometrical complexity in hydraulic fractures, complexity associated with the presence of natural fractures, and complexity associated with the non-uniformity of hydraulic fractures' apertures/widths. The specific objectives of this research thesis can be summarized in the following points:

- Develop a comprehensive numerical model of a shale gas well with multiple hydraulic fractures based on typical fluid and reservoir properties of shale gas reservoirs while incorporating complex aspects of shale gas transport mechanisms.
- Examine varying degrees of hydraulic fracture geometries in the 3D reservoir model in order to recognize and rank the magnitude of effect generated by different geometries on the two-phase flow performance of the shale gas well.
- Investigate the effect of natural fractures on the two-phase flow performance of the shale gas well by incorporating them in the 3D reservoir model. Different numbers and orientations of natural fractures is to be tested.
- Analyze the effect of varying fractures' apertures/widths on the overall two-phase flow performance of the shale gas well.
- Generate a sensitivity analysis to characterize the extent to which some reservoir and fracture properties can affect the two-phase flow performance of the shale gas well.

1.3. THESIS OUTLINE

This thesis consists of five chapters which follow the work's progression order. The first chapter introduces a background on the field of shale gas development, explains the motivation to pursue research on this area, and finally presents detailed research's objectives.

Chapter 2 covers the literature review pertaining to the research area. It incorporates general developments, and specific advancements and underachievement in publications related to the research objectives.

Chapter 3 discusses the methodology followed in the development of the research's objectives. It includes an overview of the Embedded Discrete Fracture Modeling (EDFM) tool, utilized for incorporating complex fracture geometries into the reservoir model. In addition, it contains a description of the reservoir simulation model. Finally, a verification of the methodology undertaken is presented by comparing simulation results of a simple planar case utilizing the Embedded Discrete Fracture Modeling (EDFM) approach versus the Local Grid Refinement (LGR) approach.

Chapter 4 provides the results of the research in addition to presenting analyses of these results. This chapter is divided into sections according to different levels of fracture complexity such as geometrical complexity in hydraulic fractures, complexity related to the presence of natural fractures, and complexity related to the non-uniformity of fractures' apertures/widths. In addition, this chapter presents a sensitivity analysis related to changing initial water saturation and fractures' conductivity.

Finally, Chapter 5 summarizes the results of this research and presents a conclusion of the research's findings. In addition, this chapter offers some recommendations for future related work.

Chapter 2: Literature Review

Typically, following a stimulation pumping process of a shale gas well, a flowback (cleanup) period is established, lasting for couple of days. This flowback period is dominated by water flow from the well. Subsequently as a standard procedure, the well is shut-in, before it is put on production where two-phase flow of gas and water is established and monitored.

The two-phase flow behavior of shale gas reservoirs has been analyzed in multiple studies. In regards to water recovery (load recovery) from shale gas wells, several studies and laboratory experiments have estimated that only 10-50% of the injected water is recovered (Bennion et al., 1994; Bennion et al., 1999; Engelder et al., 2014; Makhanov et al., 2014). In fact, Cheng (2012) argues that it is fairly common that only 10-20% of injected fluid is recovered during the flowback period. This low load recovery is attributed to phase trapping caused by spontaneous water imbibition into the shale matrix (Bennion et al., 1994; Bennion et al., 1999).

On the other hand, the two-phase flowback data, which incorporate the majority of the recovered water from shale gas reservoirs, have also been given its share of interest by several researchers. For example, Ilk et al. (2010) provided a comprehensive diagnostic workflow of early-time two-phase production data through the utilization of real flowback data of several shale gas wells. In their results, they presented a correlation in well performance (in terms of time-rate-pressure data) between the shale gas wells. In addition, Clarkson and Williams-Kovacs (2013) proposed a procedure for analyzing two-phase flowback data of shale gas wells for the purpose of generating a production forecast using estimated fracture half-length and permeability. Another utilization of flowback data was by Alkouh et al. (2014), where they proposed a procedure to analyze a

combined flowback and early production data in order to estimate the effective fracture volume of the hydraulic fracturing job. Furthermore, Williams-Kovacs and Clarkson (2015) proposed a model based on a material balance equation (MBE) by combining the multi-phase flow within the fracture network to the linear flow of gas coming from the matrix. Their aim was to conduct rate transient analysis on the single-phase flow data before breakthrough (BBT) and the multi-phase flow after breakthrough (ABT) to estimate some important fracture parameters such as fracture conductivity and half-length. However, gas diffusion was not incorporated in their model. Moreover, several analytical and semianalytical studies focused on modeling early production data by assuming single-line MBE approach (Adefidipe et al., 2014; Xu et al., 2015). However, their models did not incorporate some critical shale gas transport mechanisms such as gas desorption and gas slippage.

Others took a fully analytical approach in modeling early production data utilizing the dynamic relative permeability (DRP) concept to create a multi-phase dual-porosity linear model (Ezulike et al., 2013; Ezulike et al., 2014). However, their model neglected gas desorption and is not capable of modeling complex fracture geometries. On the other hand, several numerical models were run to simulate and analyze the performance of shale gas wells. Yu et al. (2014) utilized numerical simulation of shale gas wells to conduct a sensitivity analysis to examine the effect of fracture half-length, fracture spacing and uncertainty of fracture geometry on the cumulative gas production. Nevertheless, their study did not encompass the geometrical complexity in the developed fractures, but rather focused on analyzing different combinations of unequal half-lengths to examine possible interference. Another approach of utilizing numerical simulation of shale gas wells was by Shen et al. (2016), where they constructed a numerical shale gas reservoir model to examine gas and water flow dynamics and study the effect of several

reservoir properties and production parameters on the long-term production. Although their model covers most of the shale gas transport phenomena, complexity in hydraulic fracture geometries was not incorporated since their model assumed orthogonal fractures.

Despite the tremendous effort accomplished by the aforementioned studies to model and analyze shale gas reservoirs, to the best of my knowledge, few of these models considered complex hydraulic fracture geometries. In general, little research has been conducted to model the two-phase flow behavior of shale gas wells while assuming complex hydraulic fracture geometries as well as examining the interplay between these induced fractures and existing natural fractures.

The main instigator of fracture complexity is the interaction between induced fractures and existing fractures during the hydraulic fracturing job (Wu and Olson, 2015). Therefore, due to the prevalence of existing natural fractures in the majority of unconventional plays and based on several experimental studies, complex (non-orthogonal) fracture network is much more common than initially predicted (Olson, 1995; Wang et al., 2013; Dahi Taleghani and Olson, 2014). As a result, numerous researchers developed analytical, semianalytical, and numerical models in an effort to examine well performance with complex fracture geometry. First effort was through the development of the dual continuum (dual porosity and dual permeability) numerical model (Warren and Root, 1963; Blaskovich et al., 1983; Saidi, 1983; Hill and Thomas, 1985; Dean and Lo, 1988). However, a major caveat in the dual continuum model is its inability to explicitly model complex fracture networks. Discrete fracture modeling (DFM) is another effort to capture complex fracture geometries by relying on unstructured gridding (Noorishad and Mehran, 1982; Hoteit and Firoozabadi, 2006; Hui and Mallison, 2009). However, adding to its complicated gridding, DFM requires significantly high and expensive computational demand. Henceforth, an efficient

approach to model complex fracture geometry in unconventional reservoirs, and especially in shale gas reservoirs, is still lacking.

In this study, an embedded discrete fracture model (EDFM) is introduced, which was originally proposed by Li and Lee (2008). EDFM is an efficient approach which combines the accuracy of the DFM approach and the computational manageability of the dual-continuum modeling approach (Xu, 2015). Moinfar et al. (2014) further extended the development of the EDFM to incorporate inclined fractures for 3D compositional modeling. Cavalcante Filho et al. (2015) also worked in developing a preprocessing code for the EDFM. Simply, the EDFM tool can be used to explicitly and efficiently handle complex fracture geometries by modifying the input file of the simulator in a nonintrusive manner (Xu, 2015). Several studies were conducted showcasing the accuracy, applicability and capability of the EDFM approach for different research objectives (Shakiba, 2014; Panfili and Cominelli, 2014; Jiang et al., 2014; Shakiba and Sepehrnoori, 2015). Due to the successful application of the EDFM approach during the last few years, it has become a promising approach in the DFM's arena.

In this study, a 3D shale gas reservoir model was built using a commercial simulator. In addition, the EDFM tool was utilized to construct different cases of a multi-fractured shale gas horizontal well with varying degrees of hydraulic fracture complexity. In all cases, for the purpose of accurately comparing their results, both the total fracture length and the total amount of water injected to create the simulated reservoir volume (SRV) were kept constant. The objective is to examine the effect of these fracture complexities on the two-phase flow of a shale gas well. In addition, 1-set and 2-set natural fractures, interchangeably, was included into the model to test their influence on the well performance. Finally, variable fracture conductivities and initial water saturation values were tested to further assess their effect on the two-phase flow behavior of the

shale gas well. The purpose of this study is not to repeat any of the enormous effort presented in the aforementioned papers, but rather to highlight the importance of incorporating complex fracture geometries into modeling shale gas reservoirs. Specifically, this study aims to provide insight toward understanding the extent to which this fracture complexity can affect the two-phase flow performance of shale gas wells.

Chapter 3: Methodology

3.1. Embedded Discrete Fracture Model (EDFM) Description

The Embedded Discrete Fracture Model (EDFM) is an efficient tool to simulate complex fracture geometries conjointly while using a reservoir simulator. By discretizing fractures into small segments, the EDFM approach creates an additional cell in the computational domain every time a fracture segment penetrates a matrix cell in the physical domain. Subsequently, once these additional cells, which represent fracture segments, are incorporated, non-neighboring connections (NNCs) are established. These NNCs account for the flow communication between a matrix cell and a fracture segment penetrating it, between fracture segments in a single fracture, and between intersecting fracture segments. Each NNC pair (between two cells) has its own transmissibility factor (T_{NNC}), which is calculated by the EDFM preprocessor as follows:

$$T_{NNC} = \frac{k_{NNC} A_{NNC}}{d_{NNC}} \tag{1}$$

where k_{NNC}, A_{NNC}, and d_{NNC} represent permeability, contact area, and distance associated with this connection, respectively.

For NNC between a matrix cell and a fracture cell, k_{NNC} is the matrix permeability in the direction perpendicular to the plane of the fracture segment, A_{NNC} is the area of the fracture segment penetrating the matrix block, and d_{NNC} is the average normal distance from matrix block to the plane of the fracture segment. On the other hand, for NNC between fracture segments, k_{NNC} is the average fracture permeability, A_{NNC} is the common area between fracture segments, and d_{NNC} is the distance between centroids of the fracture segments. Further detailed formulation and explanation of the transmissibility factor calculation for the different NNCs can be found in Xu (2015).

Using the calculated NNC transmissibility factors (T_{NNC}), the volume flow rate of phase l between each two cells in an NNC pair is calculated as follows:

$$q = \lambda_l T_{NNC} \Delta P \tag{2}$$

where λ_l is the relative mobility of phase l and ΔP is the potential difference between the two cells.

Finally, the intersections between the wellbore and fracture segments are modeled by assigning an effective well index (WI_f) for each fracture segment intersecting the wellbore trajectory, as follows:

$$WI_f = \frac{2\pi k_f w_f}{ln(r_e/r_w)} \tag{3}$$

$$r_e = 0.14\sqrt{L^2 + W^2} \tag{4}$$

where k_f is the fracture permeability, w_f is the fracture aperture, L is the length of the fracture segment, and W is the height of the fracture segment.

Modeling complex fracture geometries has proven to be manageable with the use of the EDFM approach. By discretizing fractures into interconnected small fracture segments and adding them to the computational domain, the EDFM is able to combine traits from both dual-continuum models and discrete fracture models. Hence, the EDFM approach is capable of avoiding the high computational demand of unstructured gridding while keeping the unique functionality of the simulator in use (Xu, 2015).

This study applies the EDFM approach to a commercial simulator (CMG-GEM, 2014) to simulate complex fracture geometries in a shale gas reservoir. The following subsection will highlight the reservoir parameters used in building the synthetic reservoir simulation model. The subsection afterward will verify the EDFM approach by comparing it to the local grid refinement (LGR) approach for a simple planar base case.

3.2. RESERVOIR SIMULATION MODEL DESCRIPTION

In this simulation study, a field-scale shale gas reservoir model was built using a numerical reservoir simulator (CMG-GEM, 2014). The reservoir model was constructed based on a 3D Cartesian grid system, consisting of 170 grids in the x direction, 101 grids in the y direction, and 1 grid in the z direction. In total, the model has 17,170 grids. The reservoir is 3,400 ft in length × 2,020 ft in width × 100 ft in thickness. A horizontal well with a lateral length of 2,420 ft was considered. It was completed with 25 hydraulic fractures along the horizontal wellbore with 100-ft spacing between each two fractures and a fracture conductivity of 100 mD·ft. The base case assumed a simple fracture geometry where hydraulic fractures are orthogonal/planar. Nevertheless, the hydraulic fractures in the other cases were constructed with a varying degree of fracture complexity using the EDFM approach. The reservoir is assumed to have a matrix porosity of 6%, a matrix permeability of 0.0001 mD, and a matrix initial water saturation of 20%. In addition, to account for the complex shale gas transport mechanisms, both gas desorption and gas slippage were considered in this model. In regards to gas desorption, both the Langmuir model and the BET (Brunauer, Emmett and Teller) model were considered and tested. In regards to gas slippage, the Klinkenberg effect was considered with a reference pressure of 500 psi. Moreover, as showcased in **Figure 3.1**, fluid flow in shale matrix and fractures was described with two sets of relative permeability curves. Finally, **Table 3.1** presents a summary of the basic reservoir and fracture parameters considered in this reservoir model.

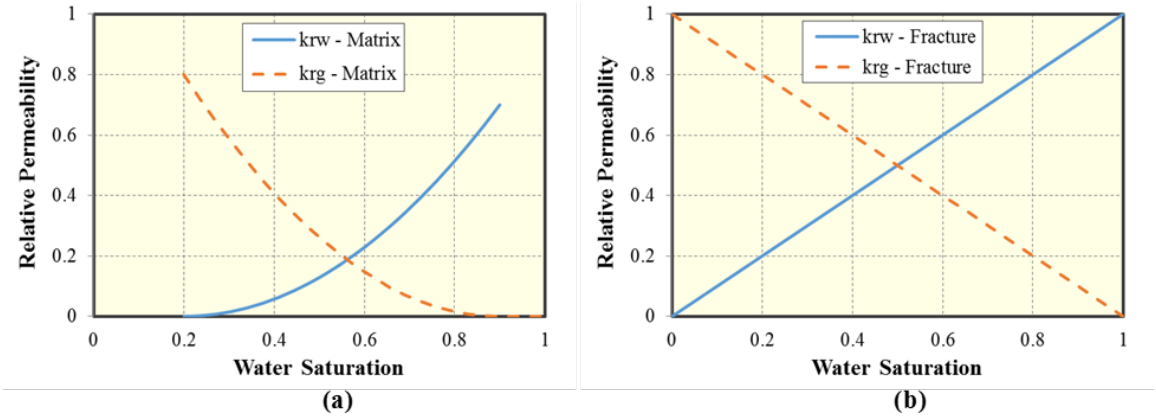

Figure 3.1: Relative permeability curves for **(a)** matrix system and **(b)** fracture system.

Parameter	**Value**	**Unit**
Model dimensions [L × W × H]	3,400 × 2,020 × 100	*ft*
Initial reservoir pressure	4,000	*psi*
Reservoir temperature	130	*°F*
Matrix porosity	6	*%*
Matrix permeability	0.0001	*mD*
Initial water saturation	0.2	*fraction*
Rock density	2.5	g/cm^3
Rock compressibility	3×10^{-6}	*1/psi*
Langmuir pressure	1,300	*psi*
Langmuir volume	140	*scf/ton*
BET V_m	124.53	*Scf/ton*
BET C	36.63	-
BET n	4.03	-
Klinkenberg reference pressure	500	*psi*
Fracture conductivity	100	*mD·ft*
Fracture spacing	100	*ft*
Fracture height	100	*ft*
Fracture aperture/width	0.01	*ft*
Base (planar) case fracture half-length	510	*ft*
Initial S_w in fractures	1	*fraction*
Minimum bottom-hole pressure	500	*psi*

Table 3.1: Basic reservoir model parameters.

3.3. VERIFICATION OF THE EMBEDDED DISCRETE FRACTURE MODEL (EDFM)

Although the EDFM approach has been implemented and verified in several reservoir simulators proving its applicability and accuracy (Panfili, 2014; Shakiba, 2014), this study presents an alternative verification specific to the proposed shale gas reservoir model. By applying the EDFM to a commercial simulator (CMG-GEM, 2014), a comparison of the two-phase flow results of the base (Planar) case was conducted between the EDFM approach and the built-in LGR approach. The verification simulation runs first considered the Langmuir model to account for gas desorption. Next, the BET model was considered. In addition, these verification runs were tested for gas slippage. Cumulative gas production and cumulative water production plots for a 30-year production cycle were used to highlight the match between LGR and EDFM for the base case (Planar case).

Using the Langmuir model to account for gas desorption, **Figure 3.2** highlights the match between the LGR and the EDFM while neglecting the gas slippage effect, whereas **Figure 3.3** highlights the match while including the gas slippage effect.

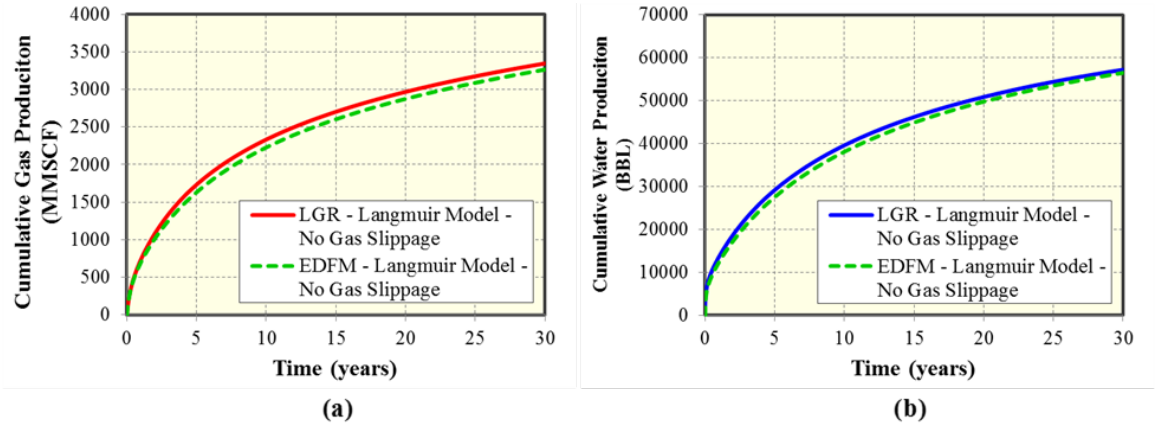

Figure 3.2: **(a)** Cumulative gas production and **(b)** Cumulative water production for LGR and EDFM using Langmuir model while neglecting gas slippage effect.

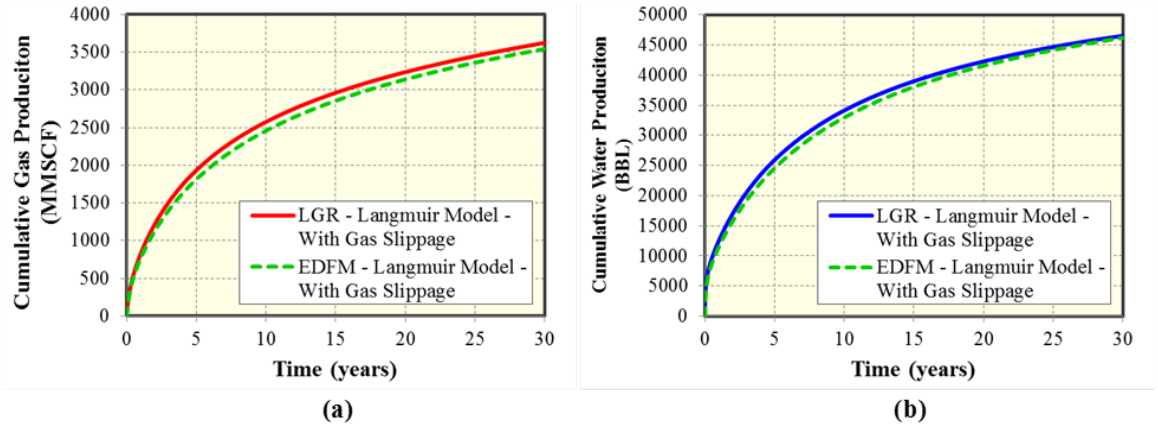

Figure 3.3: **(a)** Cumulative gas production and **(b)** Cumulative water production for LGR and EDFM using Langmuir model while including gas slippage effect.

Similarly, using the BET model to account for gas desorption, **Figure 3.4** highlights the match between the LGR and the EDFM while neglecting the gas slippage effect, whereas **Figure 3.5** highlights the match while including the gas slippage effect.

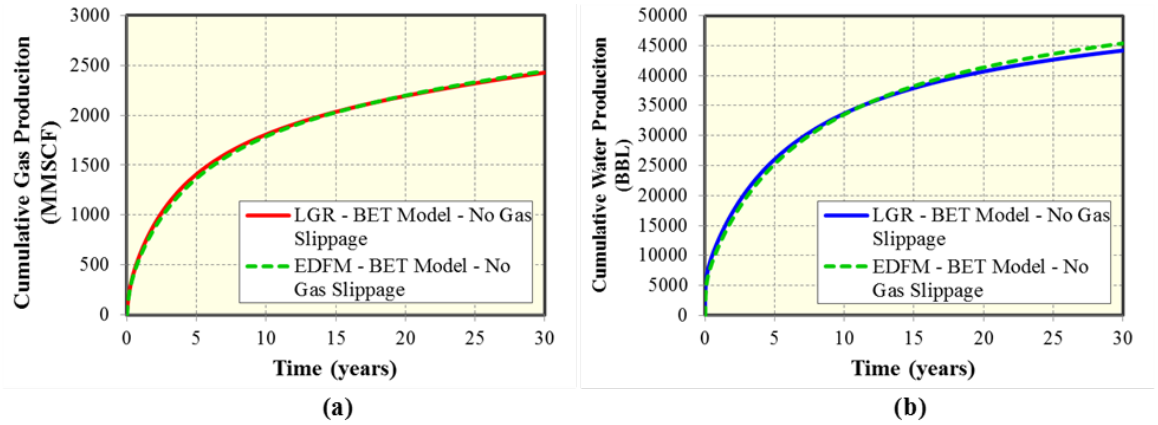

Figure 3.4: **(a)** Cumulative gas production and **(b)** Cumulative water production for LGR and EDFM using BET model while neglecting gas slippage effect.

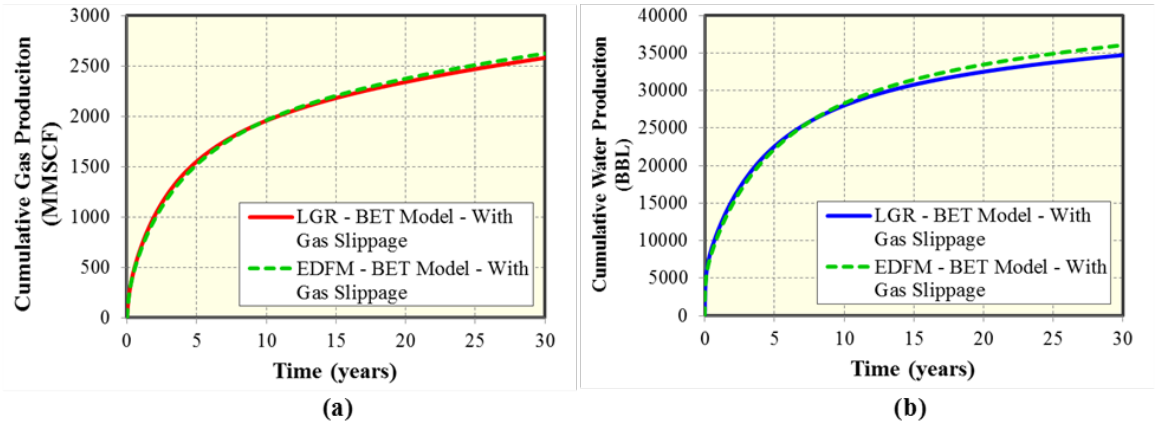

Figure 3.5: **(a)** Cumulative gas production and **(b)** Cumulative water production for LGR and EDFM using BET model while including gas slippage effect.

In all verification runs, a good agreement was obtained between the two approaches. Therefore, it's now easier to proceed with confidence and apply the EDFM approach in the subject shale gas reservoir model to simulate cases with complex fracture geometries.

In the next chapter, the BET model will be considered rather than Langmuir model to account for gas desorption. The reason for this choice is the better match achieved by the BET model with some laboratory measured data, as reported by Yu et al. (2016). In addition, the gas slippage effect will be included in modeling the different cases in the coming sections.

Chapter 4: Results and Analysis

4.1. Complex Hydraulic Fracture Geometries Case Studies

In this subsection, a field-scale synthetic representation of a shale gas horizontal well with 25 hydraulically-induced fractures is presented. The geometry of the hydraulic fractures was varied from simple to complex in order to study the effect of fracture geometries on the two-phase well performance of shale gas wells. **Figure 4.1** and **Figure 4.2** showcase the fracture geometries considered in this study, which are as follows:

- Planar Case (Base/Reference Case)
- Diagonal Case
- Reoriented Case
- Irregular Case
- Fracture Network Case
- Random Case

These cases consider varying degrees of fracture complexities, such as the striking angle between the horizontal wellbore and the created fracture, the irregular length of individual segments within a fracture, the creation of a fracture network, and the non-uniformity between the created fractures with respect to how far a fracture extends away from the horizontal wellbore. However, for these different cases to be comparable with each other, the following parameters were kept constant:

- Constant total fracture length of 25,500 ft.
- Constant total amount of water injected to create the simulated reservoir volume (SRV).

Planar Case: This case presents 25 simple planar fractures which are at 90-degree angle with respect to the horizontal wellbore. All the fractures have the same fracture half-length of 510 ft.

Diagonal Case: This case represents the first degree of complexity considered in this study and it pertains to the orientation of the created fractures with respect to the horizontal wellbore. All the 25 fractures were angled at 70° from the wellbore. In addition, they have the same half-length of 510 ft.

Reoriented Case: This case represents the second degree of complexity. It presents 25 fractures with outer fractures longer than inner ones. Each fracture is composed of two segments with different orientations (80° for the upper segment and 100° for the lower one). The fracture's segment length varies from 518 ft at for outer fractures, 512 ft for inner fractures, to 394 ft for the middle fracture.

Irregular Case: This case represents the third degree of complexity. It presents 25 fractures with multiple segments and multiple changes in orientation following a zigzag pattern. The number of segments in each fracture and the length of each segment is irregular. Nonetheless, all fractures extend away from the wellbore uniformly.

Fracture Network Case: This case represents the fourth degree of complexity. It presents 25 fractures that are composed of segments that intersect each other and intersect segments of adjacent fracture; thus, creating a fracture network.

Random Case: This case represents the fifth and last degree of complexity considered in this study. It is similar to the irregular case in which the 25 fractures are composed of multiple segments with different orientations and lengths. However, it differs from the irregular case in the non-uniformity of how far each fracture extends away from the wellbore.

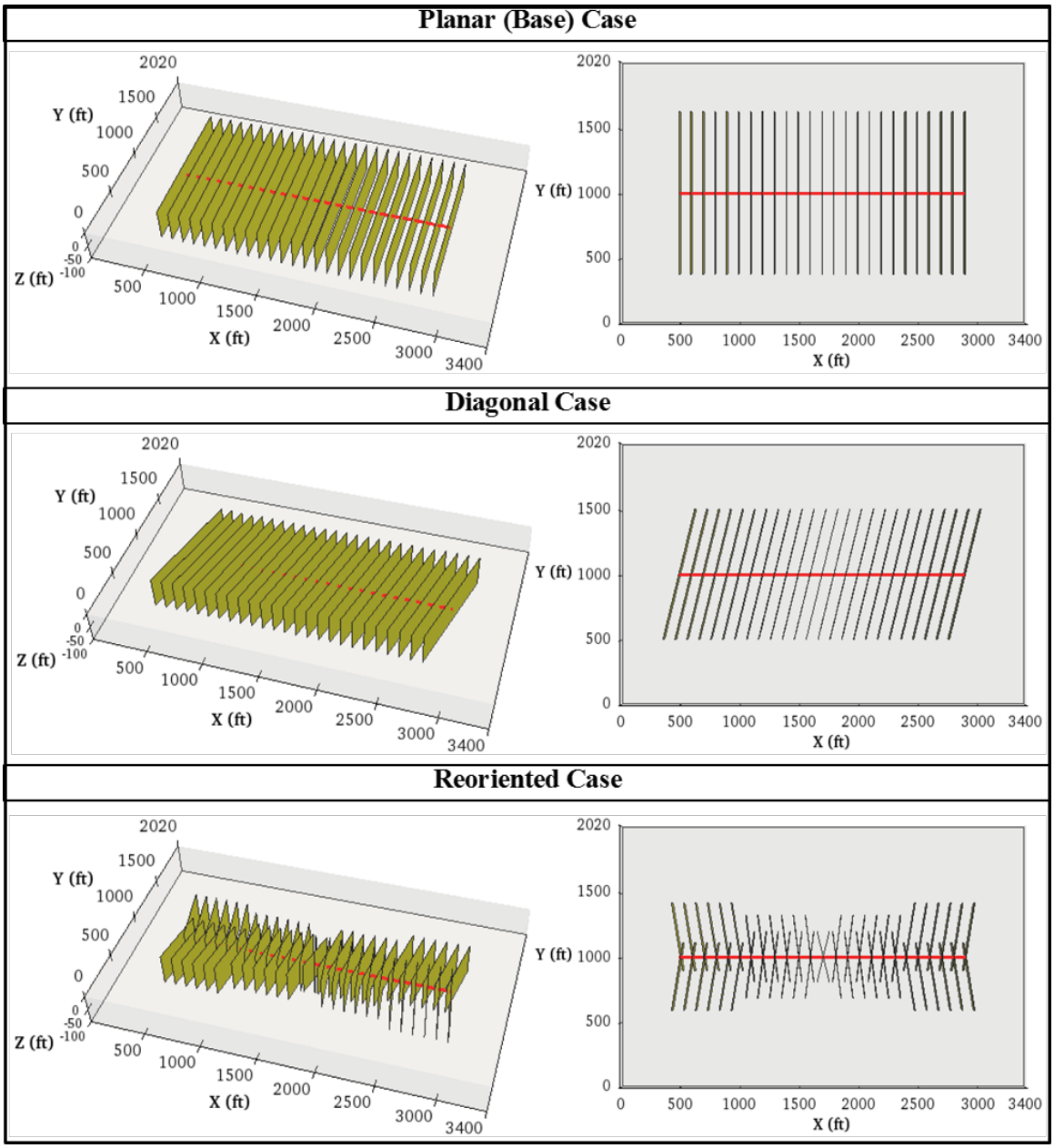

Figure 4.1: Illustrations of fracture geometries evaluated for the two-phase flow recovery of a shale gas well (*Part 1/2*).

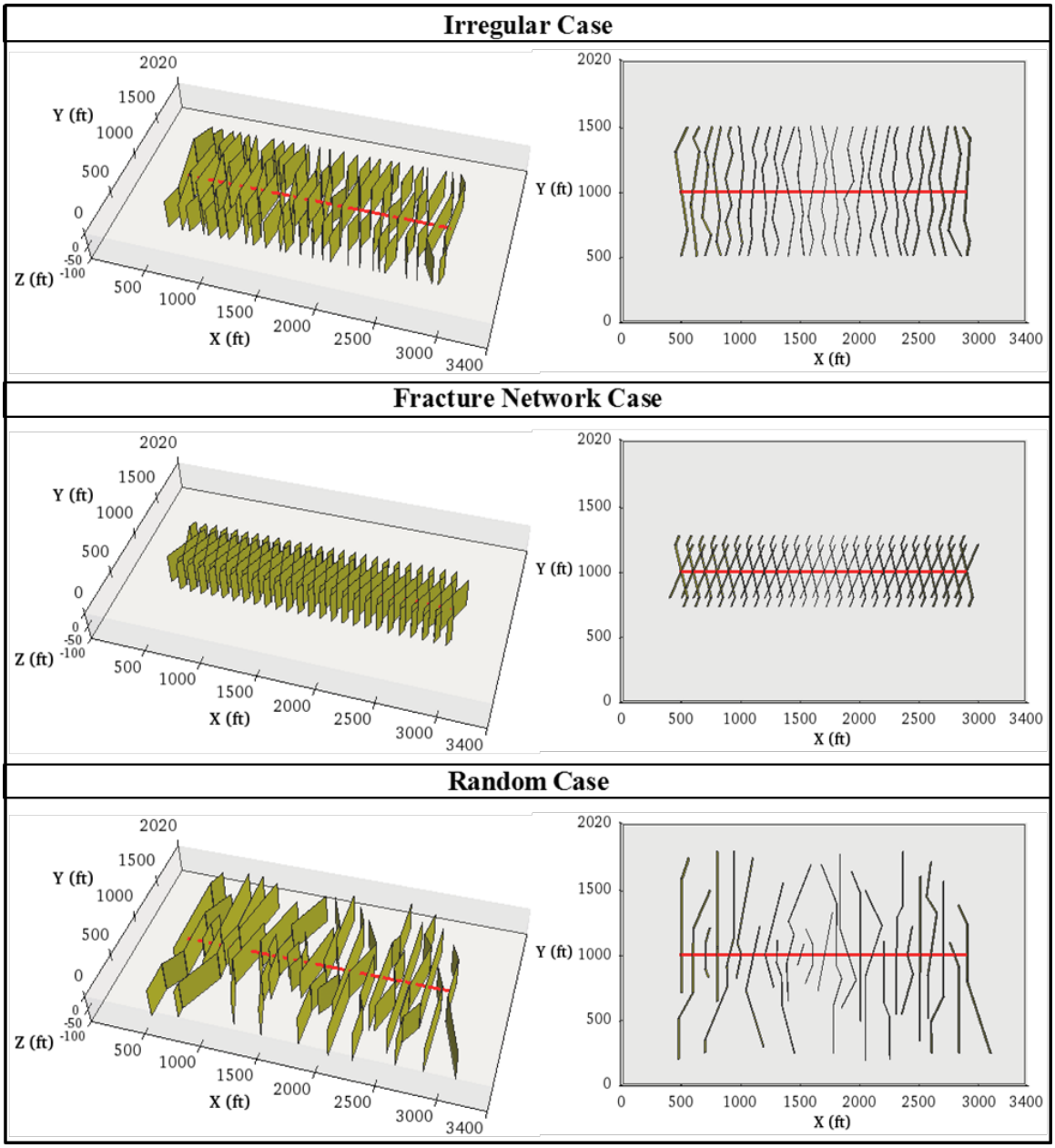

Figure 4.2: Illustrations of fracture geometries evaluated for the two-phase flow recovery of a shale gas well (*Part 2/2*).

These aforementioned cases were used to quantify the effect of increasing hydraulic fracture geometrical complexity on shale gas well performance. **Figure 4.3** and

Figure 4.4 present a comparison of cumulative gas and water productions between the five complex cases with respect to the Planar (Base) case.

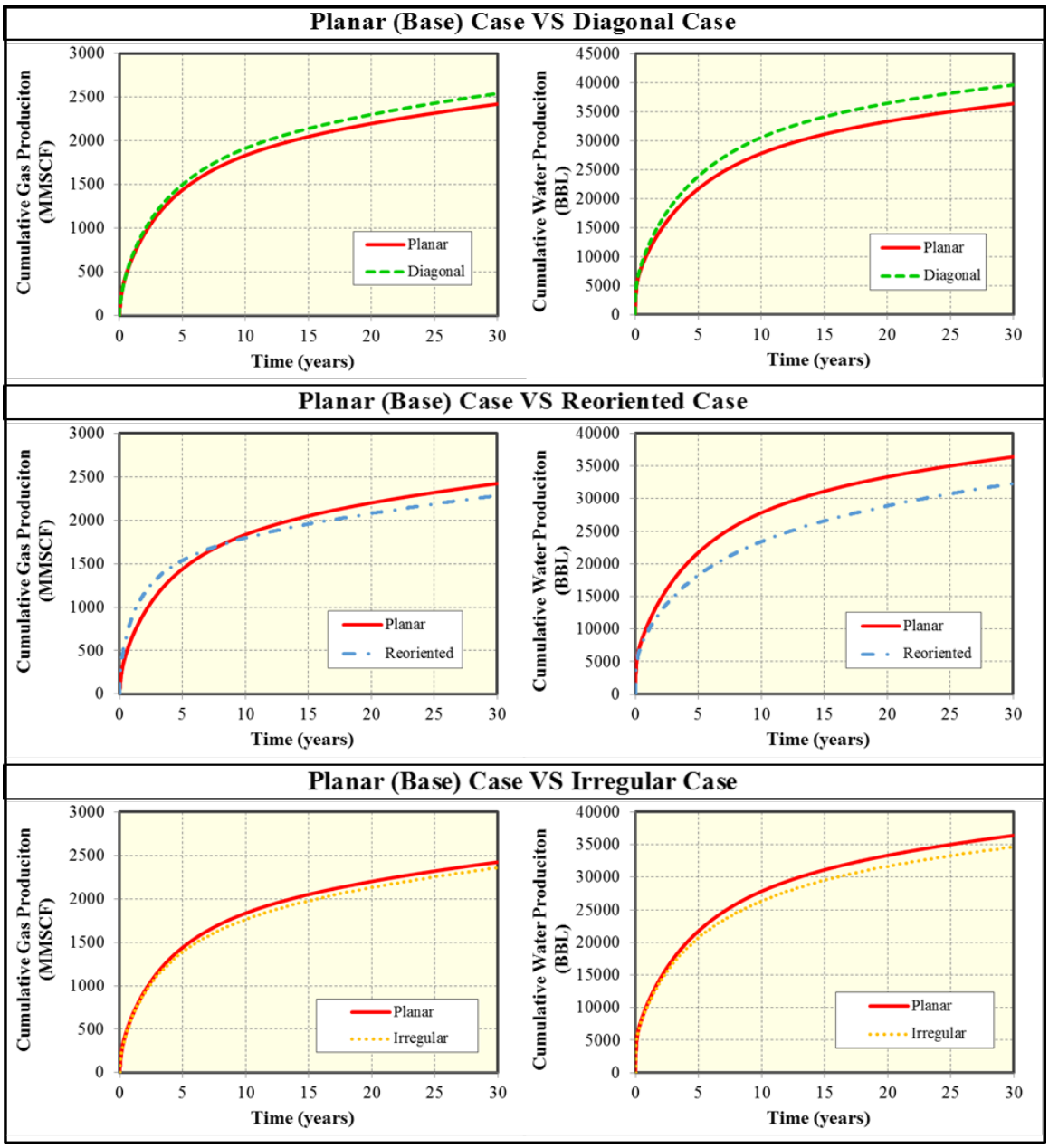

Figure 4.3: Comparison of cumulative gas production (*Left Column*) and cumulative water production (*Right Column*) between the different hydraulic fracture geometry cases with respect to the Planar (Base) case (*Part 1/2*).

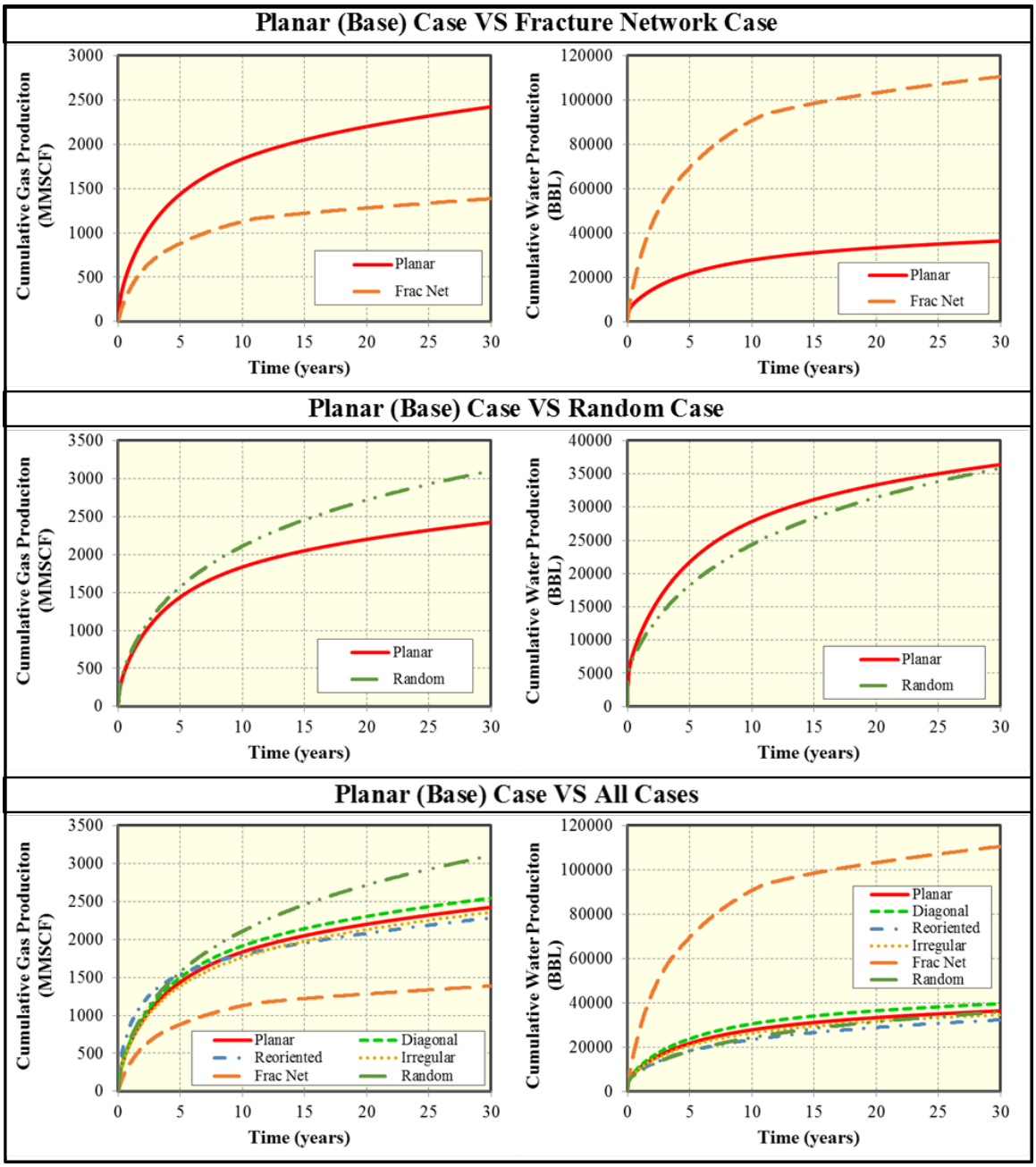

Figure 4.4: Comparison of cumulative gas production (*Left Column*) and cumulative water production (*Right Column*) between the different hydraulic fracture geometry cases with respect to the Planar (Base) case (*Part 2/2*).

As can be seen on **Figure 4.3,** the first three complex cases (Diagonal, Reoriented, and Irregular) resulted in a somewhat similar gas production throughout the 30-year production period. In fact, only 5%, -6%, and 3% changes from the Planar (Base) Case in terms of cumulative gas production at the end of 30 years, were estimated for the Diagonal, Reoriented, and Irregular cases, respectively (**Table 4.1**). Similarly, the cumulative water production plots of the three cases, on **Figure 4.3**, are insignificantly different. This indifference in productivity performance between the three case (Diagonal, Reoriented, and Irregular) and the Planar (Base) case can be attributed to the fact that these four cases create fairly the same uniform simulated reservoir volume (SRV). This means that although the first three complex cases and the Planar case have different fracture geometries, the rock volume simulated by their fractures is somewhat similar. Hence, these cases are exposed to the same drainage area and hence produce fairly the same results.

To the contrary, as can be seen on **Figure 4.4**, both the Fracture Network case and the Random case tell a different story. The Fracture Network case resulted in a significantly lower gas productivity throughout the 30-year production period. In fact, 43% decrease in gas productivity was estimated at the end of 30 years in comparison with the Planar (Base) case. In contrast, the Fracture Network case resulted in an extremely higher water flowback. As a matter of fact, the Fracture Network case has, of all cases, the lowest gas productivity and the highest water flowback. On the other hand, the Random case resulted in the highest cumulative gas production at 30 years with 28% increase from the Planar (Base) case. However, its cumulative water production throughout 30 years was negligibly different from the Planar (Base) case. These vast differences in productivity performance between these two cases (Fracture Network and Random) and the Planar (Base) case can be attributed to the different simulated reservoir

volume (SRV). The Fracture Network case has the smallest SRV resulting in the lowest gas production whereas the Random case has the largest SRV and hence the largest gas production. In particular, the Random case is the only case that has a drainage area, and thus an SRV, that is distributed non-uniformly (randomly).

Table 4.1 lists the cumulative gas productions in MMSCF at 30 years for all the six cases. In addition, it lists the percentage change in gas productivity at the 30-year mark from the Planar (Base) case for all the other five cases.

Table 4.2 lists the cumulative water productions in BBL at 30 years for all the six cases. Moreover, it summarizes the percentage change in cumulative water flowback at the end of 30 years from the Planar (Base) case for all the other five cases. Additionally, assuming that only the injected water flows back to surface during the production cycle and given that all the cases had the same amount of water injected, **Table 4.2** compares the percentage recovery of the injected water in all the six cases. All the cases recovered almost the same percentage of injected water (3 to 4%) at the end of 30 years, except the Fracture Network case which recovered more than triple what the Base case has recovered (10%). This can be attributed to the size of the simulated reservoir volume (SRV). The Fracture Network case has the smallest SRV size, which means that the injected water had to simulate and imbibe into a smaller volume of rock compared to other cases. This might have led to water fighting for a smaller volume of rock. Hence, when the well is put on production, it is plausible that a good amount of the injected water is still within close proximity to the fracture openings and hence available for flowback. Furthermore, the low gas productivity and high water flowback in the Fracture Network case can also be ascribed to fracture interference due to the fractures' closer proximity of each other or even more to when fractures intersect each other. The creation of fracture network results in a stronger and more pronounced interference between the

fractures, compared to other cases where fractures seldom intersect and are spaced uniformly. The fracture interference effect contributes to lowering the gas flow velocity into the fractures (Yu et al., 2014). This allows for more water to flow back to surface. Hence, more water and consequently less gas are cumulatively produced. In contrast, the fracture interference factor is curtailed in the Random case due to the creation of a larger SRV size which diminishes any possible fracture interference. This explains the superior gas recovery encountered in the Random case.

	Planar	**Diagonal**	**Reoriented**	**Irregular**	**Fracture Network**	**Random**
Cumulative Gas Production @ 30 Years (MMSCF)	2,421	2,544	2,282	2,356	1,386	3,097
% Change in Cumulative Gas Production @ 30 Years from the Planar (Base) Case		5%	-6%	-3%	-43%	28%

Table 4.1: Summary of cumulative gas production (MMSCF) and the percentage change from the Planar (Base) case at the end of 30 years for the different hydraulic fracture geometry cases.

	Planar	Diagonal	Reoriented	Irregular	Fracture Network	Random
Cumulative Water Production @ 30 Years (BBL)	36,397	39,578	32,322	34,638	110,561	35,838
% Change in Cumulative Water Production @ 30 Years from the Planar (Base) Case		9%	-11%	-5%	204%	-2%
% Recovery of Injected Water	3%	4%	3%	3%	10%	3%

Table 4.2: Summary of cumulative water production (BBL), the percentage change from the Planar (Base) case at the end of 30 years, and the percentage recovery of injected water for the different hydraulic fracture geometry cases.

Figure 4.5 through **Figure 4.10** highlight the pressure distribution of the 100-day, 10-year, and 30-year marks for the Planar, Diagonal, Reoriented, Irregular, Fracture Network, and Random cases, respectively. Clearly, the Fracture Network case (**Figure 4.9**) has the smallest disturbed volume while the Random case (**Figure 4.10**) has the largest and most distributed volume, of all the cases.

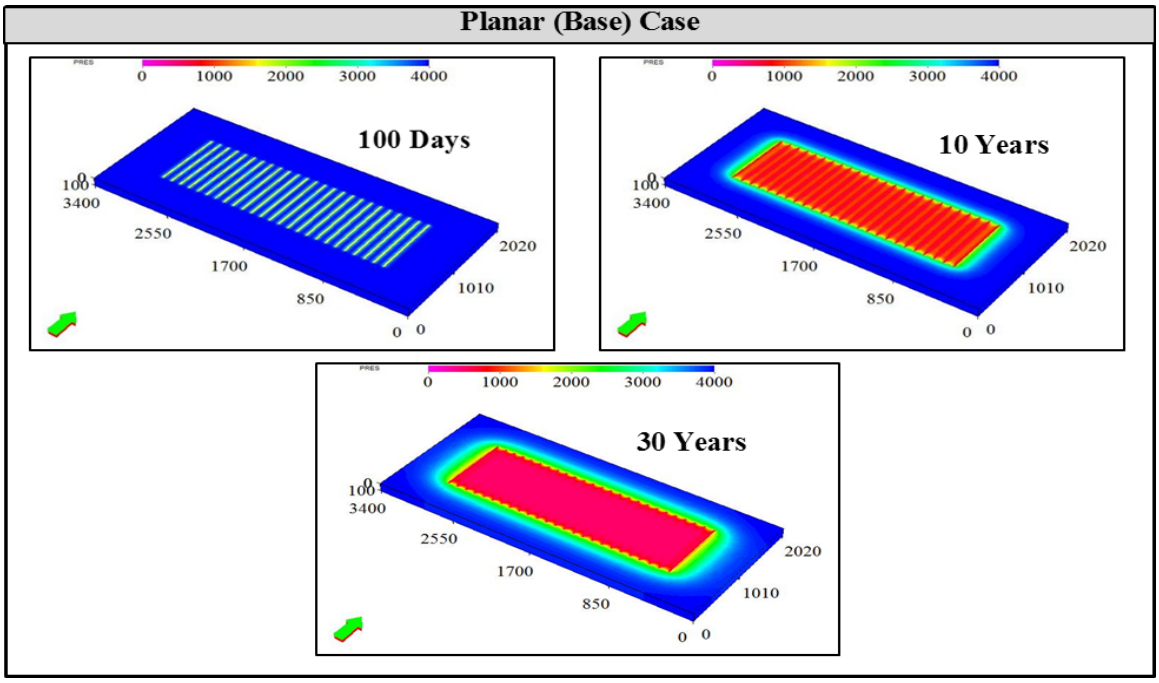

Figure 4.5: Pressure distribution maps of the Planar (Base) case simulation results for the 100-day, 10-year, and 30-year marks.

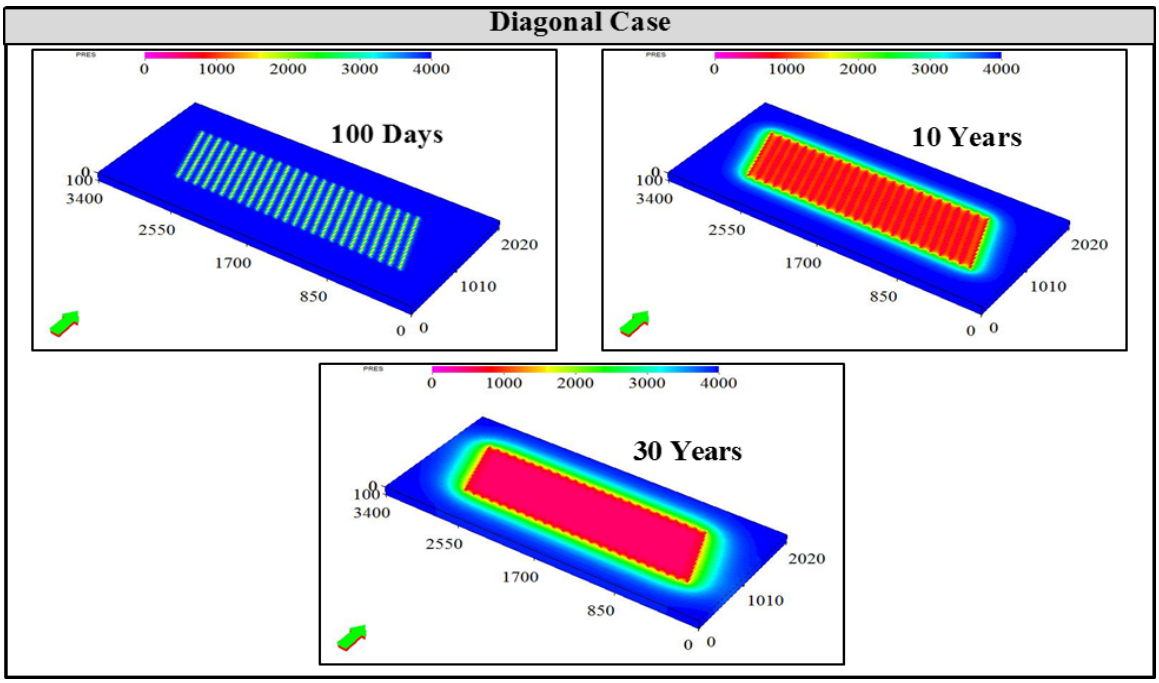

Figure 4.6: Pressure distribution maps of the Diagonal case simulation results for the 100-day, 10-year, and 30-year marks.

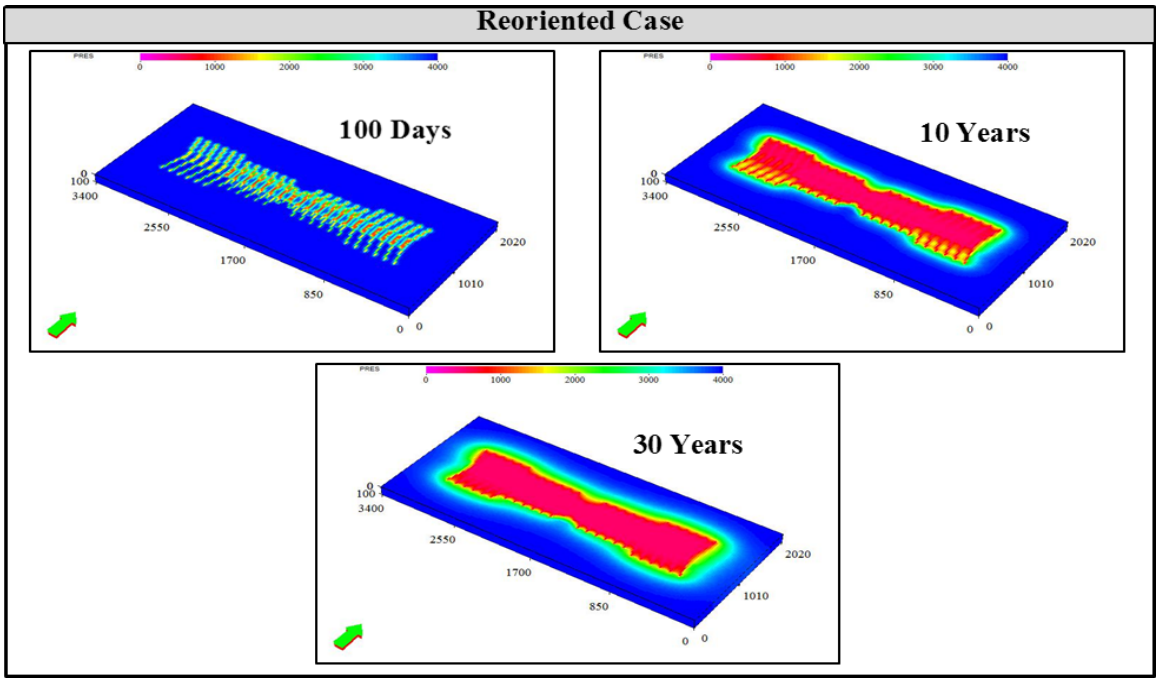

Figure 4.7: Pressure distribution maps of the Reoriented case simulation results for the 100-day, 10-year, and 30-year marks.

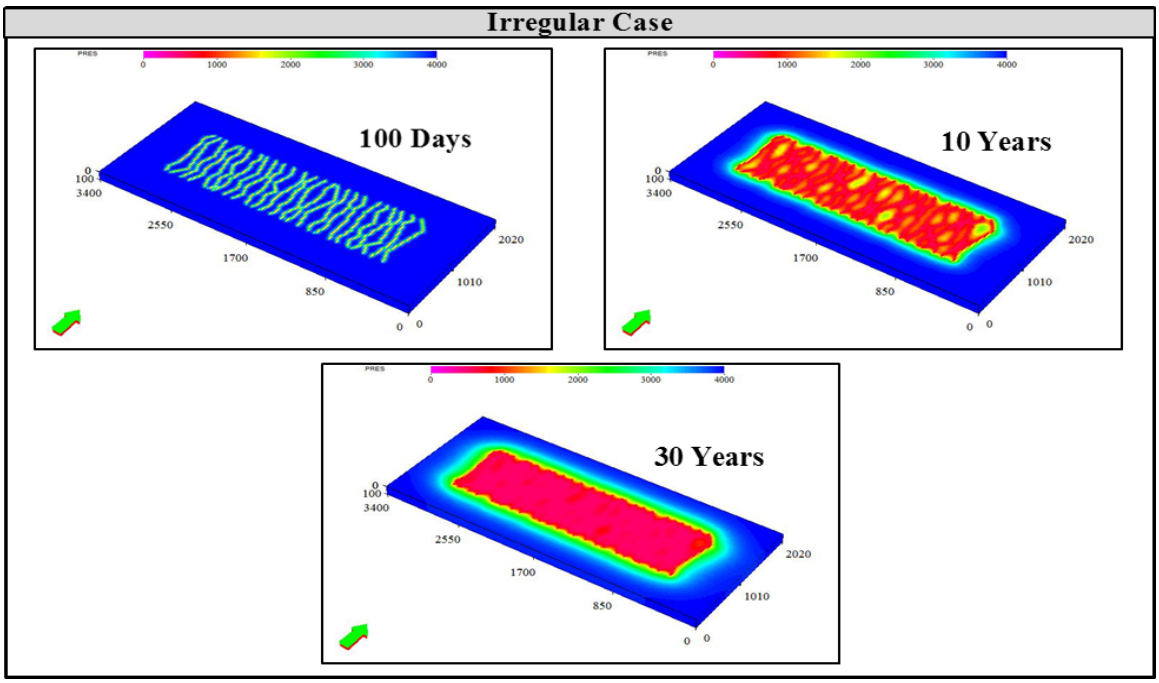

Figure 4.8: Pressure distribution maps of the Irregular case simulation results for the 100-day, 10-year, and 30-year marks.

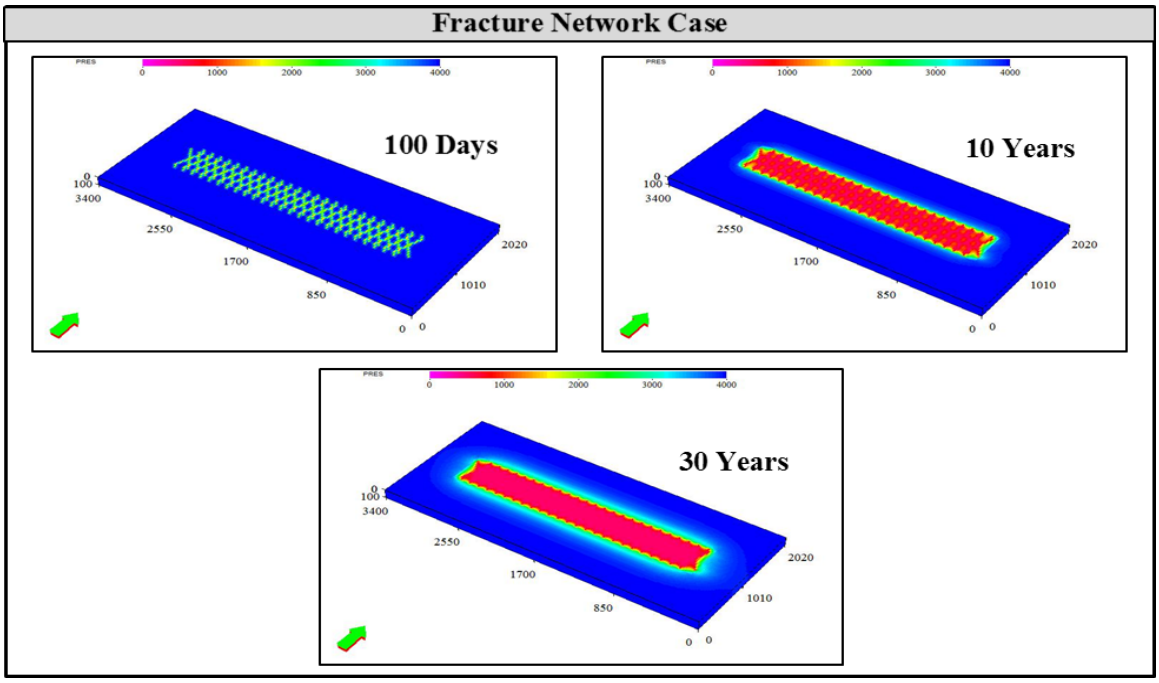

Figure 4.9: Pressure distribution maps of the Fracture Network case simulation results for the 100-day, 10-year, and 30-year marks.

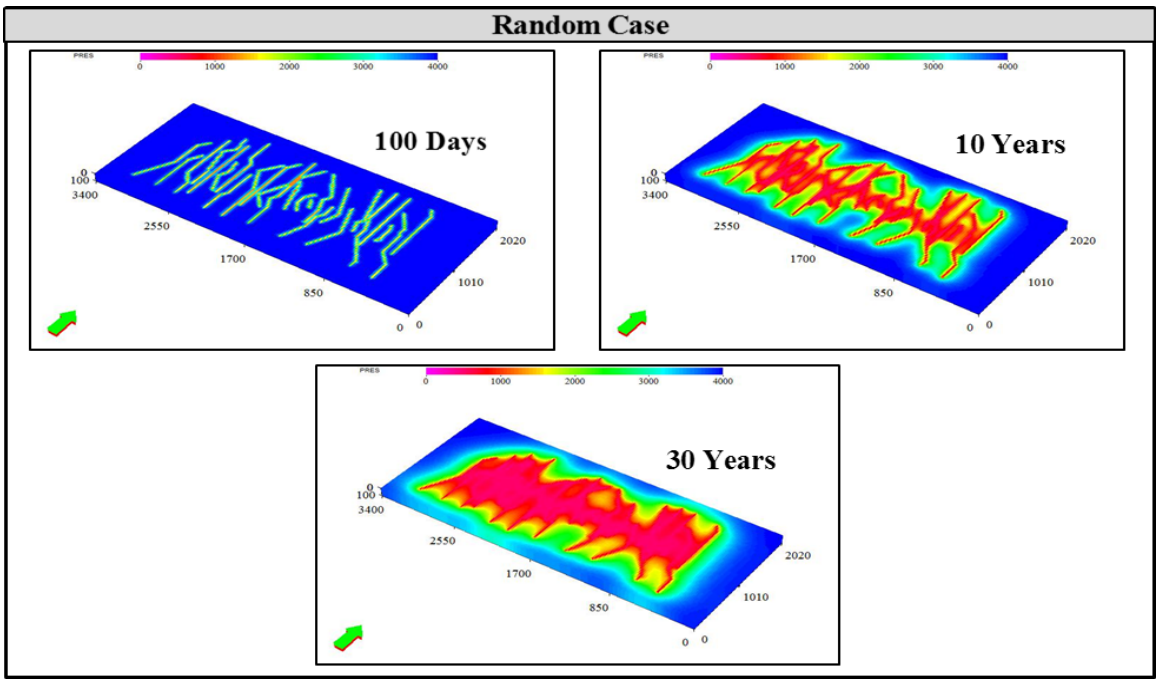

Figure 4.10: Pressure distribution maps of the Random case simulation results for the 100-day, 10-year, and 30-year marks.

4.2. EFFECT OF THE PRESENCE OF NATURAL FRACTURES

In this section, another level of complexity pertaining to the presence of natural fractures within the 3D reservoir model is evaluated. The ubiquity and orientation of natural fractures within the subject shale gas reservoir are examined. Cases with 100 and 1,000 natural fractures are constructed for the different hydraulic fracture geometries. In these cases, the orientation of the natural fractures is alternated between a 1-set orientation and a perpendicular 2-set orientation. **Table 4.3** summarizes the properties of these 1-set and 2-set natural fractures.

Parameter	Value	Unit
Natural fracture height	100	*ft*
Natural fracture length range	100-300	*ft*
Natural fracture aperture/width	0.001	*ft*
Natural fracture conductivity	0.1	*mD·ft*
Natural fracture dip angle	90	*Degrees*
1-Set natural fracture orientation range	5-10	*Degrees*
2-Set natural fracture orientation ranges	5-10 & 90-100	*Degrees*

Table 4.3: Properties of natural fractures.

Figures 4.11 through **4.16** illustrate the different scenarios of natural fractures considered for the Planar, Diagonal, Reoriented, Irregular, Fracture Network, and Random cases, respectively. Each scenario represents a unique case. These cases are used to quantify the effect of increasing the prevalence of natural fractures and their orientation on the two-phase flow performance of shale gas wells.

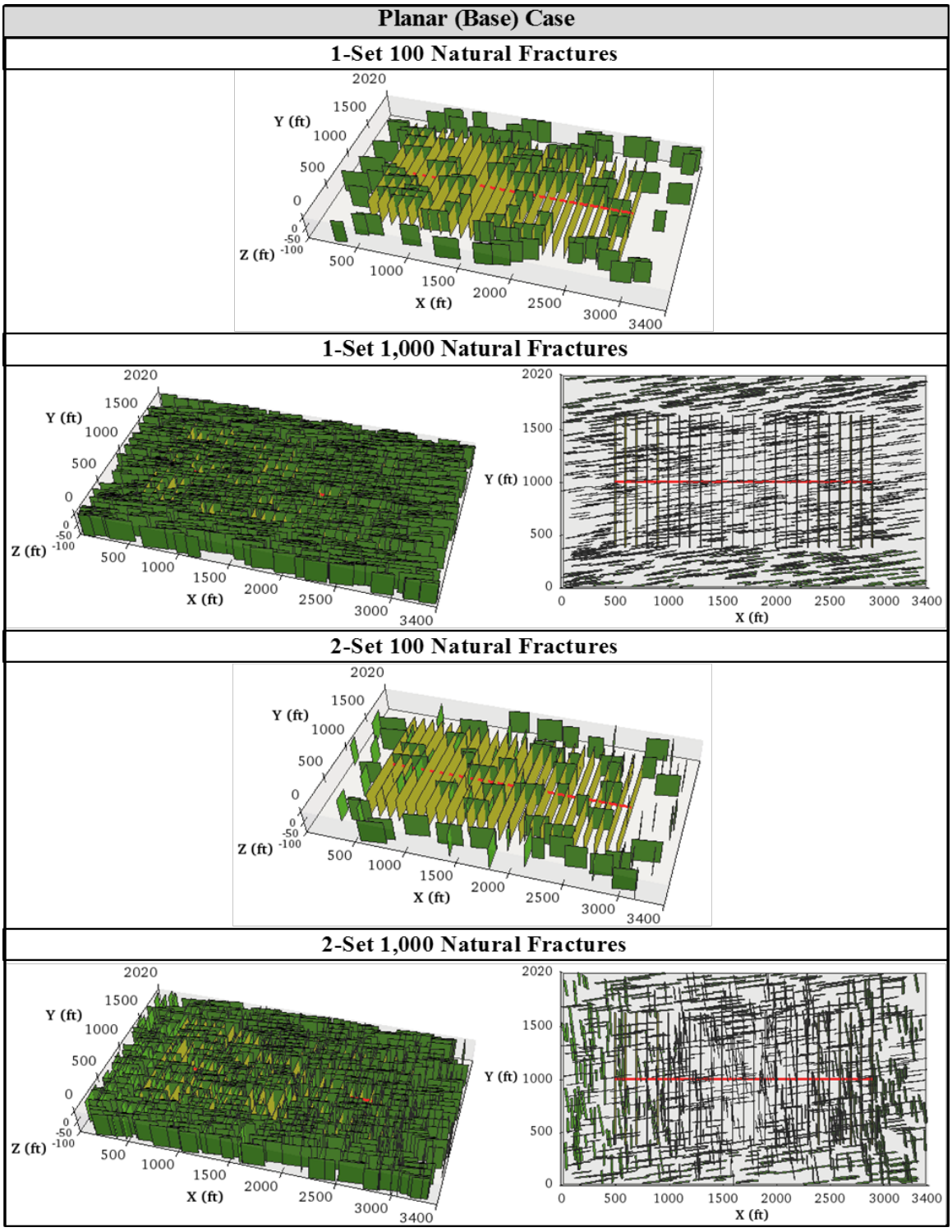

Figure 4.11: Illustrations of 1-set and 2-set natural fractures evaluated for the Planar case.

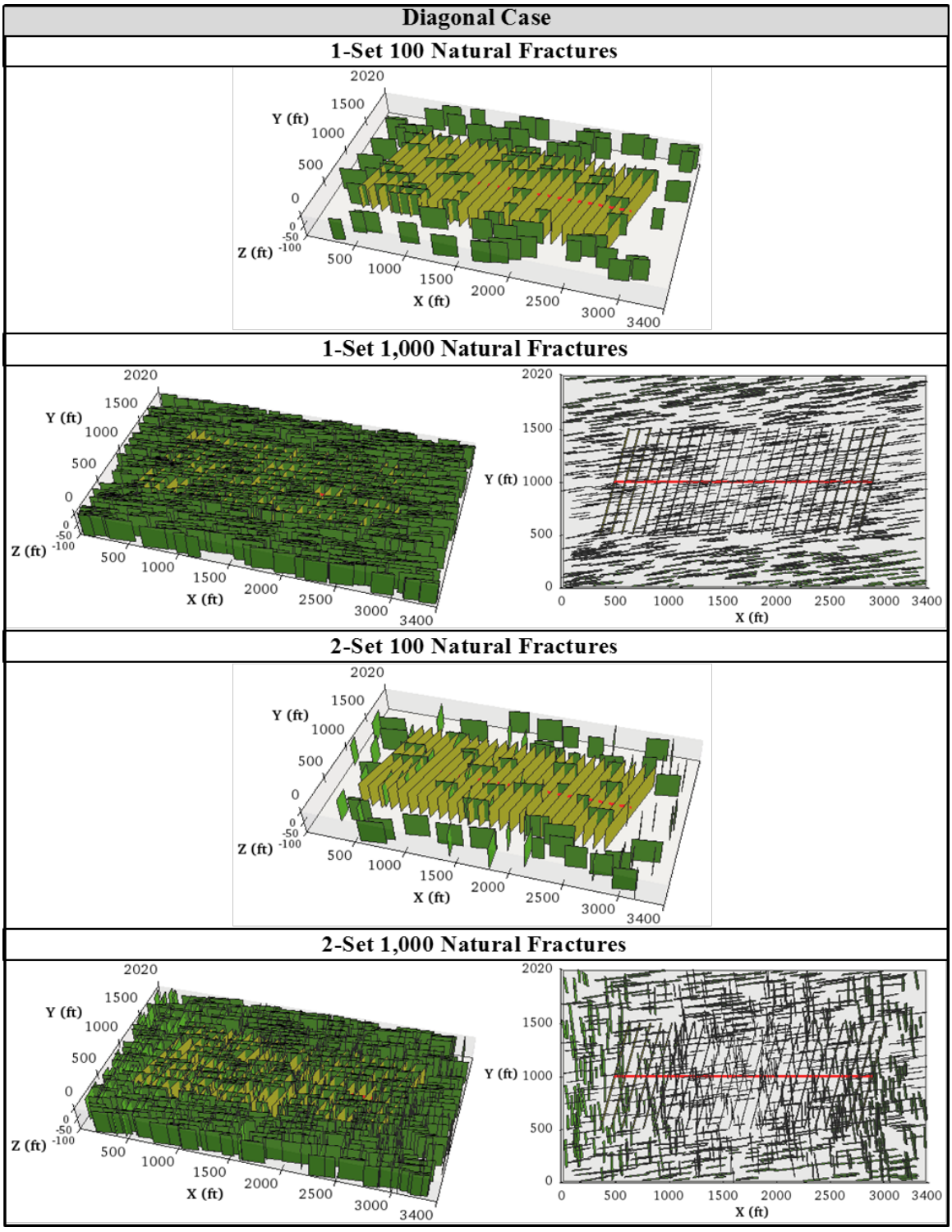

Figure 4.12: Illustrations of 1-set and 2-set natural fractures evaluated for the Diagonal case.

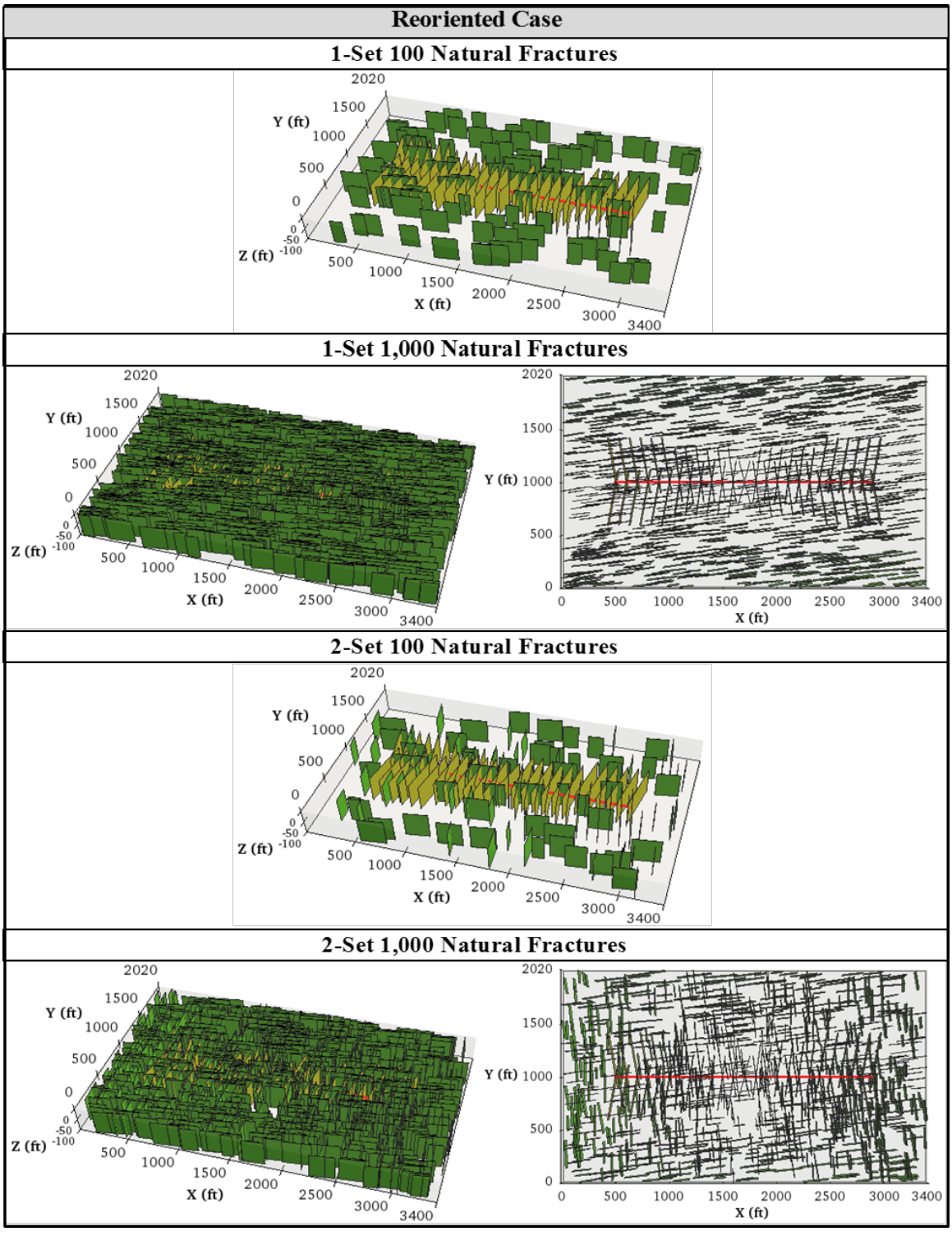

Figure 4.13: Illustrations of 1-set and 2-set natural fractures evaluated for the Reoriented case.

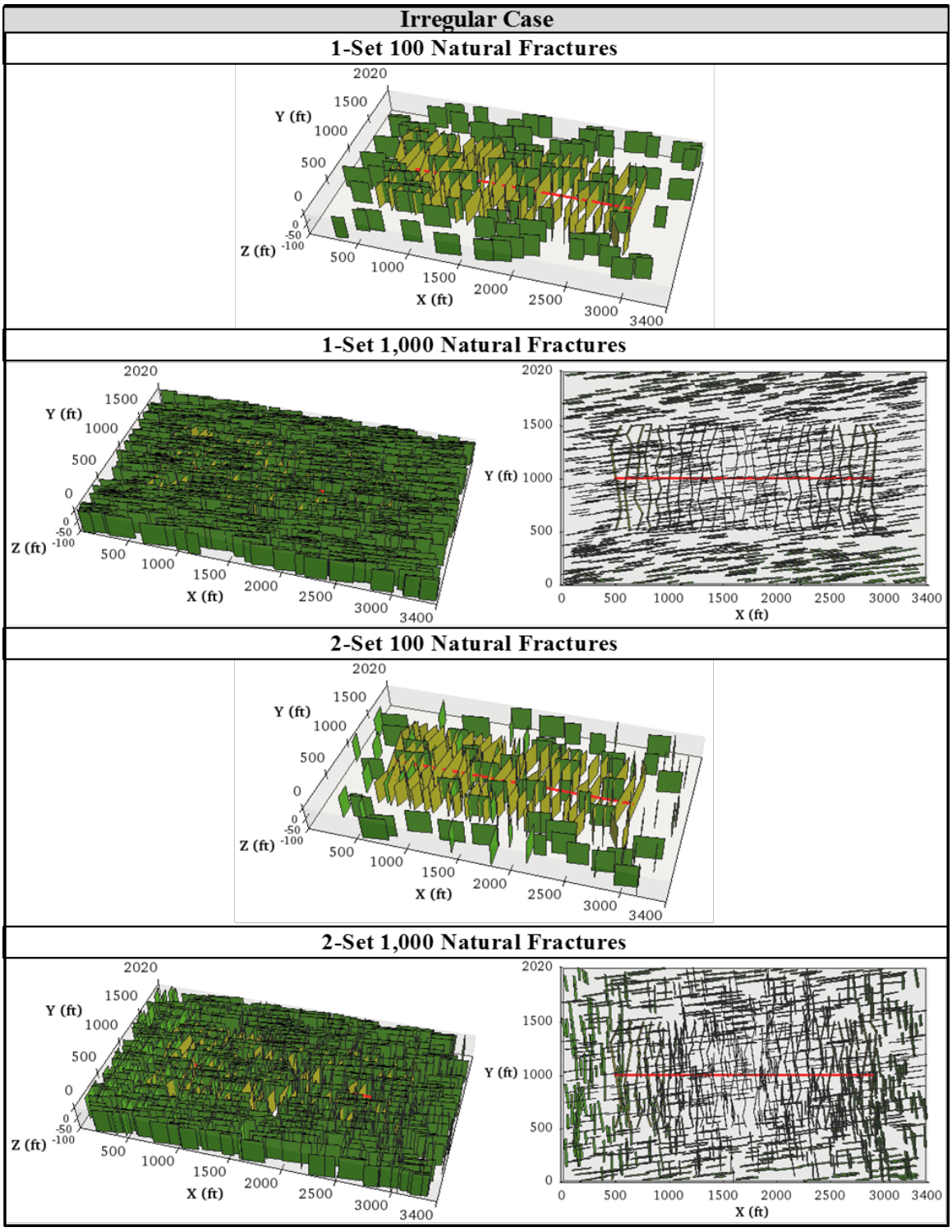

Figure 4.14: Illustrations of 1-set and 2-set natural fractures evaluated for the Irregular case.

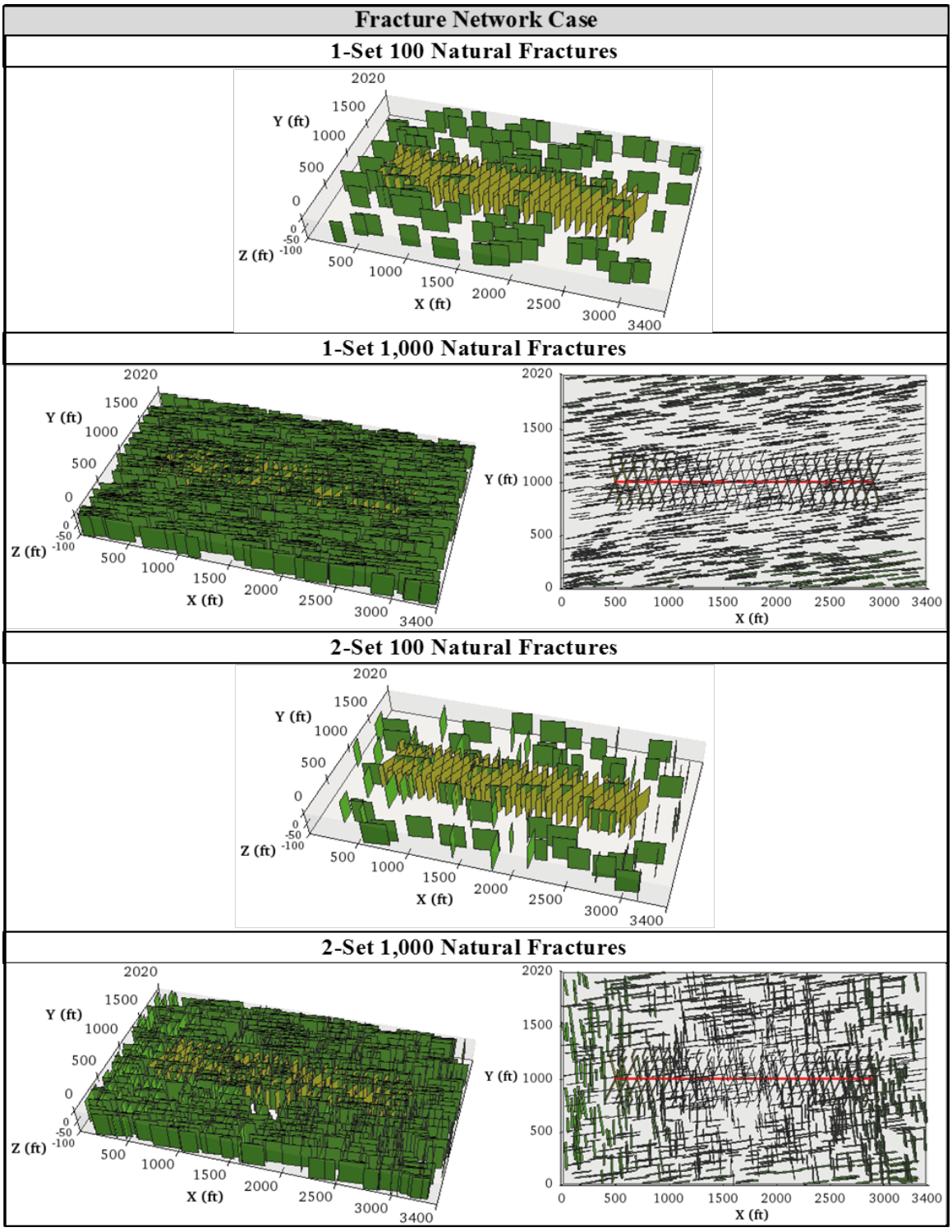

Figure 4.15: Illustrations of 1-set and 2-set natural fractures evaluated for the Fracture Network case.

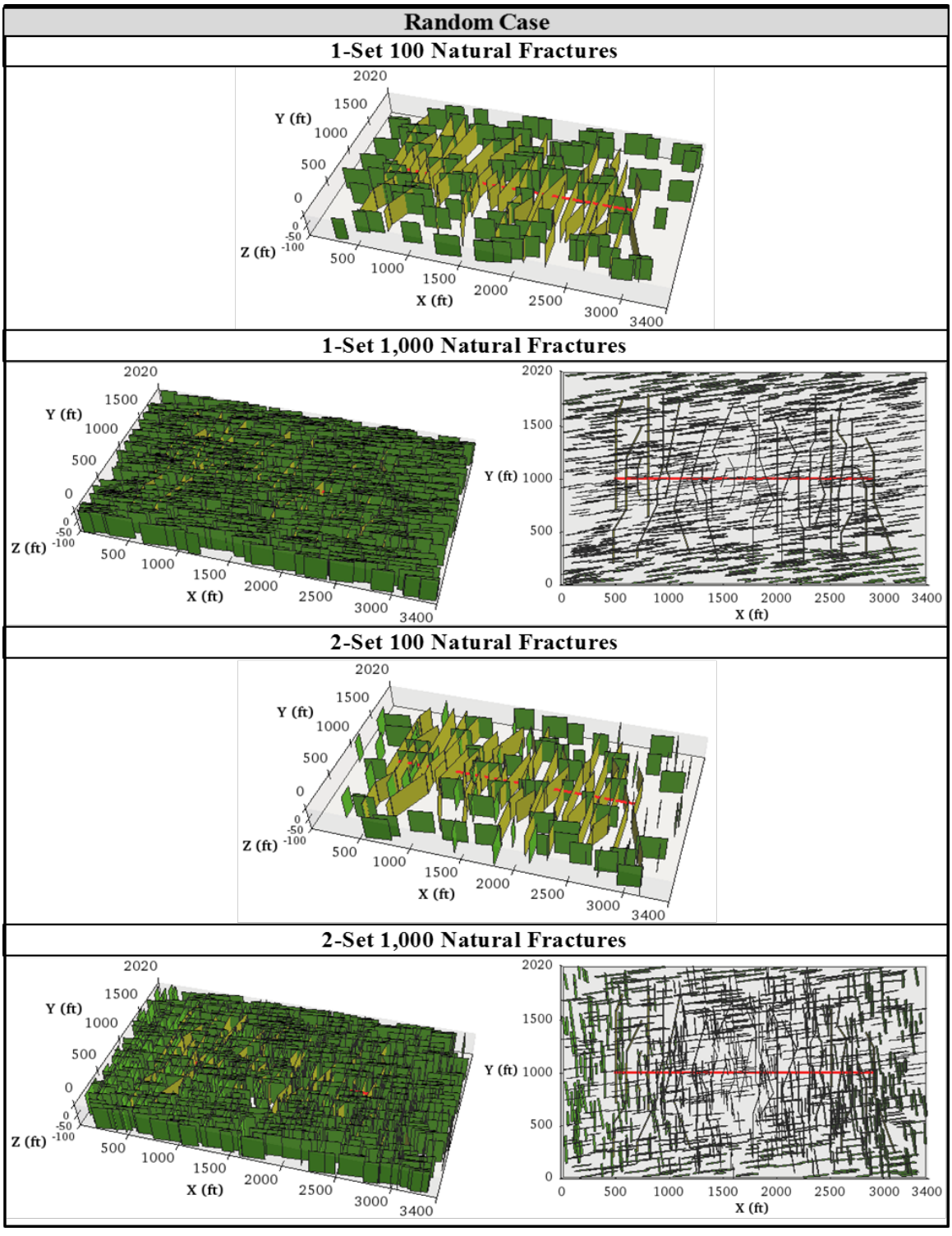

Figure 4.16: Illustrations of 1-set and 2-set natural fractures evaluated for the Random case.

Figures 4.17 and **4.18** present a comparison of the simulated scenarios of natural fractures for each of the six hydraulic fracture geometry cases, in terms of cumulative gas and water productions. As can be seen, the gas productivity in most of the cases reacted positively to the presence of natural fractures. In addition, most of the cases reacted somewhat similarly to the presence of natural fractures in which the more prevalent the natural fractures in a case, the more gas and water were produced cumulatively. Nevertheless, the magnitude of effect of increasing the number of natural fractures was not identical in all the six hydraulic fracture geometry cases. For example, compared to the cases with no natural fractures, the presence of 1-set 100 natural fractures had, at the end of 30 years, minimal contributions (2 to 6%) to the gas recovery in almost all the six hydraulic fracture geometry cases, except for the Random case where the addition of 1-set 100 natural fractures resulted in a significant jump in gas productivity at the end of 30 years by 18%. On the other hand, the addition of 100 natural fractures with 2-set orientations presented different findings where only the Planar and Fracture Network cases had significant increase in gas productivity at the end of 30 years by 45% and 15 %, respectively, from the cases with no natural fractures. To the contrary, the presence of 1,000 natural fractures (both 1-set and 2-set) resulted in extremely significant surges in gas productivity in all six hydraulic fracture geometry cases. **Table 4.4** presents a summary of the cumulative gas production and the percentage change in gas productivity at the end of 30 years from the cases with no natural fractures for all the six hydraulic fracture geometry cases with 100 and 1,000 natural fractures (both 1-set and 2-set orientations). Similarly, the cumulative flowback of water has reacted positively to the presence of natural fractures, as highlighted on **Figures 4.17** and **4.18**, and **Table 4.5**.

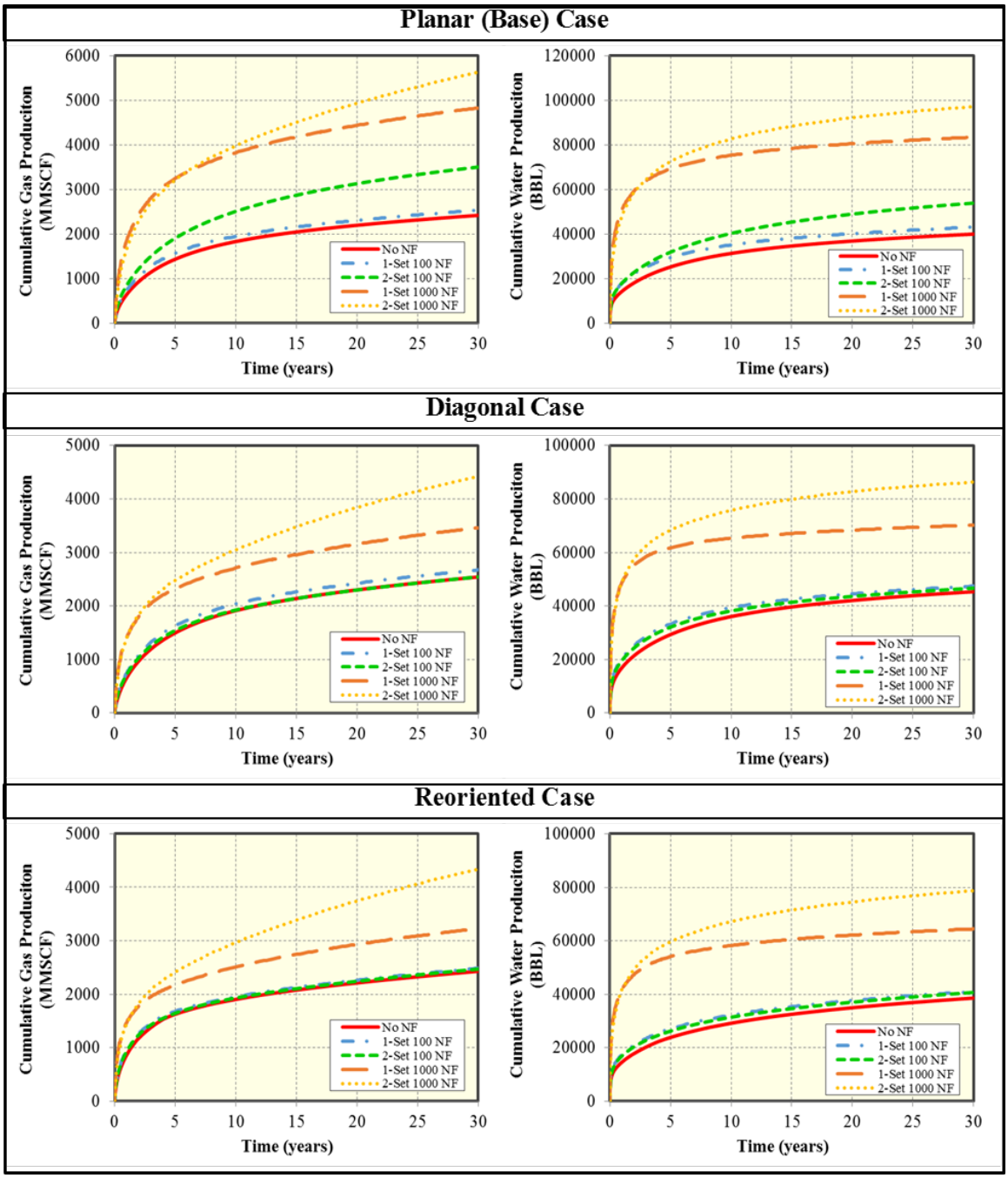

Figure 4.17: Comparison of cumulative gas production (*Left Column*) and cumulative water production (*Right Column*) between 100 and 1,000 natural fractures (both 1-set and 2-set) for the different hydraulic fracture geometry cases (*Part 1/2*)

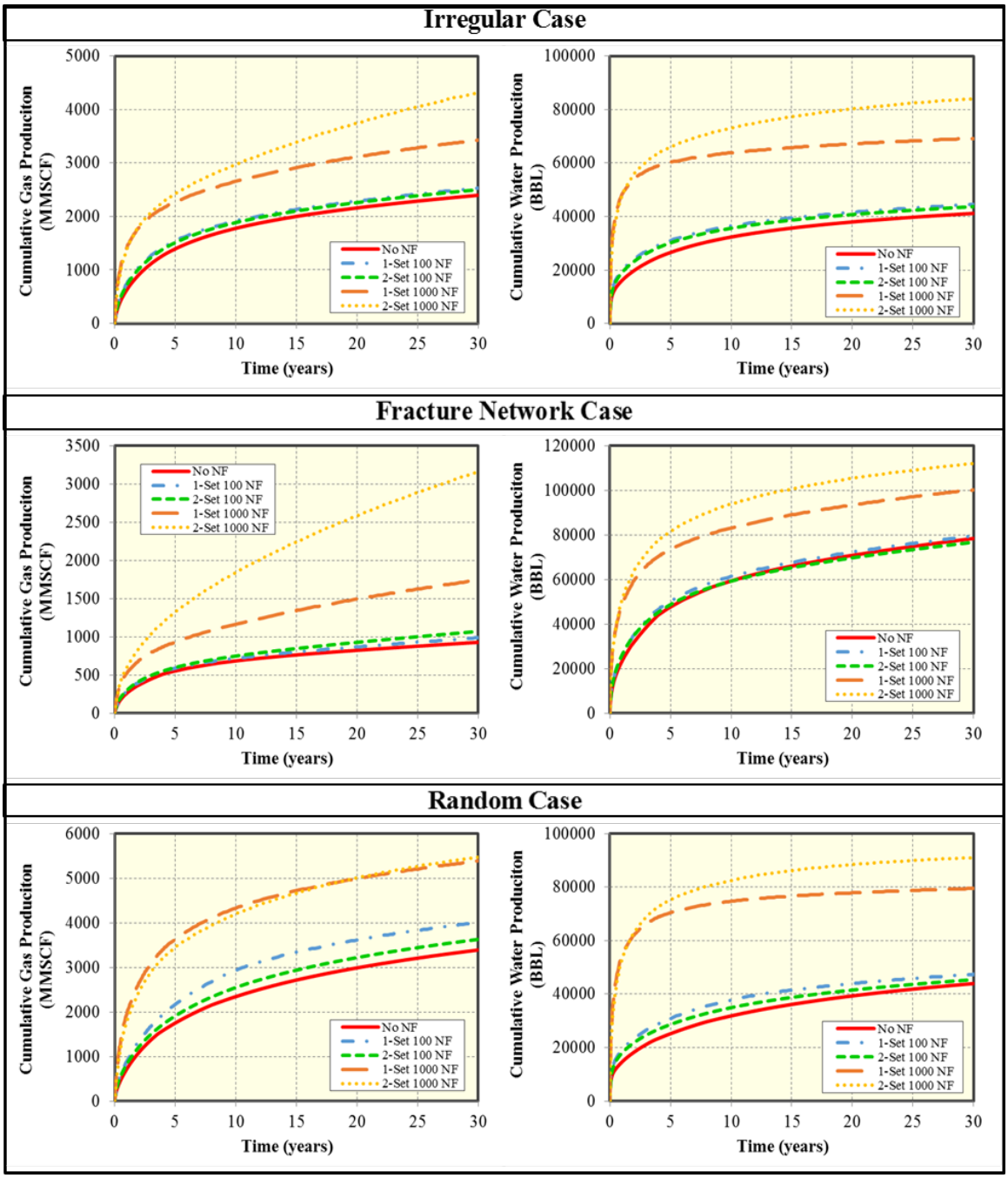

Figure 4.18: Comparison of cumulative gas production (*Left Column*) and cumulative water production (*Right Column*) between 100 and 1,000 natural fractures (both 1-set and 2-set) for the different hydraulic fracture geometry cases (*Part 2/2*)

Cumulative Gas Production (MMSCF) @ 30 Years

		No NF	1-Set 100 NF	2-Set 100 NF	1-Set 1,000 NF	2-Set 1,000 NF
Planar	**Cum. Gas Prod. @ 30 years**	2,422	2,538	3,500	4,830	5,629
	% Change from No NF		5%	45%	99%	132%
Diagonal	**Cum. Gas Prod. @ 30 years**	2,543	2,674	2,539	3,464	4,418
	% Change from No NF		5%	0%	36%	74%
Reoriented	**Cum. Gas Prod. @ 30 years**	2,431	2,487	2,470	3,228	4,344
	% Change from No NF		2%	2%	33%	79%
Irregular	**Cum. Gas Prod. @ 30 years**	2,397	2,530	2,504	3,426	4,318
	% Change from No NF		6%	4%	43%	80%
Fracture Network	**Cum. Gas Prod. @ 30 years**	930	988	1,069	1,743	3,164
	% Change from No NF		6%	15%	87%	240%
Random	**Cum. Gas Prod. @ 30 years**	3,390	4,006	3,633	5,385	5,474
	% Change from No NF		18%	7%	59%	61%

Table 4.4: Summary of cumulative gas production (MMSCF) and the percentage change, at the end of 30 years, from the case with no natural fractures for the different hydraulic fracture geometry cases with 1-set and 2-set of 100 and 1,000 natural fractures.

Cumulative Water Production (BBL) @ 30 Years

		No NF	1-Set 100 NF	2-Set 100 NF	1-Set 1,000 NF	2-Set 1,000 NF
Planar	**Cum. Water Prod. @ 30 years**	40,039	43,123	53,817	83,449	97,212
	% Change from No NF		8%	34%	108%	143%
Diagonal	**Cum. Water Prod. @ 30 years**	45,358	47,440	46,664	70,261	86,306
	% Change from No NF		5%	3%	55%	90%
Reoriented	**Cum. Water Prod. @ 30 years**	38,603	41,051	40,598	64,442	78,719
	% Change from No NF		6%	5%	67%	104%
Irregular	**Cum. Water Prod. @ 30 years**	41,183	44,521	43,706	69,217	84,082
	% Change from No NF		8%	6%	68%	104%
Fracture Network	**Cum. Water Prod. @ 30 years**	78,491	79,657	76,735	100,257	112,175
	% Change from No NF		1%	-2%	28%	43%
Random	**Cum. Water Prod. @ 30 years**	43,971	47,401	45,376	79,505	91,089
	% Change from No NF		8%	3%	81%	107%

Table 4.5: Summary of cumulative water production (BBL) and the percentage change, at the end of 30 years, from the case with no natural fractures for the different hydraulic fracture geometry cases with 1-set and 2-set of 100 and 1,000 natural fractures.

Alternatively, **Figure 4.19** presents a comparison of cumulative gas and cumulative water productions by combining all six hydraulic fracture geometry cases with 100 natural fractures on a single plot. As can be seen, the Random case persist to be the highest in gross gas productivity in both 1-set and 2-set orientations. Nonetheless, its lead is greatly diminished by the Planar case when considering 2-set orientation. This can be attributed to the increase in probability of intersections, for the Planar case, between the planar hydraulic fractures and natural fractures when considering wider ranges of natural fractures orientations as provided by the 2-set cases. On the other hand, the Fracture Network case continue to under deliver in terms of gas recovery in both cases. Whereas, the cumulative gas recovery in the Diagonal, Reoriented and Irregular cases was almost unfazed to the presence of 100 natural fractures in both cases of orientations. In contrast to gas recovery, cumulative water flowback was at its highest level with the Fracture Network case. Nonetheless, the addition of 100 natural fractures had not significantly contribute to increasing the water flowback recovery in any of the six hydraulic fracture geometry cases, except for the Planar case, which saw an increase of 34%, at the end of 30 years, in water recovery due to the addition of 2-set 100 natural fractures.

In the same way, **Figure 4.20** presents a similar comparison to **Figure 4.19** but for the cases with 1,000 natural fractures. As can be seen, both the Planar and Random cases continue to dominate the scene in cumulative gas recovery. This domination in gas recovery, as explained in the previous section, is partially attributed to the larger SRV covered by the Planar and Random cases compared to the other hydraulic fracture geometry cases. In addition, it's worth noting that the Planar case has, for the first time, surpassed the Random case in cumulative gas recovery when 2-set 1,000 natural fractures were considered. This can be accredited to the greater chances of intersection between

hydraulic and natural fractures provided by the 2-set orientation of natural fractures as opposed to 1-set orientation. On the other hand, even though the Fracture Network case had reacted positively to the addition of 1,000 natural fractures, its reaction is still unparalleled to other cases. The Fracture Network case continue to be the lowest and highest in gas cumulative recovery and water flowback recovery, respectively. Finally, the addition of 1,000 natural fractures has benefited the Diagonal, Reoriented, and Irregular cases in terms of increasing their gas productivity, though their responses were almost identical.

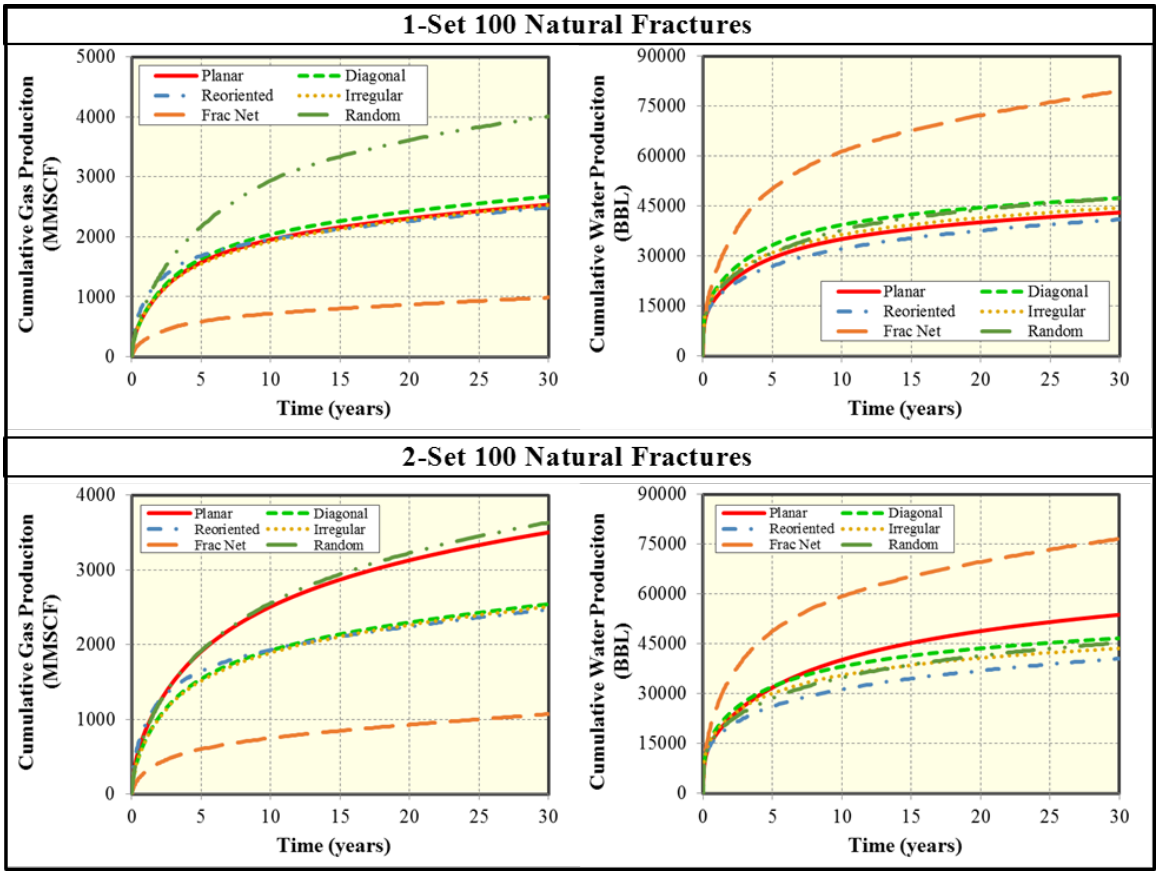

Figure 4.19: Comparison of cumulative gas production (*Left Column*) and cumulative water production (*Right Column*) between the different hydraulic fracture geometry cases with 1-set and 2-set 100 natural fractures.

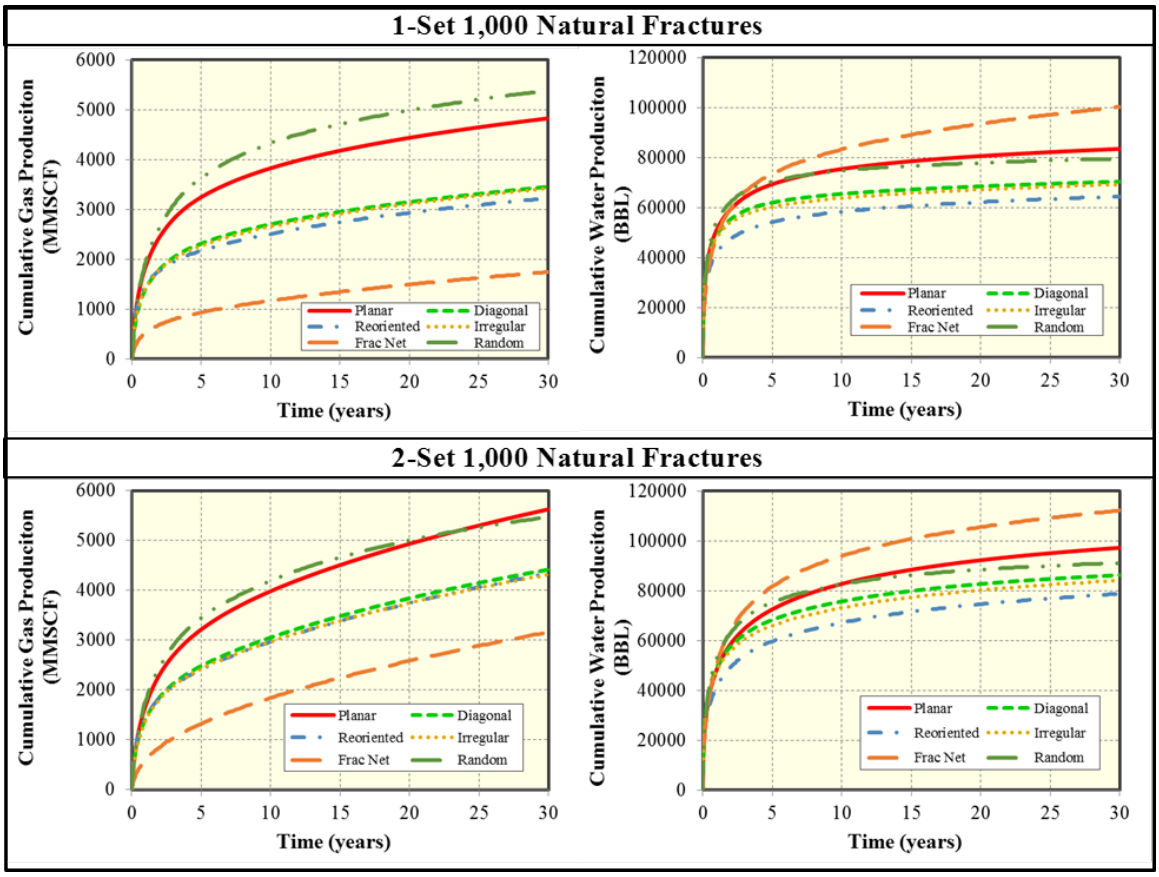

Figure 4.20: Comparison of cumulative gas production (*Left Column*) and cumulative water production (*Right Column*) between the different hydraulic fracture geometry cases with 1-set and 2-set 1,000 natural fractures.

Another way to examine the effect of the presence of natural fractures in the different hydraulic fracture geometry cases is depicted on **Figures 4.21** and **4.22**. These two figures rank the cumulative gas and water recoveries at the end of 30 years, respectively, for the different hydraulic fracture geometries with and without natural fractures. As can be noted, three hydraulic fracture geometry cases (Diagonal, Reoriented, and Irregular) had reacted somewhat similarly to the presence of natural fractures in terms of their two-phase cumulative productions. As a matter of fact, the two-phase production in these three aforementioned cases were almost idle to the presence of 100 natural fractures. On the other hand, the Random case has overall reacted positively in terms of gas cumulative recovery to any presence of natural fractures, though 1-set orientation was more favorable than 2-set orientation. Additionally, the cumulative water flowback of the Random case has only experienced a rise when 1,000 natural fractures were added. Nonetheless, this rise in cumulative water recovery was proportionally comparable to rises in the other cases. Similar to the Random case, the Planar case had a positive reaction to the presence of natural fractures, except for the case with 1-set 100 natural fractures. However, opposite to the Random case, the Planar case seems to favor the 2-set orientation in terms of increasing cumulative gas recovery. Lastly, the gas and water recoveries from Fracture Network case, as shown in **Figures 4.21** and **4.22**, respectively, stalled to the presence of 100 natural fractures in both orientations, and reacted increasingly to the presence of 1,000 natural fractures in both orientations.

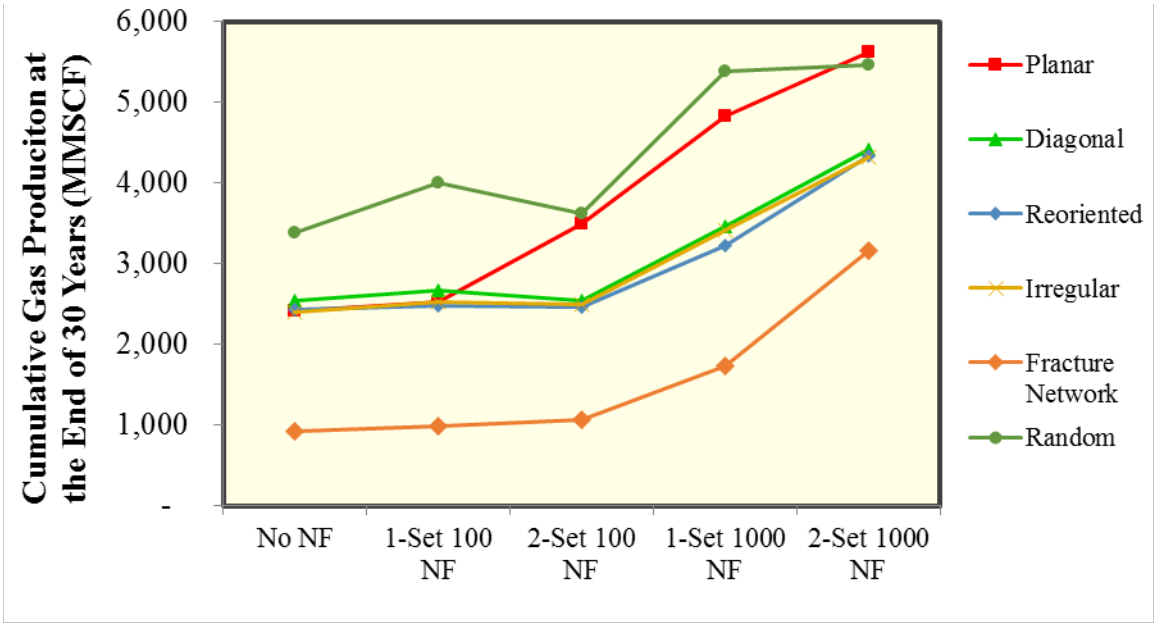

Figure 4.21: Cumulative gas recovery at the end of 30 years for the different fracture geometry cases with and without natural fractures.

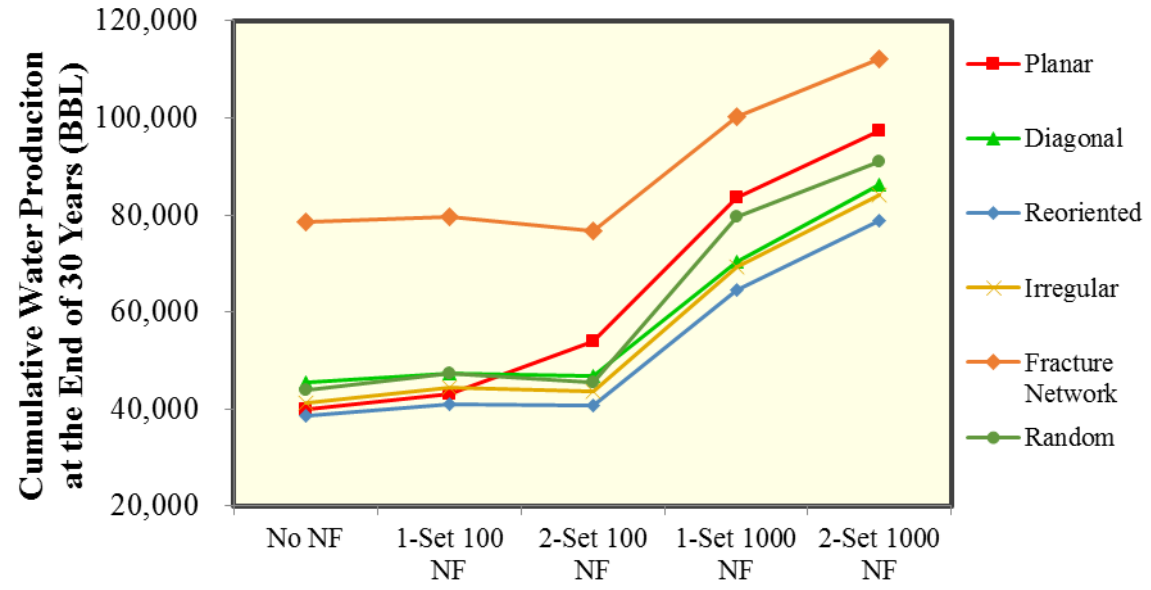

Figure 4.22: Cumulative water recovery at the end of 30 years for the different fracture geometry cases with and without natural fractures.

The aforementioned enhancements in recovery, which are attributed to the addition of natural fractures, are expected since the presence of natural fractures results in a more exposure to the rock when intersected by hydraulic fractures. This consequently enhances the drainage area available for the well. Nevertheless, the previous statements only hold if you assume that these natural fractures are characteristically open and are not sealed, which was the case in this model. Overall, the presence of natural fractures in shale rocks, theoretically, presents an opportunity, albeit governed by the characteristic of these natural fractures (open or closed). This means that the more ubiquitous these natural fractures in a shale rock, the better the expected recovery. In addition, based on analysis of the results, the orientation of these natural fractures seem to play a big factor in altering recovery. As a matter of fact, the orientation that results in a higher likelihood of intersections between hydraulic and natural fractures, will eventually gain the well a better recovery. For that reason, since orientation of natural fractures is governed by rock stresses, well placement is crucial in order to take advantage of a larger drainage area.

Figures 4.23 through **4.46** highlight the pressure distribution of the 100-day, 10-year, and 30-year marks for all the six hydraulic fracture geometry cases with 1-Set 100, 2-Set 100, 1-Set 1,000, and 2-Set 1,000 natural fractures, respectively. Clearly, the more natural fractures present in a case, the larger the drainage area accumulated for flow, and thus the better the well's productivity.

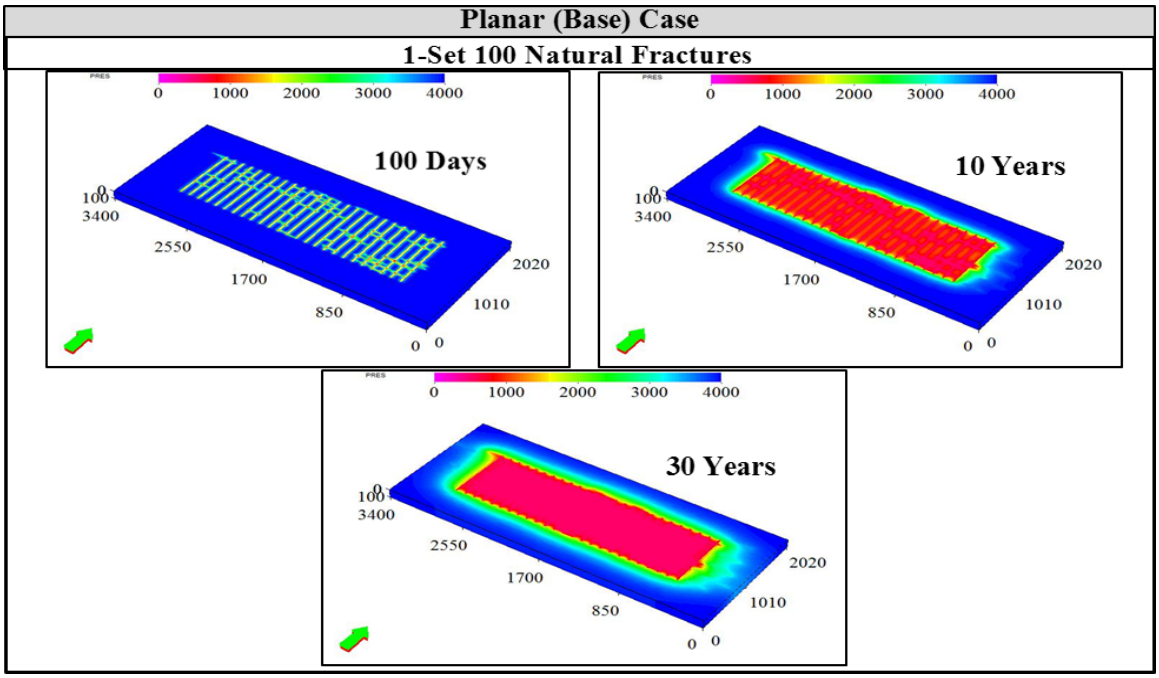

Figure 4.23: Pressure distribution maps of the Planar case with 1-set 100 natural fractures for the 100-day, 10-year, and 30-year marks.

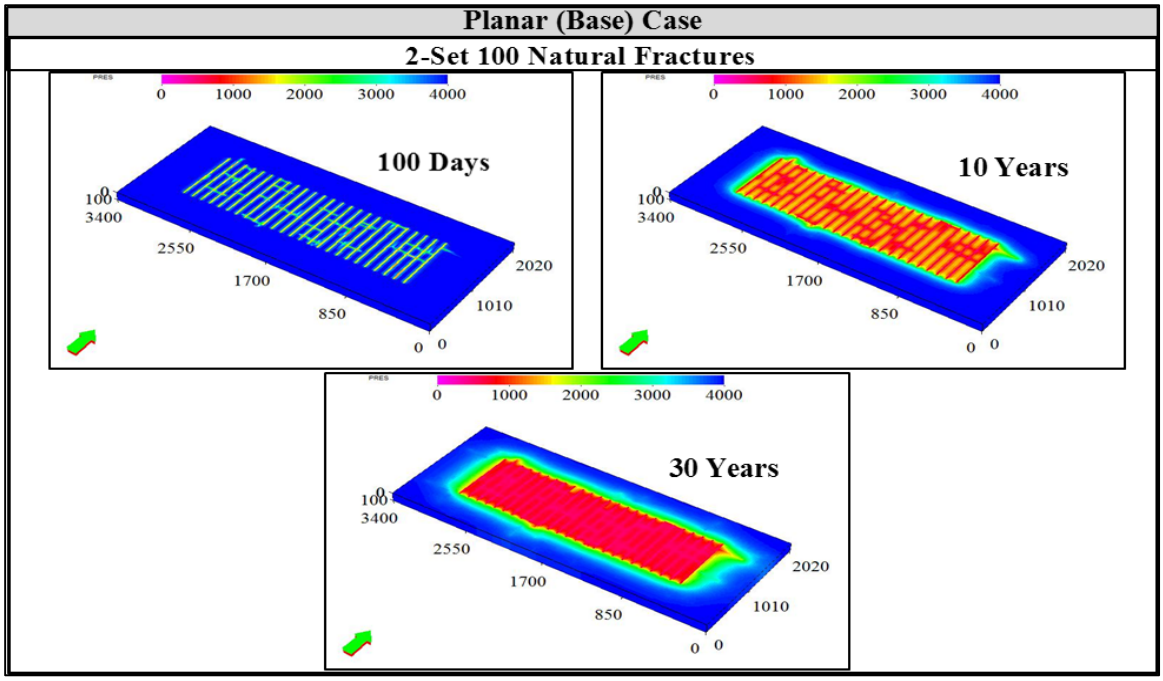

Figure 4.24: Pressure distribution maps of the Planar case with 2-set 100 natural fractures for the 100-day, 10-year, and 30-year marks.

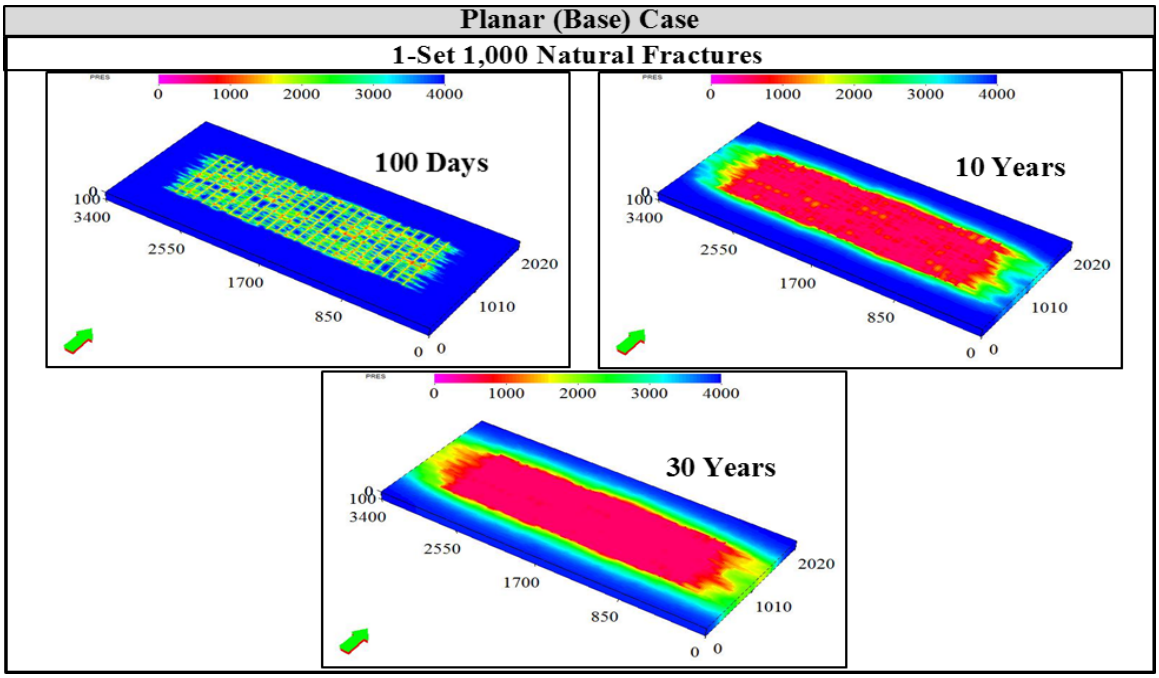

Figure 4.25: Pressure distribution maps of the Planar case with 1-set 1,000 natural fractures for the 100-day, 10-year, and 30-year marks.

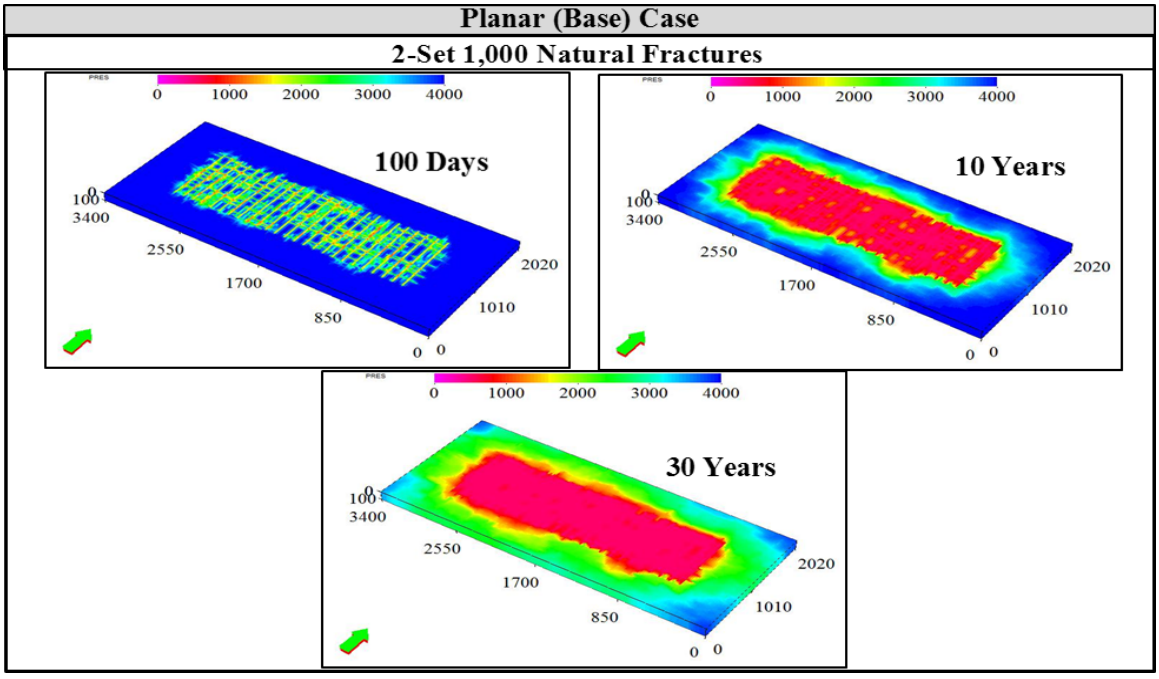

Figure 4.26: Pressure distribution maps of the Planar case with 2-set 1,000 natural fractures for the 100-day, 10-year, and 30-year marks.

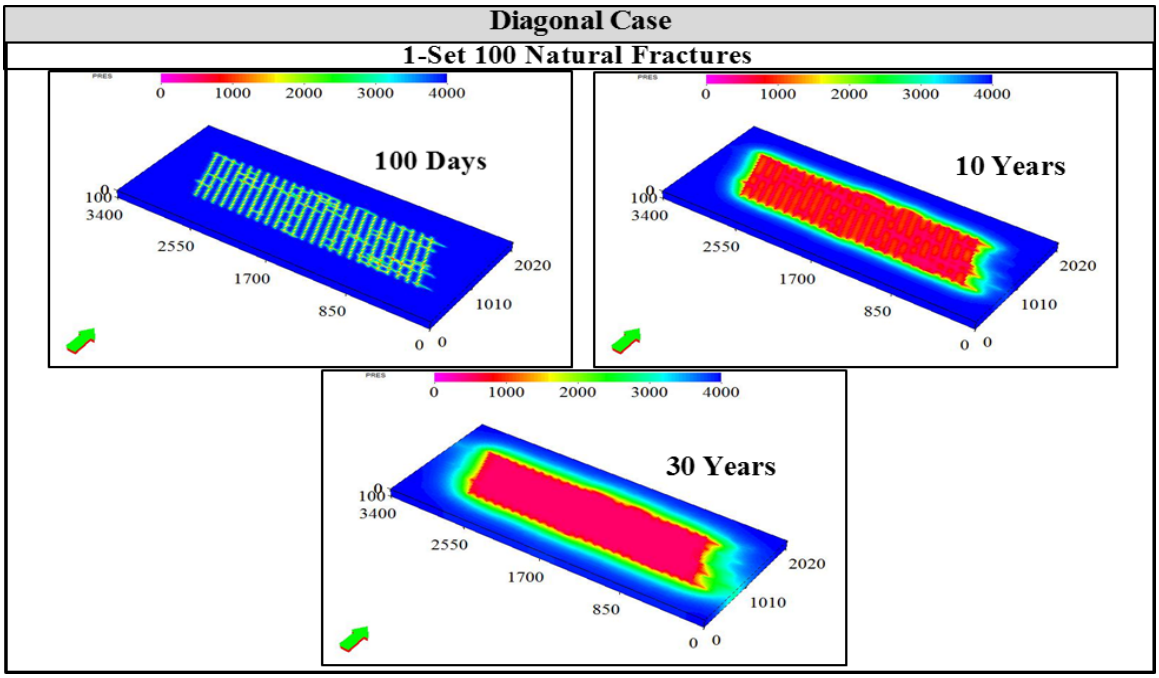

Figure 4.27: Pressure distribution maps of the Diagonal case with 1-set 100 natural fractures for the 100-day, 10-year, and 30-year marks.

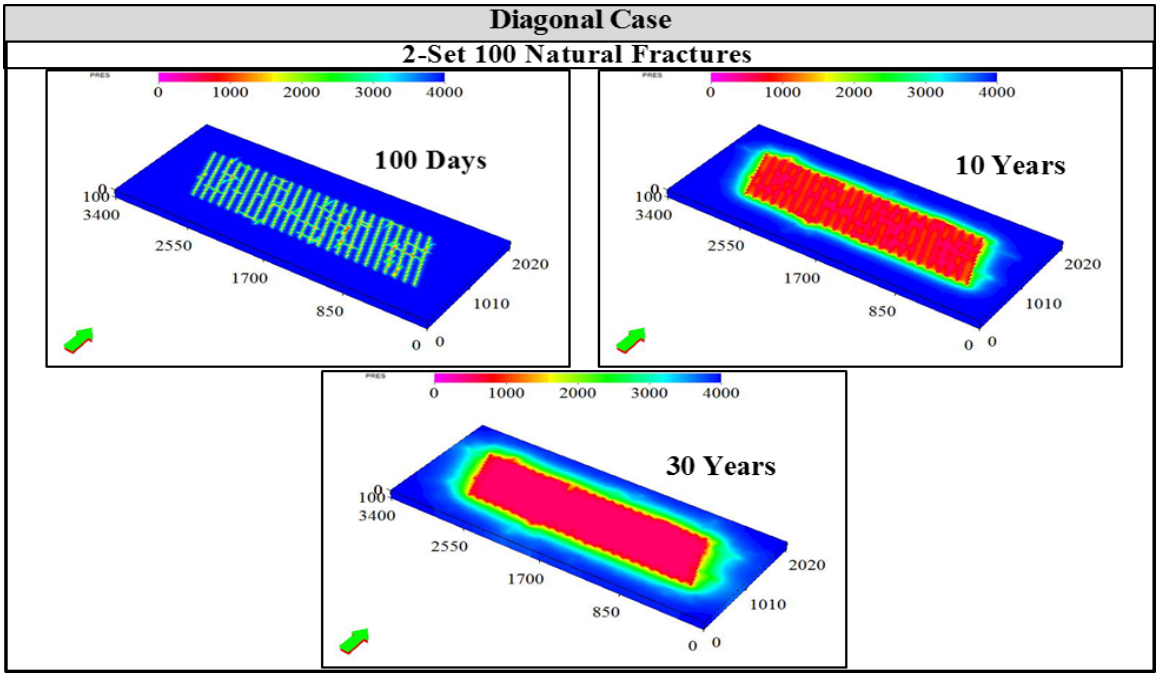

Figure 4.28: Pressure distribution maps of the Diagonal case with 2-set 100 natural fractures for the 100-day, 10-year, and 30-year marks.

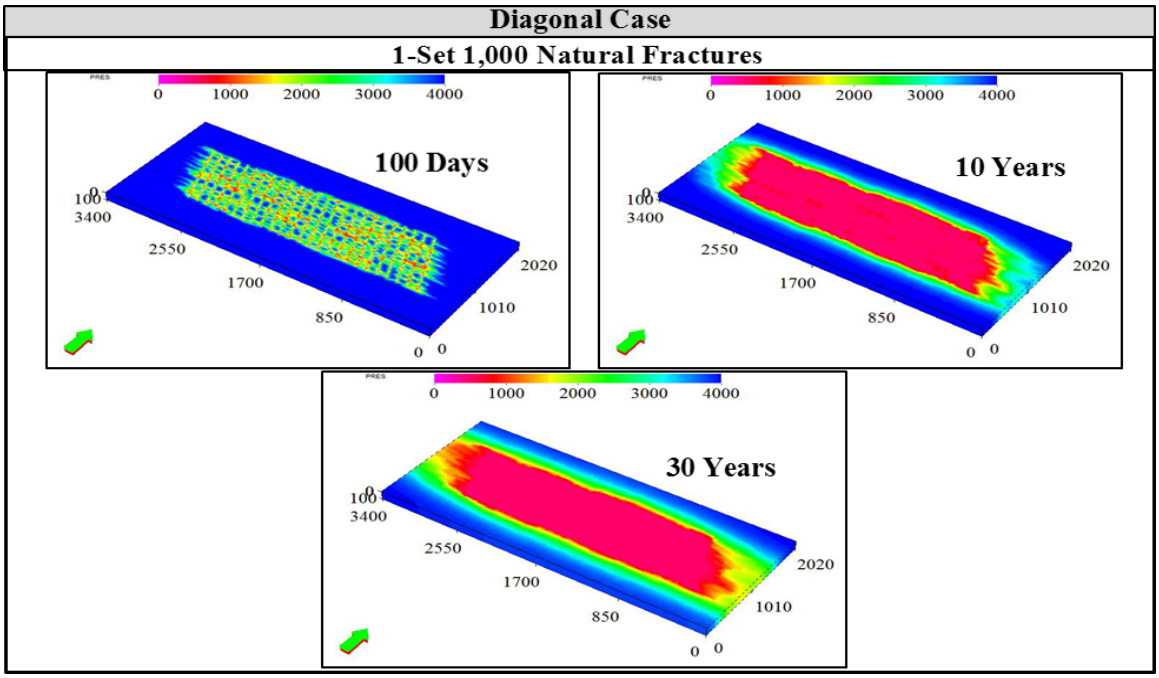

Figure 4.29: Pressure distribution maps of the Diagonal case with 1-set 1,000 natural fractures for the 100-day, 10-year, and 30-year marks.

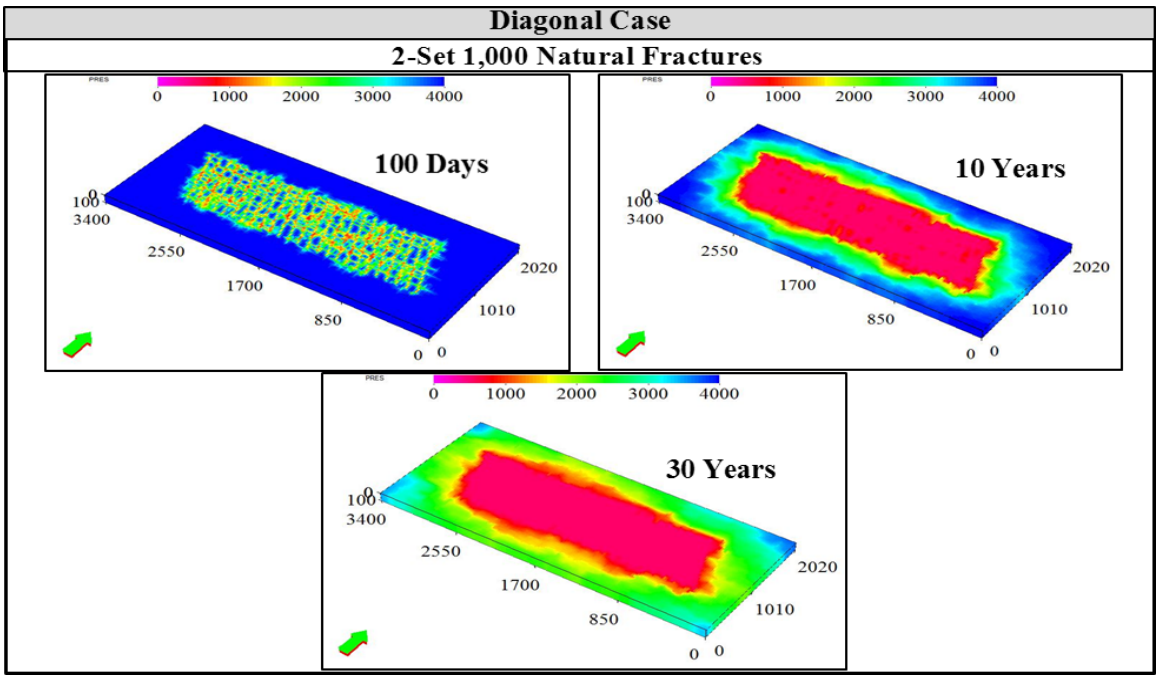

Figure 4.30: Pressure distribution maps of the Diagonal case with 2-set 1,000 natural fractures for the 100-day, 10-year, and 30-year marks.

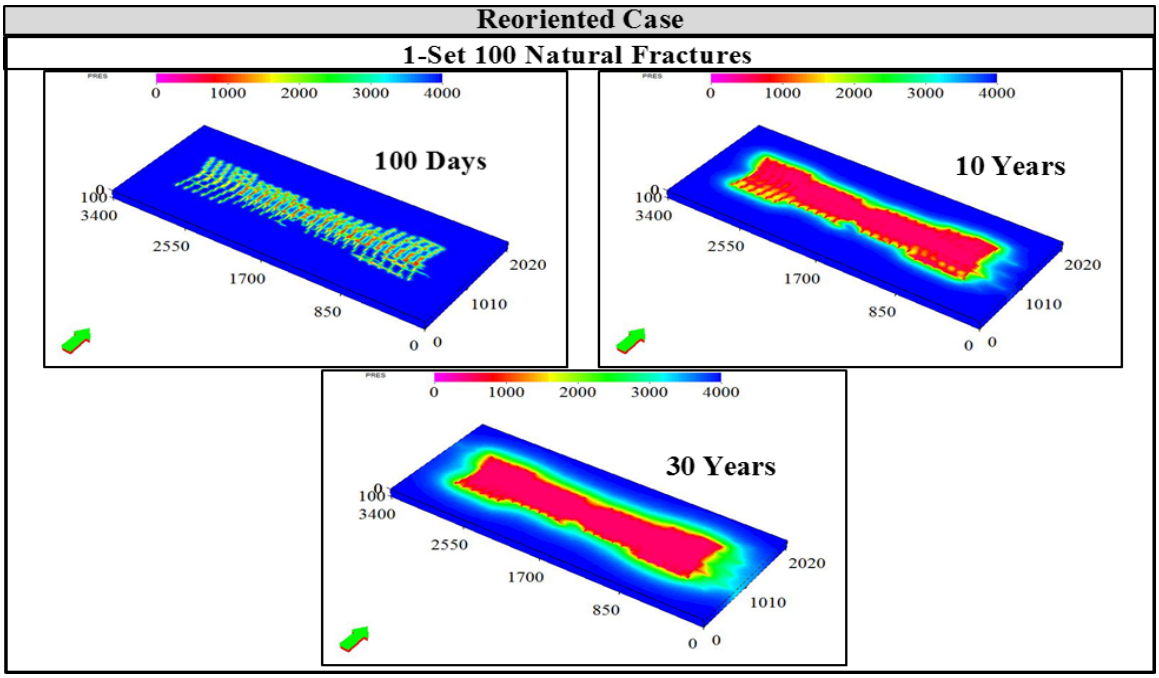

Figure 4.31: Pressure distribution maps of the Reoriented case with 1-set 100 natural fractures for the 100-day, 10-year, and 30-year marks.

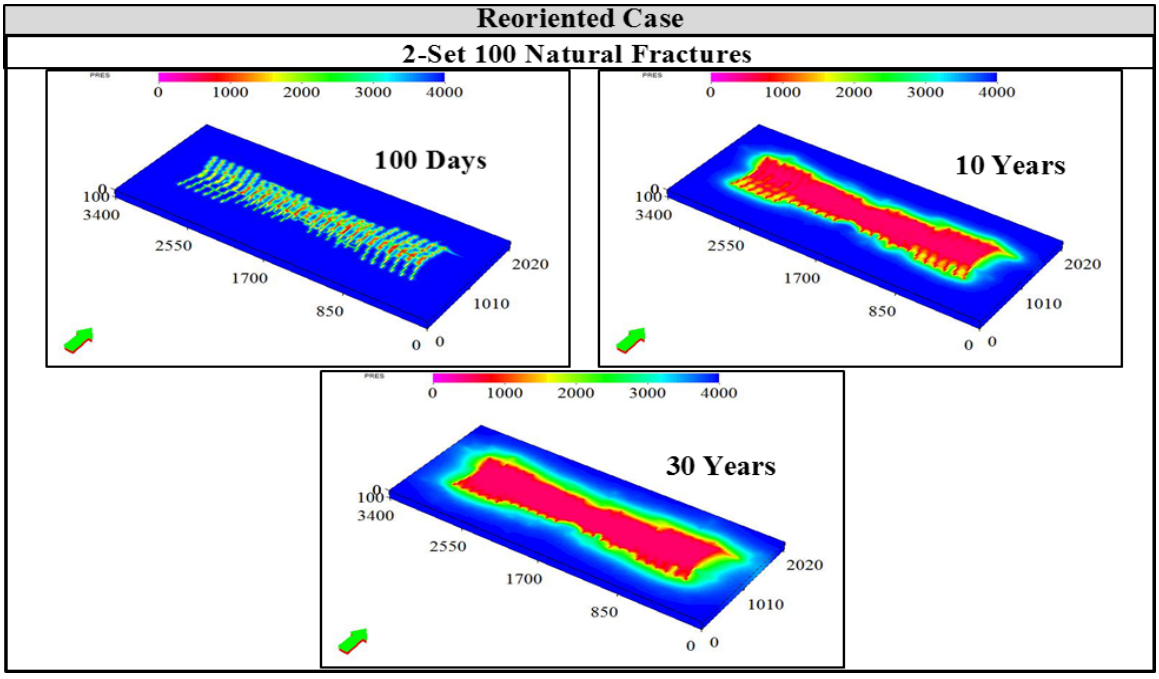

Figure 4.32: Pressure distribution maps of the Reoriented case with 2-set 100 natural fractures for the 100-day, 10-year, and 30-year marks.

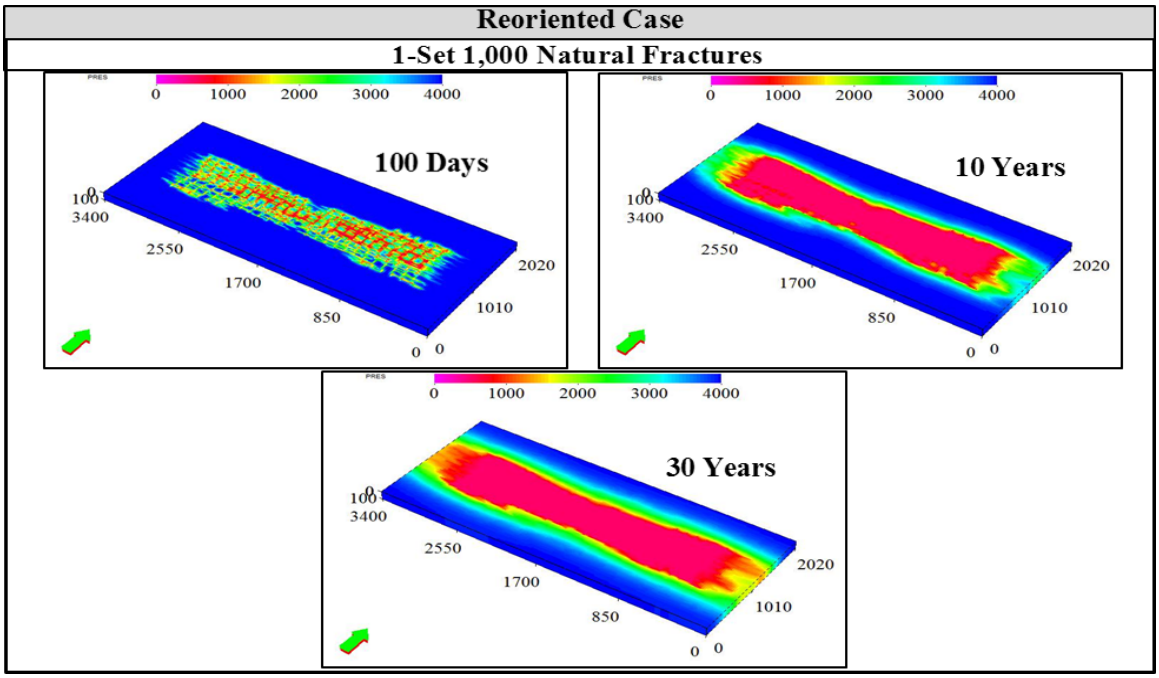

Figure 4.33: Pressure distribution maps of the Reoriented case with 1-set 1,000 natural fractures for the 100-day, 10-year, and 30-year marks.

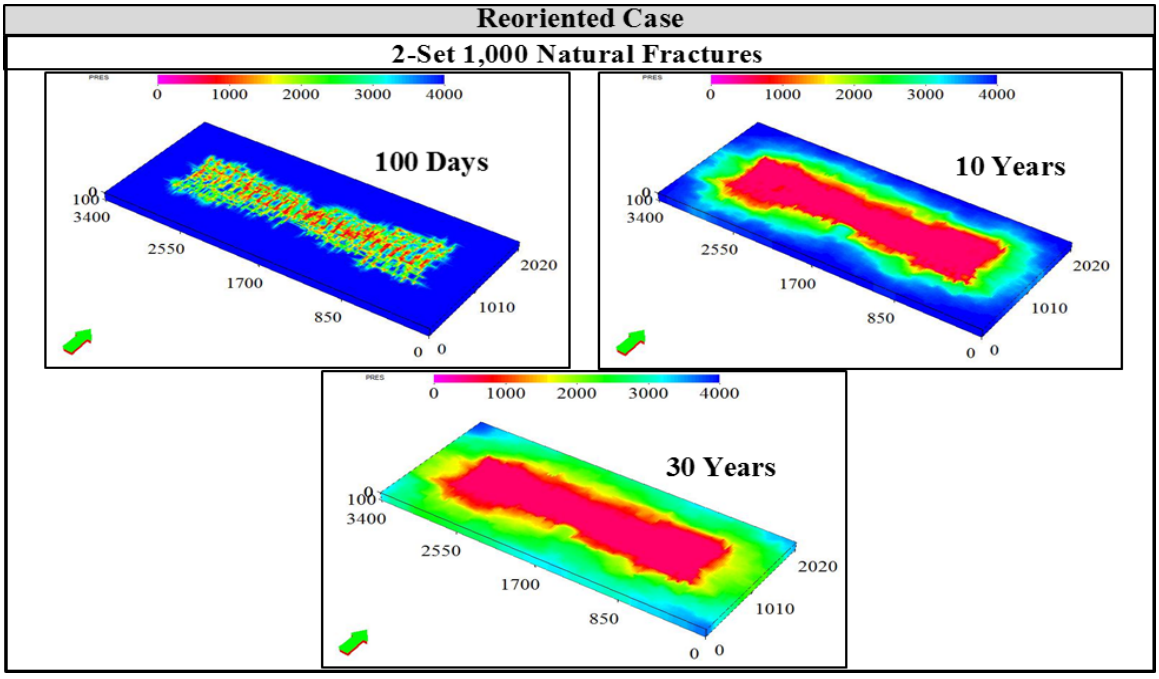

Figure 4.34: Pressure distribution maps of the Reoriented case with 2-set 1,000 natural fractures for the 100-day, 10-year, and 30-year marks.

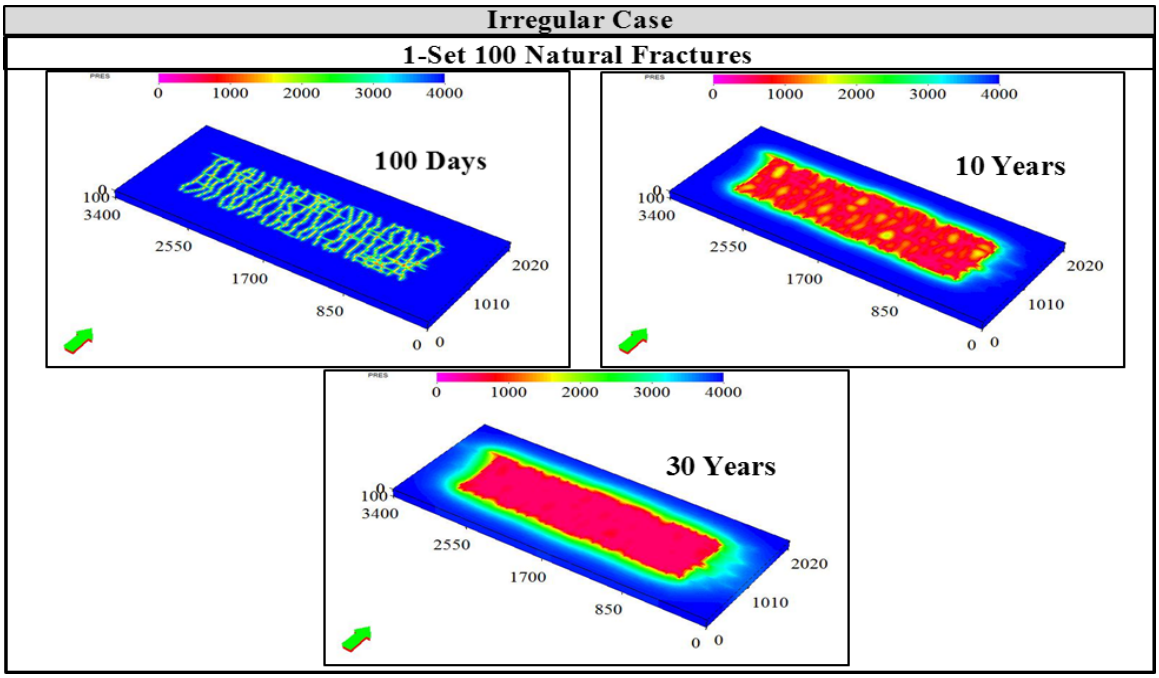

Figure 4.35: Pressure distribution maps of the Irregular case with 1-set 100 natural fractures for the 100-day, 10-year, and 30-year marks.

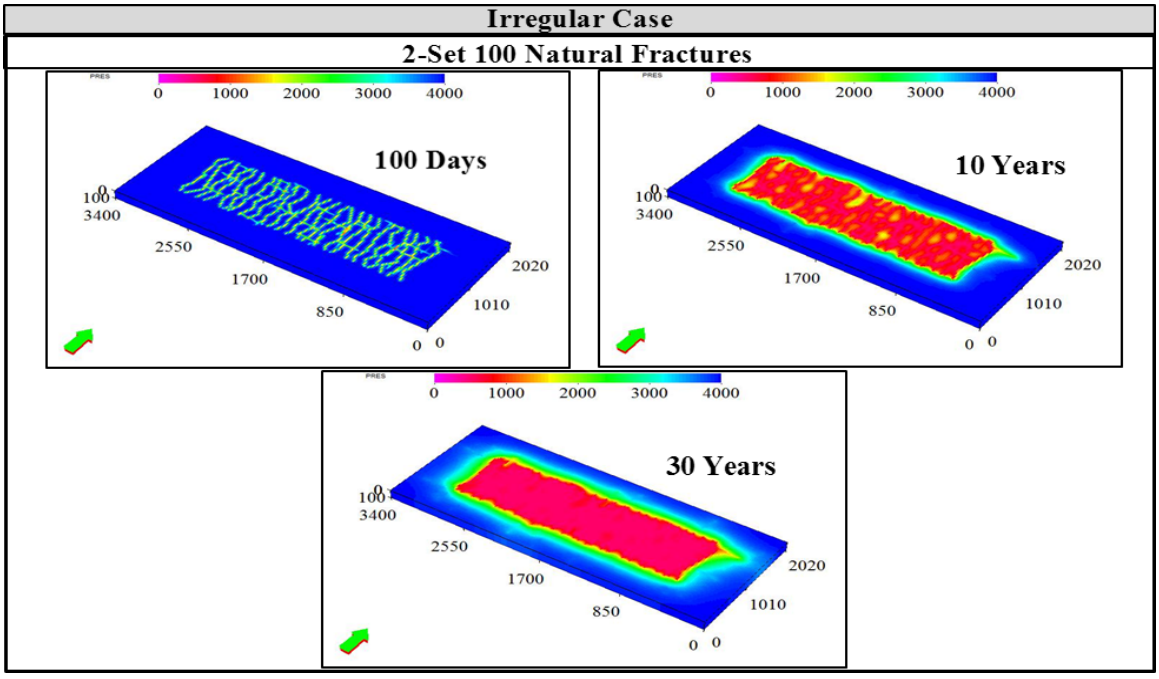

Figure 4.36: Pressure distribution maps of the Irregular case with 2-set 100 natural fractures for the 100-day, 10-year, and 30-year marks.

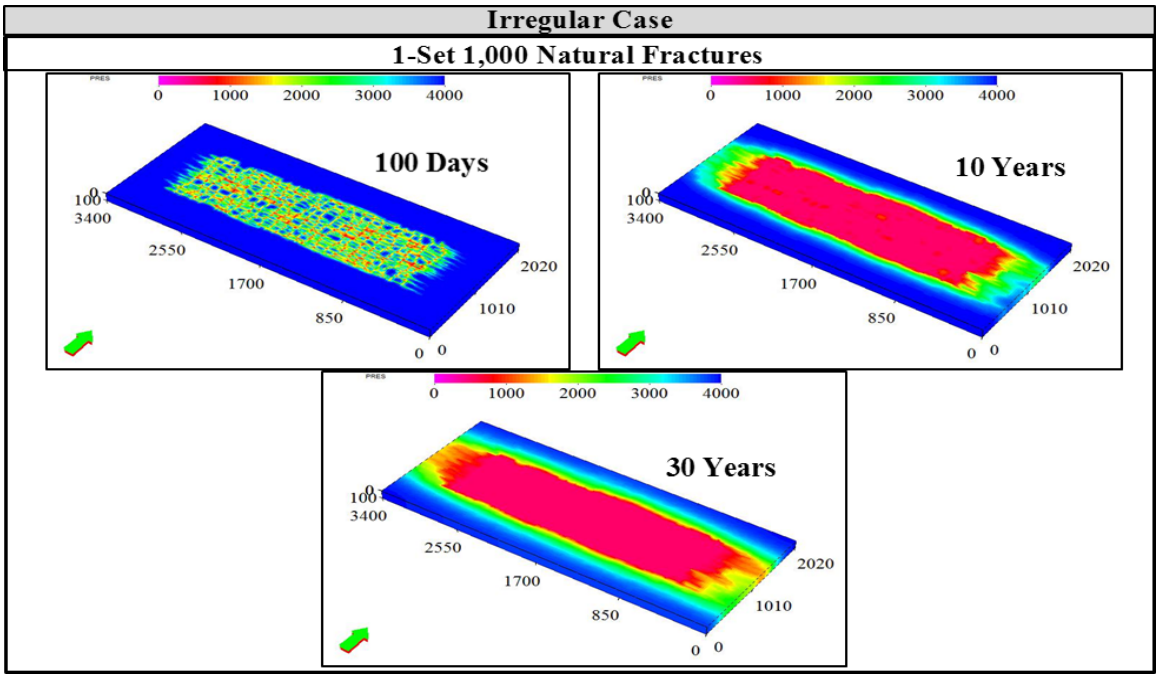

Figure 4.37: Pressure distribution maps of the Irregular case with 1-set 1,000 natural fractures for the 100-day, 10-year, and 30-year marks.

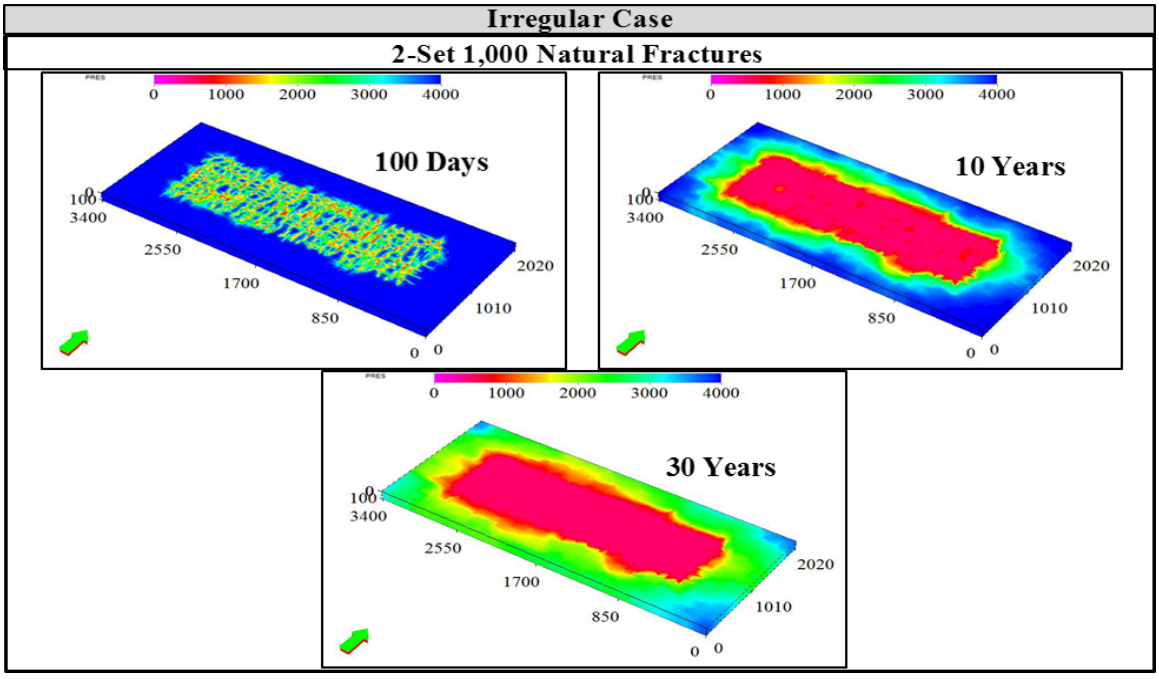

Figure 4.38: Pressure distribution maps of the Irregular case with 2-set 1,000 natural fractures for the 100-day, 10-year, and 30-year marks.

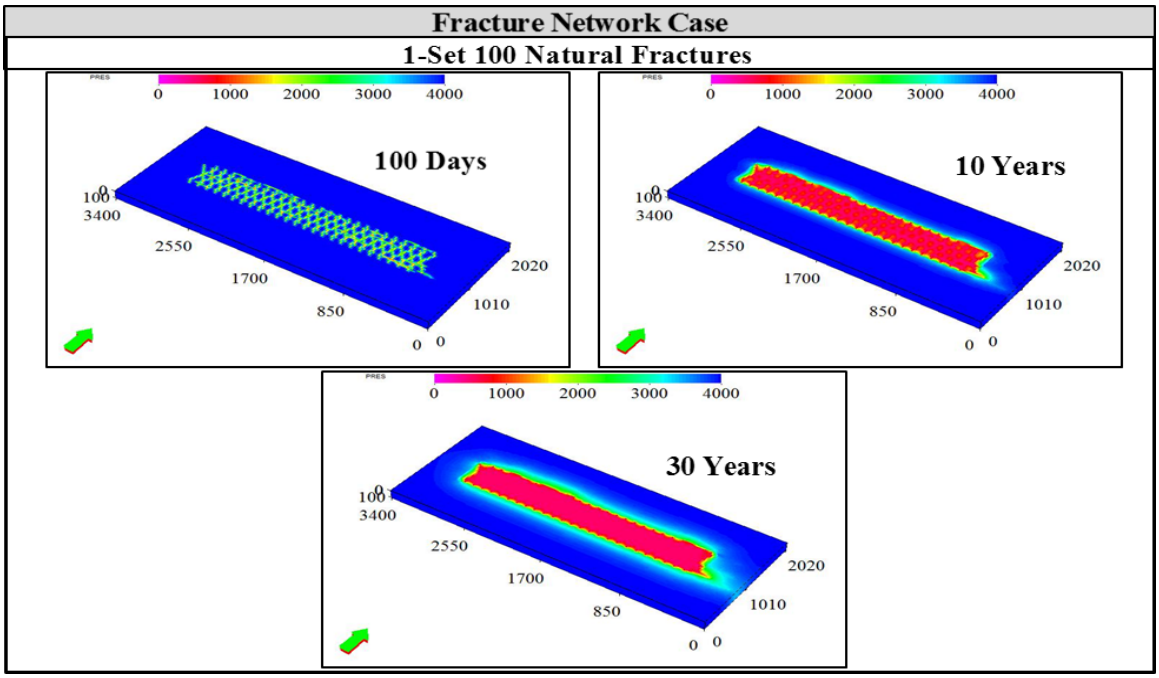

Figure 4.39: Pressure distribution maps of the Fracture Network case with 1-set 100 natural fractures for the 100-day, 10-year, and 30-year marks.

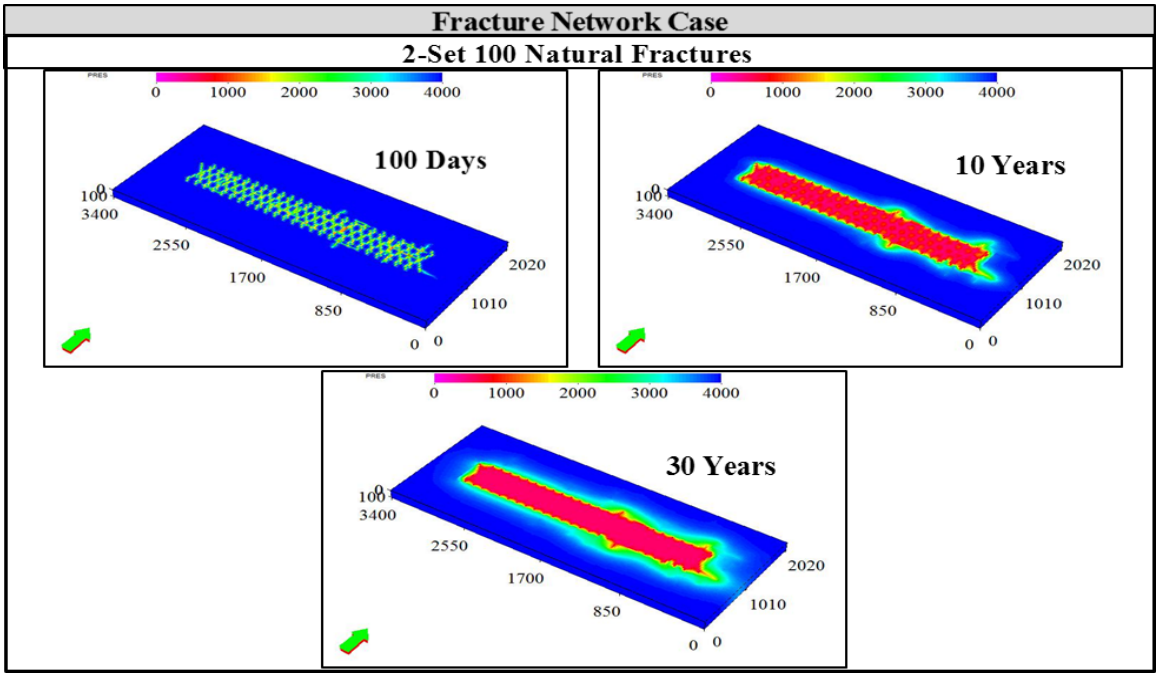

Figure 4.40: Pressure distribution maps of the Fracture Network case with 2-set 100 natural fractures for the 100-day, 10-year, and 30-year marks.

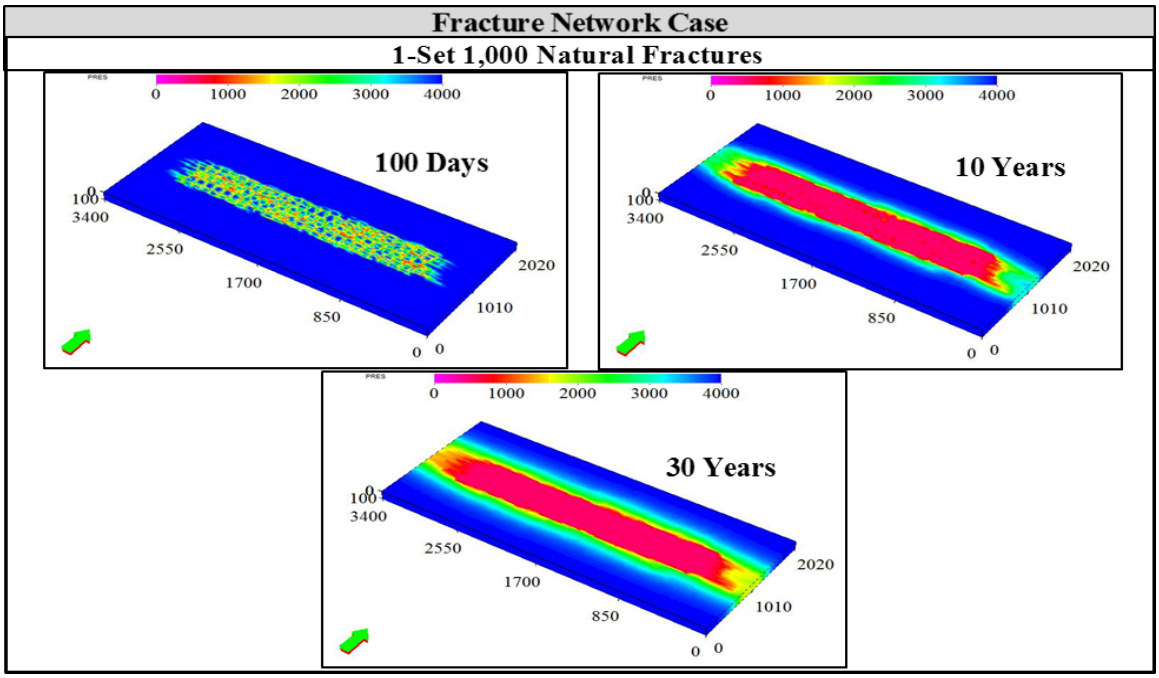

Figure 4.41: Pressure distribution maps of the Fracture Network case with 1-set 1,000 natural fractures for the 100-day, 10-year, and 30-year marks.

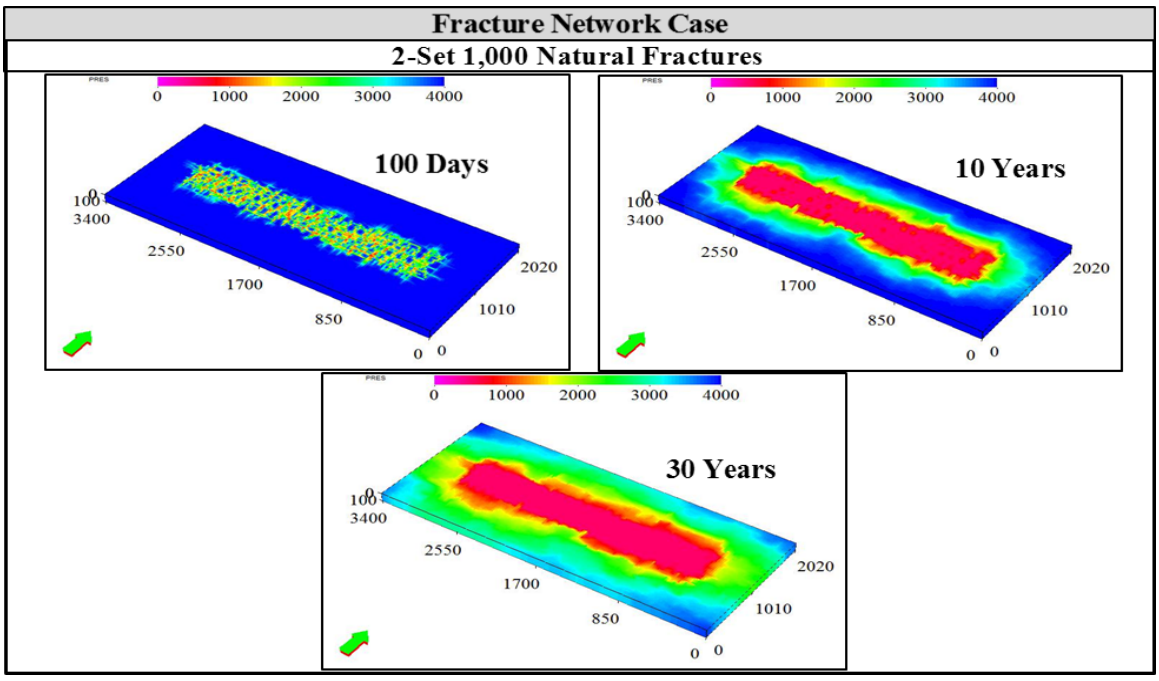

Figure 4.42: Pressure distribution maps of the Fracture Network case with 2-set 1,000 natural fractures for the 100-day, 10-year, and 30-year marks.

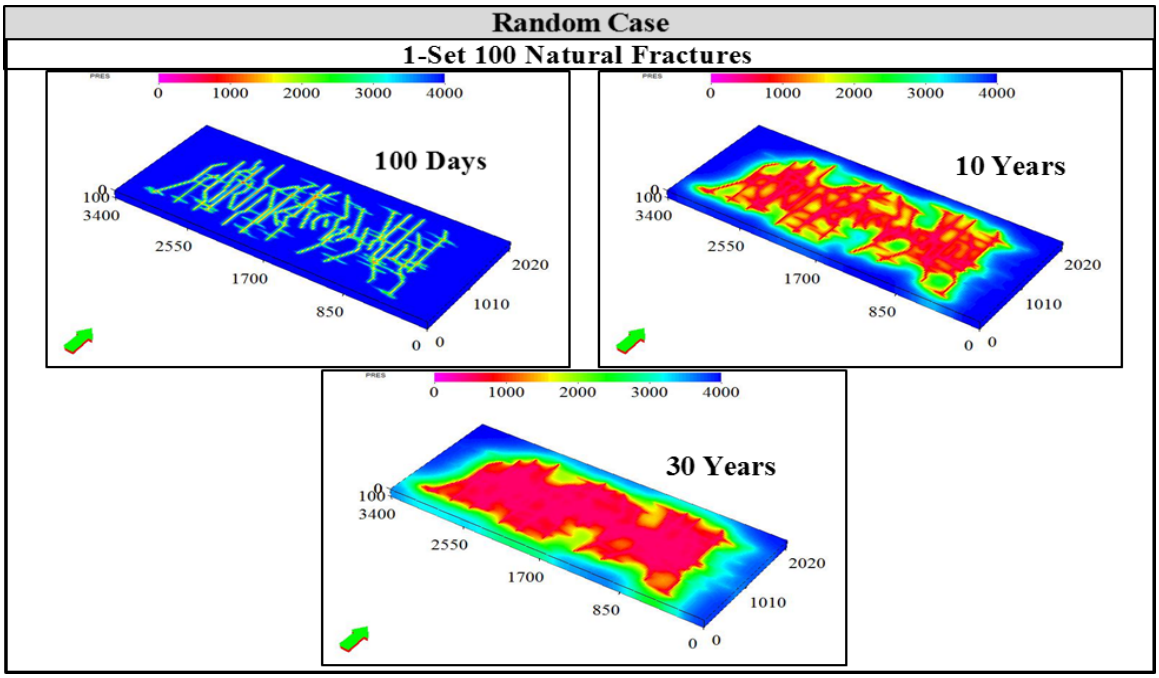

Figure 4.43: Pressure distribution maps of the Random case with 1-set 100 natural fractures for the 100-day, 10-year, and 30-year marks.

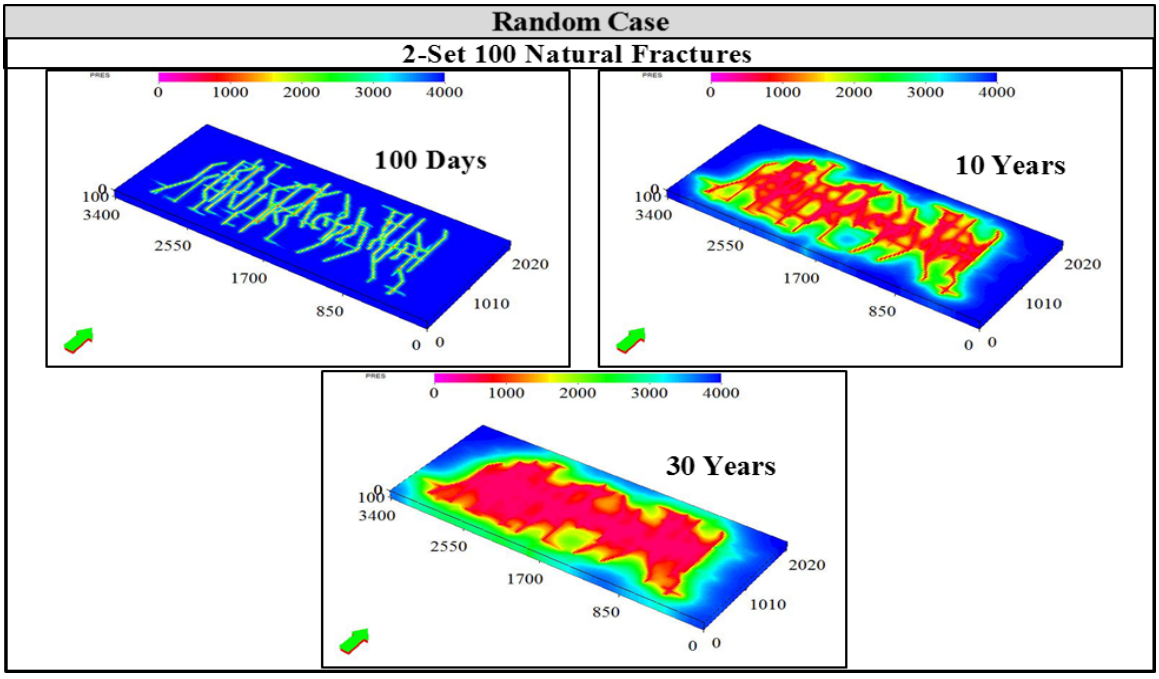

Figure 4.44: Pressure distribution maps of the Random case with 2-set 100 natural fractures for the 100-day, 10-year, and 30-year marks.

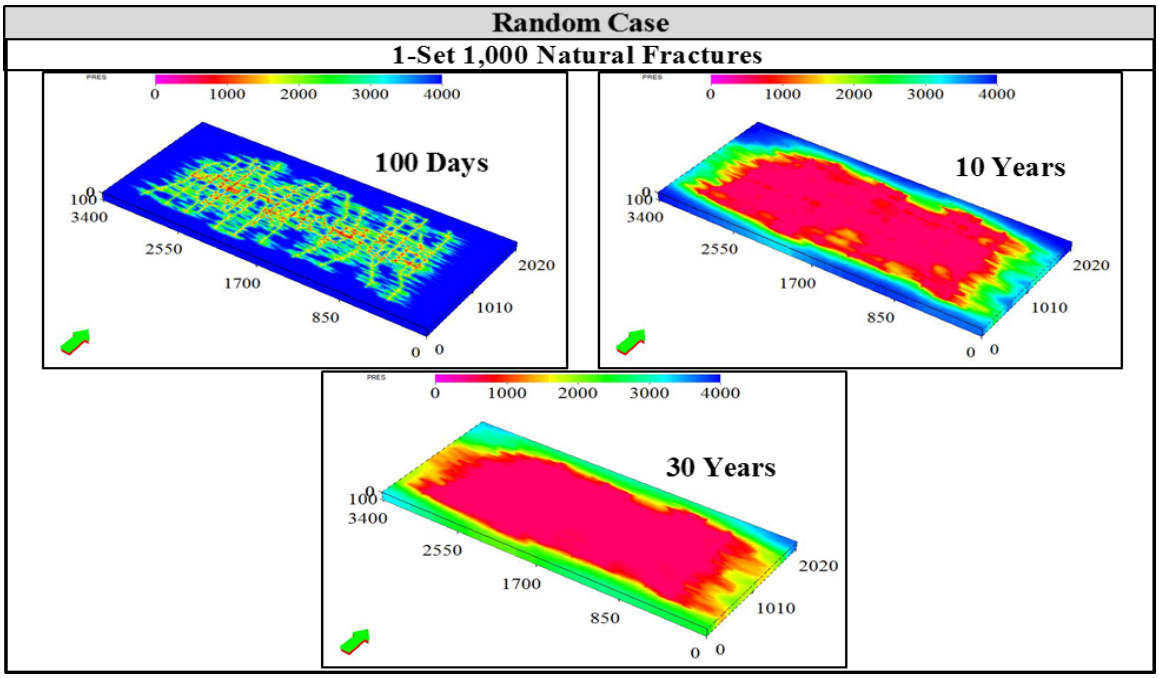

Figure 4.45: Pressure distribution maps of the Random case with 1-set 1,000 natural fractures for the 100-day, 10-year, and 30-year marks.

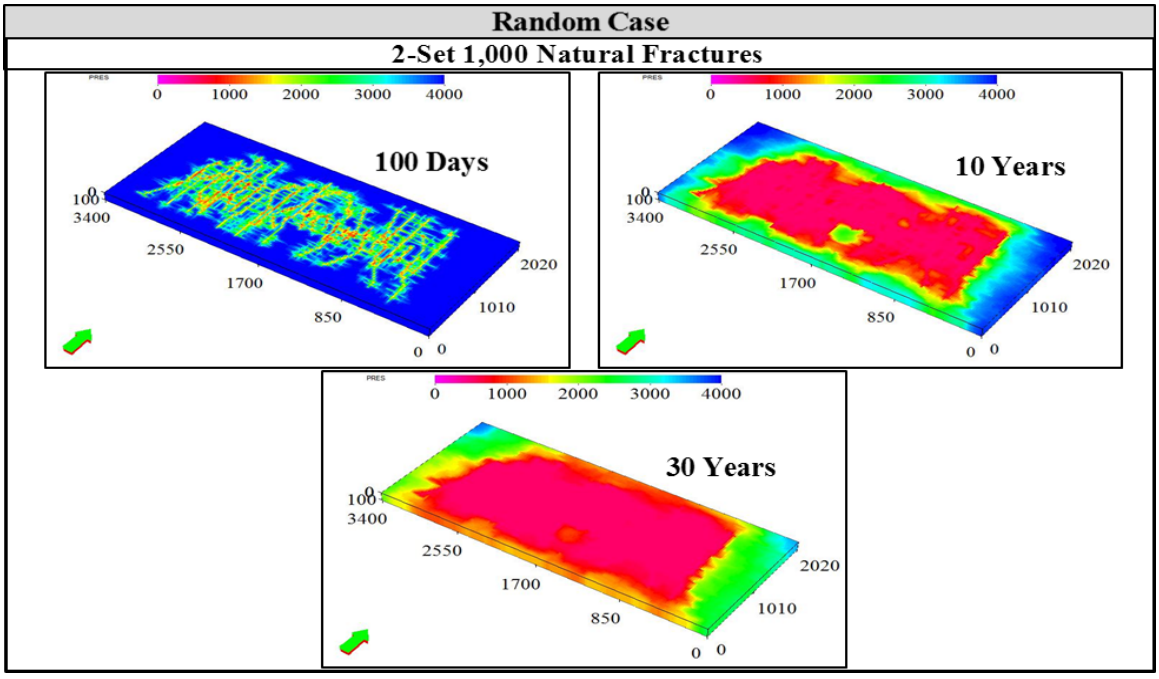

Figure 4.46: Pressure distribution maps of the Random case with 2-set 1,000 natural fractures for the 100-day, 10-year, and 30-year marks.

4.3. VARYING FRACTURE WIDTH CASES

In the previous sections, all hydraulic fractures were assumed to have a constant fracture aperture/width of 0.01 ft. In this section, another type of complexity pertaining to the width of these hydraulic fractures is investigated. The Random fracture geometry in the previous sections was used for this investigation. Four runs with different fracture conductivity values were conducted. In each run, two cases were created: one that adopts a constant fracture width and the other adopts varying fracture widths. Nonetheless, the sum of the fractures' widths in both cases of each run was kept constant. This means that the total fractures' volume and the total fractures' conductivity in both cases of each run are similar. **Table 4.6** summarizes the values considered in each run. The runs are arranged in descending total fractures' conductivity.

Run #	Cases	Single Fracture Width (*ft*)	Single Fracture Conductivity (*mD·ft*)	Total Fractures' Width (*ft*)	Total Fractures' Volume (ft^3)	Total Fractures' Conductivity (*mD·ft*)
Run 1	Constant Fracture Width	0.01	100	0.71	25,500	7,100
	Varying Fracture Width	Varies*	Varies*			
Run 2	Constant Fracture Width	0.001	10	0.071	2,550	710
	Varying Fracture Width	Varies**	Varies**			
Run 3	Constant Fracture Width	0.0001	1	0.0071	255	71
	Varying Fracture Width	Varies***	Varies***			
Run 4	Constant Fracture Width	0.00001	0.1	0.00071	25.5	7.1
	Varying Fracture Width	Varies****	Varies****			

* Fractures widths average at 0.01 *ft* and fractures conductivities average at 100 *mD·ft*

** Fractures widths average at 0.001 *ft* and fractures conductivities average at 10 *mD·ft*

*** Fractures widths average at 0.0001 *ft* and fractures conductivities average at 1 *mD·ft*

**** Fractures widths average at 0.00001 *ft* and fractures conductivities average at 0.1 *mD·ft*

Table 4.6: Summary of the runs of constant and varying fracture width cases considered in the study.

For each run, a comparison between the constant and varying fracture width cases is made. **Figures 4.47** through **4.50** showcases these comparisons in terms of cumulative gas and water productions for the four runs, respectively. As can be seen, in almost all runs, the varying fracture width cases had a lower gas and water recoveries compared to the constant fracture width cases. In addition, the difference in cumulative recoveries between the constant and the varying fracture width cases seem to be widening as you move from one run to the next. This is can be correlated to the decrease in total fractures' conductivity as you move from Run 1 through Run 4.

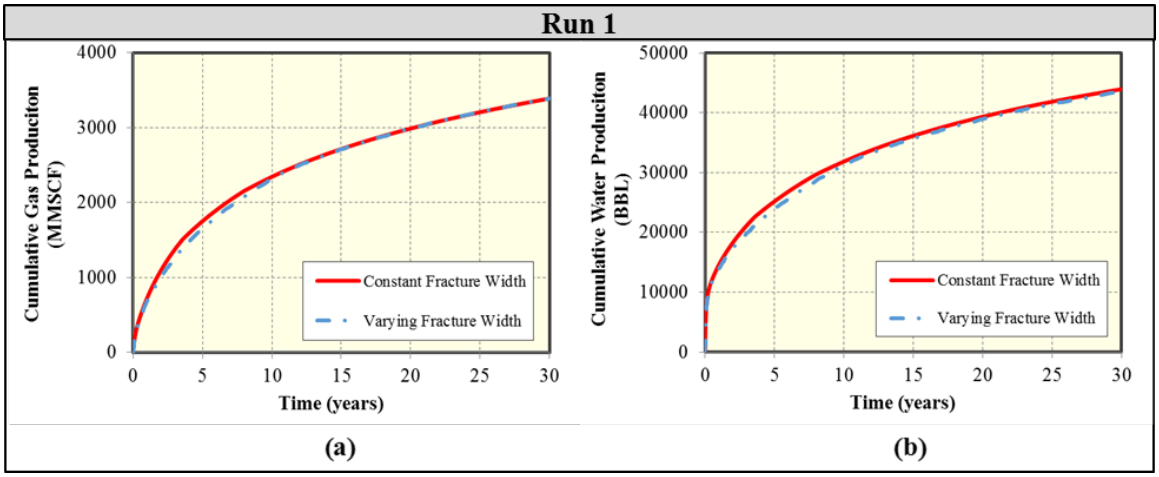

Figure 4.47: Comparison of **(a)** Cumulative gas production and (**b)** Cumulative water production between the constant fracture width case and the varying fracture width case for Run 1

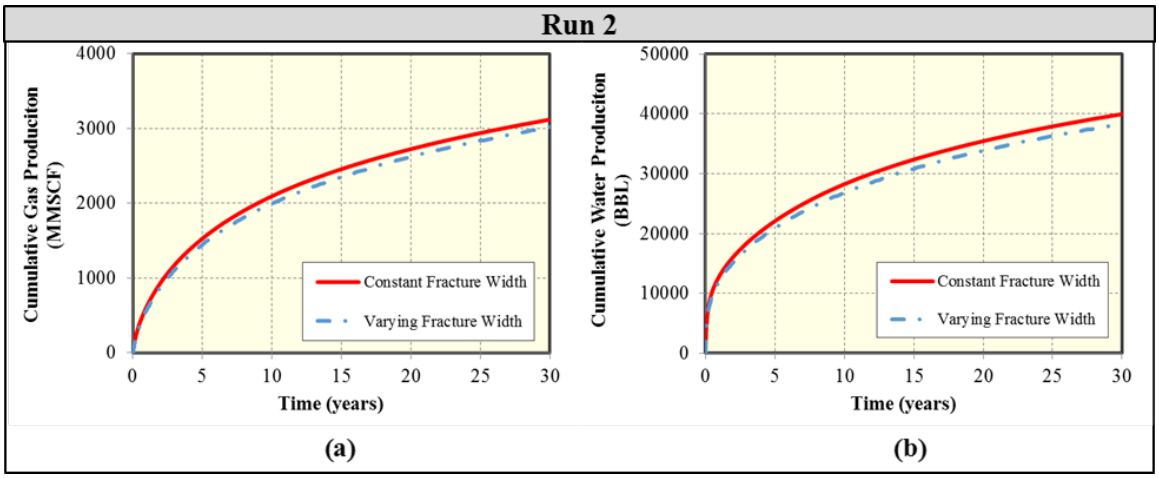

Figure 4.48: Comparison of **(a)** Cumulative gas production and (**b)** Cumulative water production between the constant fracture width case and the varying fracture width case for Run 2

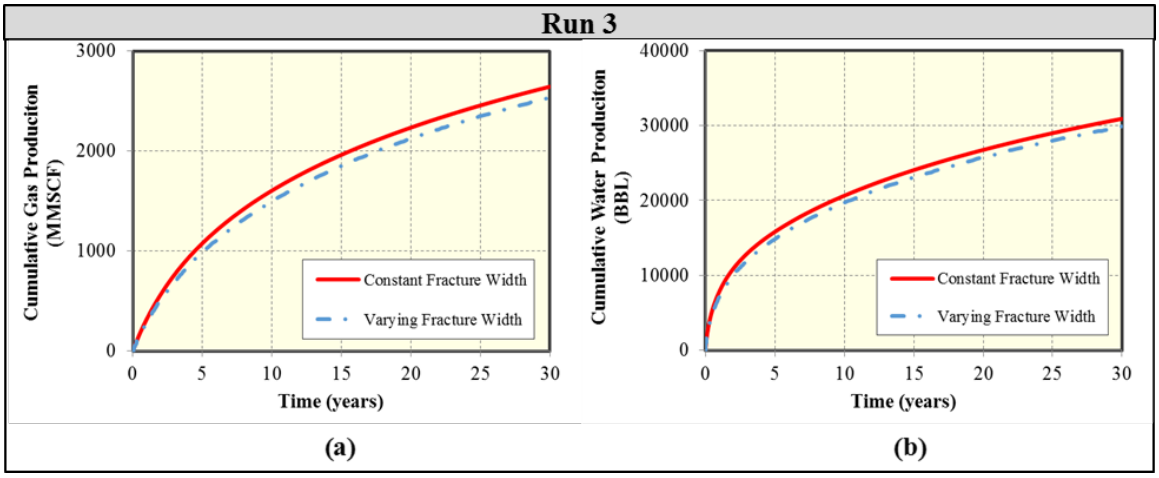

Figure 4.49: Comparison of **(a)** Cumulative gas production and (**b)** Cumulative water production between the constant fracture width case and the varying fracture width case for Run 3

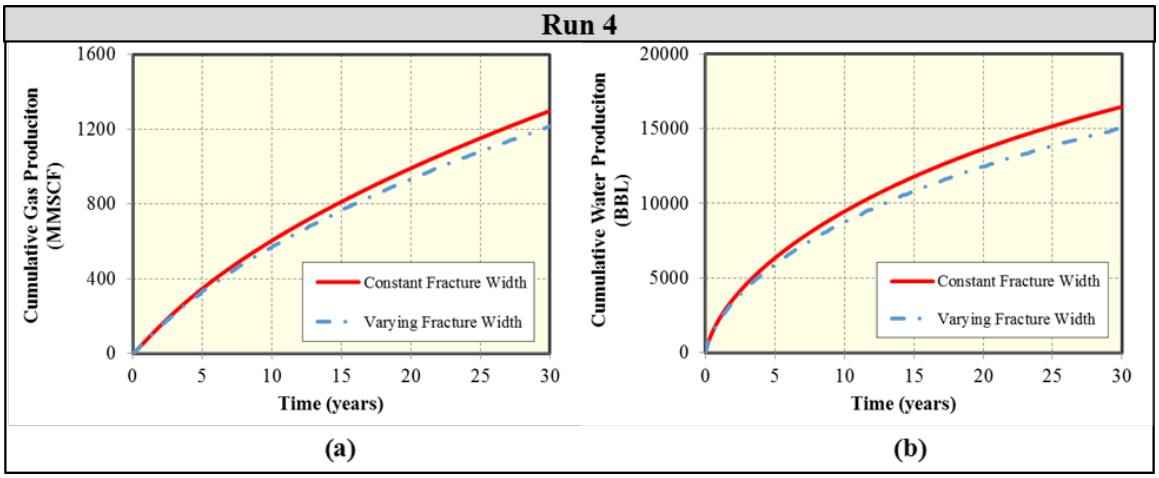

Figure 4.50: Comparison of **(a)** Cumulative gas production and (**b)** Cumulative water production between the constant fracture width case and the varying fracture width case for Run 4

To get a better glimpse of the difference in recoveries, **Tables 4.7** and **4.8** highlight the percentage differences in cumulative gas and water productions at 30 years, respectively, between the constant and the varying fracture width cases for all four runs. As can be seen, there are almost no differences in gas and water recoveries between the two cases for Run 1, which has the highest total fractures' conductivity. However, differences in recoveries between constant and varying fracture width cases appear as you move on to the next runs. As a matter of fact, an increasing trend in absolute difference between the two cases in terms of gas recovery is observed. This indicates that the difference in gas recoveries between the constant fracture width case and the varying fracture widths case is exacerbated as the gross conductivity of these fractures is at its lowest. Water flowback recoveries follow a somewhat similar pattern in which the difference in water cumulative between the two cases is intensified as the total conductivity of the fractures is lowered.

Cumulative Gas Production @ 30 Years (MMSCF)

Run #	Constant Fracture Width	Varying Fracture Width	Difference (%)
Run 1	3390.2	3393.2	0%
Run 2	3120.1	3016.2	-3%
Run 3	2643.7	2535.0	-4%
Run 4	1297.4	1213.9	-6%

Table 4.7: Summary of cumulative gas productions (MMSCF) at the end of 30 years, and the percentage difference between constant and varying fracture width cases for all four runs.

Cumulative Water Production @ 30 Years (BBL)

Run #	Constant Fracture Width	Varying Fracture Width	Difference (%)
Run 1	43970.2	43599.8	-1%
Run 2	39962.4	38324.5	-4%
Run 3	30908.0	29851.6	-3%
Run 4	16465.2	15037.7	-9%

Table 4.8: Summary of cumulative water productions (BBL) at the end of 30 years, and the percentage difference between constant and varying fracture width cases for all four runs.

In summary, hydraulic fractures are seldom uniform and a major part of their non-uniformity is related to their changing apertures/widths. This section investigated this irregularity and found that non-uniform fractures' widths resulted in lowering both gas and water outcomes compared to constant fractures' widths. However, this aggravation in productivity is more apparent in low fracture conductivity setting. This means that when the reservoir rock is characterized by its low conductivity for induced fractures, which is the case for shale gas reservoirs, it's more imperative to consider varying the fractures' apertures in reservoir simulation modeling.

4.4. SENSITIVITY ANALYSIS

To characterize the sensitivity of both the reservoir and fracture properties in the two-phase flow performance of this shale gas model, two sensitivity analyses on the Planar (Base) case was performed. The first sensitivity analysis pertains to the effect of changing the initial water saturation (Sw) inside the simulated reservoir volume (SRV). This parameter represents the amount of water injected into the reservoir during the stimulation process. On the other hand, the second sensitivity analysis pertains to the effect of changing the fracture conductivity. **Table 4.9** lists the values tested under the sensitivity analysis for each of the two parameters.

Parameter	**Values Tested**	**Unit**
Initial water saturation (S_w) inside the SRV	0.15, 0.25, 0.5*, 0.75	*Fraction*
Fracture conductivity (FC)	0.1, 1, 10, 100*	*mD·ft*

* Represents Base case.

Table 4.9: Summary of reservoir and fracture parameters under sensitivity analysis.

Figure 4.51 showcases the result of the first sensitivity analysis. As can be seen, increasing the initial water saturation inside the SRV from 0.5 (Base case) to 0.75 negatively impacted gas productivity throughout the 30-year production cycle with estimated 50% decrease in cumulative recovery at the end of the 30 years. Oppositely, reducing the initial water saturation inside the SRV by half to 0.25 positively impacted gas productivity with 47% increase in cumulative recovery at the end of 30 years. As can be seen, there's a symmetrical effect between reducing and increasing by half the initial Sw value. However, further reduction in Sw value to 0.15 didn't results in proportionally similar impact as the decrease from 0.5 to 0.25.

On the contrary, as depicted on **Figure 4.51**, increasing the initial water saturation inside the SRV from 0.5 (Base case) to 0.75 had a positive impact on the cumulative water flowback during the 30-year production cycle. Specifically, 360% increase in the amount of water recovered was estimated as a result of this increase in Sw. On the other hand, decreasing the initial water saturation inside the SRV to 0.25 and 0.15 resulted in reducing the cumulative water production throughout the 30 years by almost the same amount in both cases (0.25 and 0.15).

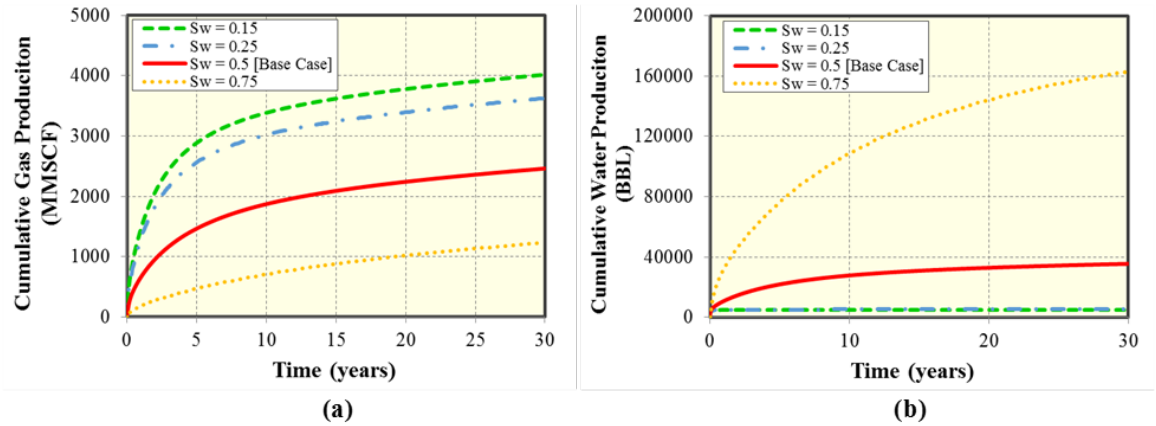

Figure 4.51: Comparison of **(a)** Cumulative gas production and **(b)** Cumulative water production between different values of initial water saturation (S_w) inside the SRV.

Figure 4.52 presents the result of the second sensitivity analysis pertaining to fracture conductivity. As can be seen, decreasing the fracture conductivity beyond 1 mD·ft results in the most pronounced deterioration of the cumulative gas recovery. On the other hand, cumulative water recovery sees the effect of decreasing fracture conductivity in a more consistent manner. This means that, to some extent, the reduction of fracture conductivity from 100 mD·ft (Base case) to 10, 1, and then 0.1 mD·ft results in decreasing water recovery proportionately.

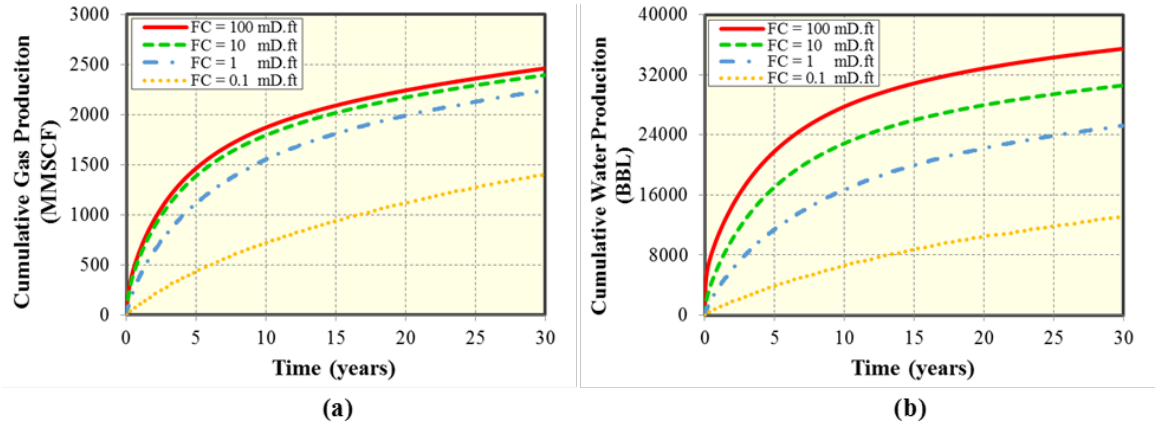

Figure 4.52: Comparison of (a) Cumulative gas production and (b) Cumulative water production between different values of fracture conductivity.

Chapter 5: Conclusions and Recommendations

5.1. Conclusions

With the help of numerical simulation, this research presents a 3D shale gas reservoir model to examine the two-phase (gas and water) flow performance of a shale gas well. Utilizing the Embedded Discrete Fracture Model (EDFM), the subject 3D reservoir model is capable of modeling complex fracture geometries. The research study first succeeded in verifying this EDFM approach by comparing it to the Local Grid Refinement (LGR) approach. Subsequently, the research thesis examined the effect of changing the hydraulic fracture geometries from simple geometry (Planar case) to more complex geometries (Diagonal, Reoriented, Irregular, Fracture Network, and Random cases). For comparability, all these cases share the same total fracture length and the same total amount of water injected into them. The following observations and conclusions were made on the simulation results:

Observations	Analyses & Conclusions
The Random case resulted in the highest cumulative gas production at the end of simulation cycle. Whereas, its water recovery hasn't been affected.	The complexity pertaining to the non-uniformity between the created fractures with respect to how far a fracture extends away from the horizontal wellbore, results in a non-uniform drainage area (also non-uniform SRV). This randomness, coupled with minimum fracture interference, contribute to the improved gas recovery.

Observations	Analyses & Conclusions
The first four cases (Planar, Diagonal, Reoriented, and Irregular) have fairly similar performance in terms of gas and water cumulative recoveries.	As long as the created fractures results in fairly the same simulated fracture volume (SRV), the following fracture complexity are rather irrelevant to the performance of shale gas wells: • The complexity pertaining to changing the angle between the horizontal wellbore and created fracture, which is imposed on the Diagonal and Reoriented cases. • The complexity pertaining to the length irregularity of individual fracture segments within a fracture, which is imposed on the Irregular case.
The Fracture Network case has, of all cases, the lowest gas productivity and the highest water flowback.	The creation of fracture network results in a stronger and more distinct interference between the fractures, compared to other cases where fractures seldom intersect and are spaced uniformly. This fracture interference effect results in lowering the gas velocity flowing into the fractures, which allows for more water, and hence less gas, to flow back to surface.

Furthermore, the research examined another level of complexity by incorporating natural fractures to the 3D reservoir model. Both quantity and orientation of these natural

fractures were tested while assuming that all added fractures are open and not sealed. The following conclusions were made on the simulation results:

- The more ubiquitous natural fractures in a shale rock, the higher the chances of intersections between hydraulic and natural fractures, and hence the larger the drainage area accessible to the well, which lead to a better expected recovery.
- The orientation of these natural fractures plays a major role in altering productivity. In fact, the orientation of natural fractures that promises a higher number of intersections between hydraulic and natural fractures will, eventually, reap the benefit of a better recovery. Hence, given that rock stresses govern the orientation of these natural fractures, well placement is critical in order to achieve a larger drainage area, and thus an enhanced recovery.

Additionally, the research thesis investigated a level of complexity related to the non-uniformity of fractures' apertures/widths. The investigation used the Random fracture geometry, highlighted in previous section, to incorporate varying fractures' widths in a case and compare it to the case where constant fractures' widths is assumed. For comparability, both cases had a constant total fractures' width. The two cases were run four times while decreasing the total fractures' conductivity from one run to the next. The following conclusion were made on the results of these simulation runs:

- The varying fracture width cases had an overall lower cumulative gas and water productions than the constant fracture width cases.
- The magnitude of differences between the two cases is intensified as the total fractures' conductivity is lowered.

Finally, the research study provided a sensitivity study to illustrate the effect of changing some reservoir and fracture parameters incorporated in the subject 3D reservoir model. Two parameters were considered. The initial water saturation inside the simulated

reservoir volume (SRV) and the fracture conductivity. The following observations were made:

- In general, the higher the initial water saturation inside the SRV, the lower the expected gas cumulative recovery and the higher the water cumulative recovery, and vice versa. Nevertheless, thresholds exist in which further decrease or increase in this saturation value doesn't affect the gas and water recoveries. These thresholds represent an opportunity to establish the optimum value of water saturation which can help in deciding the appropriate amount of water that should be injected during the stimulation process.
- Expectedly, reduction of fracture conductivity results in decreasing both gas and water cumulative recoveries. However, specific to the gas recovery, this effect is more pronounced if the fracture conductivity is lowered beyond unit mD·ft.

In conclusion, this research provides useful insights toward understanding the effect of fracture complexities on the two-phase performance of shale gas wells. The fracture complexities tested pertain to either the geometrical complexity of hydraulic fractures and or to the presence of natural fractures.

5.2. RECOMMENDATIONS FOR FUTURE WORK

Reservoir simulation modeling of shale gas reservoirs is constantly developing. This work provides a glimpse to the importance of incorporating fracture complexities to the development endeavor of reservoir simulation applications of shale gas reservoirs in particular and unconventional reservoirs in general. However, a broader and more exhaustive view of the issue of fracture complexity in unconventional reservoir setting is still pressing. This section provides recommendations for future related work which include and not limited to the following:

- Use of microseismic events detected after stimulation treatment is highly advised to decide on hydraulic fractures' propagation as well as mapping out the possible distribution of fracture segments and the intersections between hydraulic and natural fractures' segments. This will help in building a more accurate fracture network case that mimic the distribution of microseismic events.
- Since the ability to adequately simulate shale gas formations rely on the rock in-situ stresses, rock geomechanics is recommended to be included in future work. More specifically, pressure-related geomechanics is integral for shale reservoirs as it alters important rock parameters such as permeability.
- More sensitivity analyses of reservoir and fracture properties are needed to examine the possible intricate performance-related changes given the inclusion of fracture complexity factor.

Glossary

ABT	=	after breakthrough
A_{NNC}	=	contact area of non-neighboring connection
BBL	=	Barrels
BBT	=	before breakthrough
BET	=	Brunauer, Emmett and Teller
C_BET	=	constant related to the net heat of adsorption
DFM	=	discrete fracture modeling
d_{NNC}	=	distance of non-neighboring connection
DRP	=	dynamic relative permeability
EDFM	=	embedded discrete fracture model
FC	=	fracture conductivity
k_f	=	fracture permeability
k_{NNC}	=	permeability of non-neighboring connection
k_{re}	=	water relative permeability
k_{rg}	=	gas relative permeability
LGR	=	local grid refinement
MBE	=	material balance equation
MMSCF	=	million standard cubic feet
n_BET	=	maximum number of adsorption layers
NF	=	natural fracture
NNC	=	non-neighboring connection
q	=	volume flow rate
SRV	=	simulated reservoir volume
S_w	=	water saturation
Tcf	=	trillion cubic feet
T_{NNC}	=	transmissibility factor of non-neighboring connection
V_m_BET	=	maximum adsorption-gas volume for a complete unimolecular layer
w_f	=	fracture aperture
WI_f	=	fracture's effective well index
ΔP	=	potential difference between the two cells
λ_l	=	relative mobility of phase l

Bibliography

Adefidipe, O. A., Dehghanpour, H., & Virues, C. J. (2014). Immediate Gas Production from Shale Gas Wells: A Two-Phase Flowback Model. Society of Petroleum Engineers. doi:10.2118/168982-MS.

Alkouh, A., McKetta, S., & Wattenbarger, R. (2014). Estimation of Effective-Fracture Volume Using Water-Flowback and Production Data for Shale-Gas Wells. Journal Of Canadian Petroleum Technology, 53(05), 290-303. http://dx.doi.org/10.2118/166279-pa

Bennion, D., Bietz, R., Thomas, F., & Cimolai, M. (1994). Reductions In the Productivity of Oil And Low Permeability Gas Reservoirs Due to Aqueous Phase Trapping. *Journal Of Canadian Petroleum Technology*, *33*(09). http://dx.doi.org/10.2118/94-09-05

Bennion, D., Thomas, F., Bietz, R., & Bennion, D. (1999). Remediation of Water And Hydrocarbon Phase Trapping Problems In Low Permeability Gas Reservoirs. *Journal Of Canadian Petroleum Technology*, *38*(08). http://dx.doi.org/10.2118/99-08-01

Blaskovich, F. T., Cain, G. M., Sonier, F., Waldren, D., & Webb, S. J. (1983, January 1). A Multicomponent Isothermal System for Efficient Reservoir Simulation. Society of Petroleum Engineers. doi:10.2118/11480-MS.

BP (2017). Statistical review of world energy 2017. [online] Available at: http://www.bp.com/en/global/corporate/energy-economics/statistical-review-of-world-energy.html

Cavalcante Filho, J. S., Shakiba, M., Moinfar, A., & Sepehrnoori, K. (2015). Implementation of a Preprocessor for Embedded Discrete Fracture Modeling in an IMPEC Compositional Reservoir Simulator. Society of Petroleum Engineers. Presented at the SPE Reservoir Simulation Symposium held in Houston, Texas, 23-25 February 2015. doi:10.2118/173289-MS.

Cheng, Y. (2012). Impact of Water Dynamics in Fractures on the Performance of Hydraulically Fractured Wells in Gas-Shale Reservoirs. *Journal Of Canadian Petroleum Technology*, *51*(02), 143-151. http://dx.doi.org/10.2118/127863-pa

Clarkson, C., & Williams-Kovacs, J. (2013). Modeling Two-Phase Flowback of Multifractured Horizontal Wells Completed in Shale. *SPE Journal*, *18*(04), 795-812. http://dx.doi.org/10.2118/162593-PA.

CMG-GEM (Version 2014.1). (2014)

Dahi Taleghani, A., & Olson, J. E. (2014). How Natural Fractures Could Affect Hydraulic-Fracture Geometry. Society of Petroleum Engineers. doi:10.2118/167608-PA.

Dean, R. H., & Lo, L. L. (1988). Simulations of Naturally Fractured Reservoirs. Society of Petroleum Engineers. doi:10.2118/14110-PA.

EIA (2013). Technically Recoverable Shale Oil and Shale Gas Resources. [online] Available at: https://www.eia.gov/analysis/studies/worldshalegas/

EIA (2017). Annual Energy Outlook. [online] Available at: https://www.eia.gov/outlooks/aeo/pdf/0383(2017).pdf

Engelder, T., Cathles, L., & Bryndzia, L. (2014). The fate of residual treatment water in gas shale. *Journal Of Unconventional Oil And Gas Resources*, *7*, 33-48. http://dx.doi.org/10.1016/j.juogr.2014.03.002

Ezulike, D. O., Dehghanpour, H., & Hawkes, R. V. (2013). Understanding Flowback as a Transient 2-Phase Displacement Process: An Extension of the Linear Dual-Porosity Model. Society of Petroleum Engineers. doi:10.2118/167164-MS.

Fisher, M. K., Heinze, J. R., Harris, C. D., Davidson, B. M., Wright, C. A., & Dunn, K. P. (2004). Optimizing Horizontal Completion Techniques in the Barnett Shale Using Microseismic Fracture Mapping. Society of Petroleum Engineers. doi:10.2118/90051-MS.

Hill, A. C., & Thomas, G. W. (1985). A New Approach for Simulating Complex Fractured Reservoirs. Society of Petroleum Engineers. doi:10.2118/13537-MS.

Hoteit, H., & Firoozabadi, A. (2006). Compositional Modeling of Discrete-Fractured Media Without Transfer Functions by the Discontinuous Galerkin and Mixed Methods. *SPE Journal*, 11(03), 341-352. http://dx.doi.org/10.2118/90277-pa

Hui, M., & Thomas Mallison, B. (2009). System and method of grid generation for discrete fracture modeling. US Patent US9026416.

Ilk, D., Currie, S. M., Symmons, D., Rushing, J. A., Broussard, N. J., & Blasingame, T. A. (2010). A Comprehensive Workflow for Early Analysis and Interpretation of Flowback Data from Wells in Tight Gas/Shale Reservoir Systems. Society of Petroleum Engineers. doi:10.2118/135607-MS.

Jenkins, C. D., & Boyer, C. M. (2008). Coalbed- and Shale-Gas Reservoirs. Society of Petroleum Engineers. doi:10.2118/103514-JPT.

Jiang, J., Shao, Y., & Younis, R. M. (2014). Development of a Multi-Continuum Multi-Component Model for Enhanced Gas Recovery and CO2 Storage in Fractured Shale Gas Reservoirs. Society of Petroleum Engineers. doi:10.2118/169114-MS.

Li, L., & Lee, S. H. (2008). Efficient Field-Scale Simulation of Black Oil in a Naturally Fractured Reservoir Through Discrete Fracture Networks and Homogenized Media. Society of Petroleum Engineers. doi:10.2118/103901-PA.

Makhanov, K., Habibi, A., Dehghanpour, H., & Kuru, E. (2014). Liquid uptake of gas shales: A workflow to estimate water loss during shut-in periods after fracturing operations. *Journal Of Unconventional Oil And Gas Resources*, *7*, 22-32. http://dx.doi.org/10.1016/j.juogr.2014.04.001

Moinfar, A., Varavei, A., Sepehrnoori, K., & Johns, R. T. (2014). Development of an Efficient Embedded Discrete Fracture Model for 3D Compositional Reservoir Simulation in Fractured Reservoirs. Society of Petroleum Engineers. doi:10.2118/154246-PA.

Noorishad, J., & Mehran, M. (1982). An upstream finite element method for solution of transient transport equation in fractured porous media. *Water Resources Research,* 18(3), 588-596. http://dx.doi.org/10.1029/wr018i003p00588

Olson, J. E. (1995). Fracturing from Highly Deviated and Horizontal Wells: Numerical Analysis of Non-planar Fracture Propagation. Society of Petroleum Engineers. doi:10.2118/29573-MS.

Panfili, P., & Cominelli, A. (2014). Simulation of Miscible Gas Injection in a Fractured Carbonate Reservoir using an Embedded Discrete Fracture Model. Society of Petroleum Engineers. doi:10.2118/171830-MS.

Saidi, A. M. (1983). Simulation of Naturally Fractured Reservoirs. Society of Petroleum Engineers. doi:10.2118/12270-MS.

Shakiba, M. (2014). Modeling and Simulation of Fluid Flow in Naturally and Hydraulically Fractured Reservoirs Using Embedded Discrete Fracture Model (EDFM) (MS Thesis). The University of Texas at Austin.

Shakiba, M., & Sepehrnoori, K. (2015). Using Embedded Discrete Fracture Model (EDFM) and Microseismic Monitoring Data to Characterize the Complex Hydraulic Fracture Networks. Society of Petroleum Engineers. Presented at the SPE Annual Technical Conference and Exhibition, Houston, Texas, 28-30 September, 2015. doi:10.2118/175142-MS.

Shen, W., Xu, Y., Li, X., Huang, W., & Gu, J. (2016). Numerical simulation of gas and water flow mechanism in hydraulically fractured shale gas reservoirs. Journal Of Natural Gas Science And Engineering, 35, 726-735. http://dx.doi.org/10.1016/j.jngse.2016.08.078

Vassilellis, G. D., Moos, D., Li, C., & Seager, R. J. H. (2010). Investigating the Expected Long-Term Production Performance of Shale Reservoirs. Society of Petroleum Engineers. doi:10.2118/138134-MS.

Virues, C., Budge, J., & Von Lunen, E. (2015). Microseismic-Derived Ultimate Expected Fracture Half-Length in Unconventional Stimulated Reservoir Volume in a Multi-Fractured Horizontal 8 Well Full Pad - Canadian Horn River Basin Case Study. Unconventional Resources Technology Conference. doi:10.15530/URTEC-2015-2153989.

Wang, W., Olson, J. E., & Prodanovic, M. (2013). Natural and Hydraulic Fracture Interaction Study Based on Semi-Circular Bending Experiments. Unconventional Resources Technology Conference.

Warren, J. E., & Root, P. J. (1963). The Behavior of Naturally Fractured Reservoirs. Society of Petroleum Engineers. doi:10.2118/426-PA.

Williams-Kovacs, J. D., & Clarkson, C. R. (2015). A Modified Approach For Modelling 2-Phase Flowback From Multi-Fractured Horizontal Shale Gas Wells. Unconventional Resources Technology Conference. doi:10.15530/URTEC-2015-2149183.

Wu, K., & Olson, J. E. (2015). Numerical Investigation of Complex Hydraulic Fracture Development in Naturally Fractured Reservoirs. Society of Petroleum Engineers. doi:10.2118/173326-MS.

Xu, Y., Adefidipe, O. A., Dehghanpour, H., & Virues, C. J. (2015). Volumetric Analysis of Two-Phase Flowback Data for Fracture Characterization. Society of Petroleum Engineers. doi:10.2118/174023-MS.

Xu, Y. (2015). Implementation and application of the embedded discrete fracture model (EDFM) for reservoir simulation in fractured reservoirs (MS Thesis). The University of Texas at Austin.

Yu, W., Luo, Z., Javadpour, F., Varavei, A., & Sepehrnoori, K. (2014). Sensitivity analysis of hydraulic fracture geometry in shale gas reservoirs. Journal Of Petroleum Science And Engineering, 113, 1-7. http://dx.doi.org/10.1016/j.petrol.2013.12.005

Yu, W., Sepehrnoori, K., & Patzek, T. W. (2016). Modeling Gas Adsorption in Marcellus Shale With Langmuir and BET Isotherms. Society of Petroleum Engineers. doi:10.2118/170801-PA.